BES 96

The Proceedings of the 5th BES Annual Meeting

FIFTH BES ANNUAL MEETING

ZHANGJIAJIE, HUNAN . 1996

BES Collaboration

CONTENTS

TOF of BES-II

Jun-Guang LU (The TOF Group)
Institute of High Energy Physics, Beijing 100039, People's Republic of China

1 The New TOF

The new TOF barrel, still composed of 48 units and with the scintillators of the same size as those in the old TOF detector, was constructed from June 1994 and mounted onto the MDC after its completion in October 1995. The machining and optically polishing of the all light-guides had been finished before June 1995. At the same time we had made the voltage dividers of PMT's and performed a test of them. In the same year from June to August the light-guides were sticked onto the scintillators. After then, the protecting gluepaper outside the scintillators was removed. Instead, we covered the scintillators with aluminium-coated film and black tap. In the two months afterward, we performed a cosmic rays test on all of the TOF counters. The TOF system was assembled from October 1995 to December 1995.

1.1 The Comparision of New TOF and BES TOF

As shown in Fig. 1.

1.2 The Test of TOF Counter With Cosmic Rays

As shown in Fig. 2.

1.3 Laser Monitor System

As shown in Fig. 3.

1.4 New TOF Data and Runing

As shown in Fig. 4.

2 Conclusion

The analysis with the data acquistioned within 20 days this May indicates that the new TOF detector with time resolution less than 200ps (including the contribution from the beam bunch length) was very successfully designed and manufactured. Here, we are grateful to all colleagues from University of Hawaii and Physical Dvision 2 at IHEP for their cooperation.

1. **Comparision of New TOF and BES TOF**

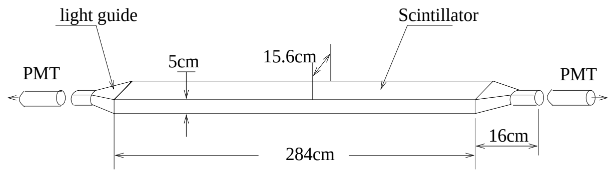

New TOF counter

	New TOF	BES TOF
Scintillator:		
size:	**15.6cm * 5cm * 284cm**	**15.6cm * 5cm * 284cm**
type:	BC-408	NE110
decay time:	**2.1 ns**	**3.3 ns**
attenuation:	**4.4 m**	**2.5 m**
Light guide:		
size:	**16cm (L)**	**112cm (L)**
material:	UVT plexiglass	air 2# plexiglass
	New TOF	***BES TOF***
wraping:	Aluminum foil + black plastic tape	Black paper + black plastic tape
PMTs :	R2490-05 (FM)	XP2020
photocathode sensitivity:	$\phi 36$	$\phi 44$
gain:	5×10^6 (at 2500v)	3×10^7 (at 2200v)
transit time:	8.5 ns	28ns
transit time variation(σ)	150 ps	250ps
Laser monitor:	dye liquid	N_2
photo pulse:	100 ps	300 ps
fibers location:	two end	middle

Figure 1: The Comparision of the New TOF and BES TOF

2. Testing TOF counter with cosmic rays

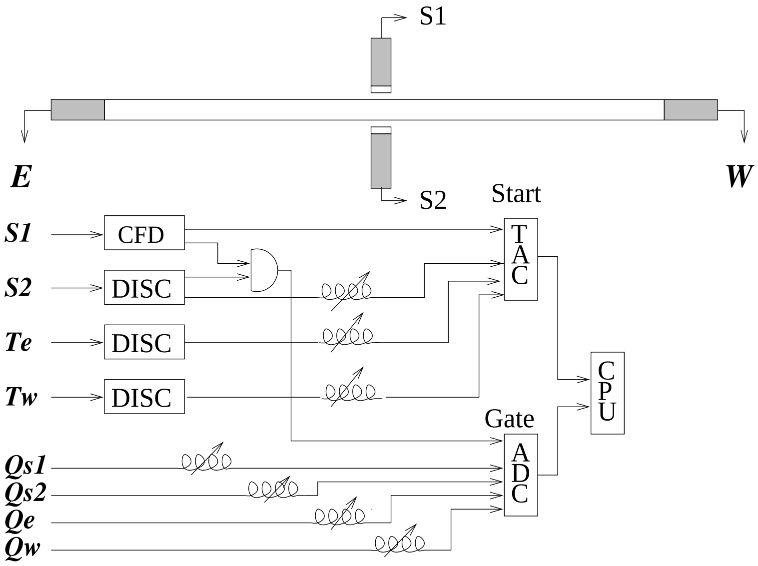

Schematic diagram for the testing readout

* Testing one counter carfully

(a) *S1 : 3cm x 3cm x 1cm*

S2 : 2cm x 2cm x 3cm

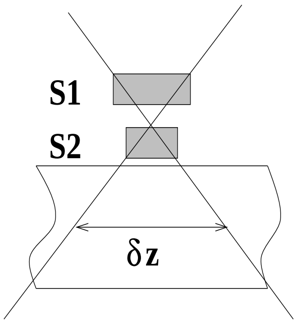

(b) *S1 : 2cm x 2cm x 1cm*

S2 : 3cm x 3cm x 1cm

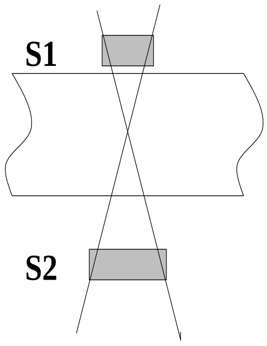

* **Transit time (cosmic rays)**

~ 62.5 ps / cm

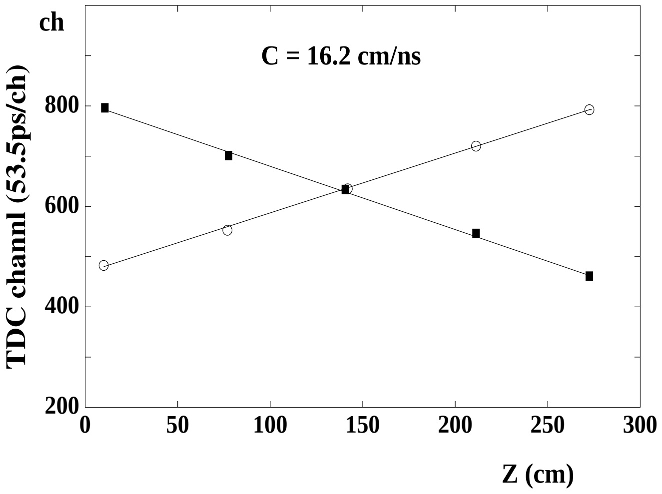

* **Attenuation lengths**

λ=3.8 **m**

Intrinsic time resolution (cosmic rays)

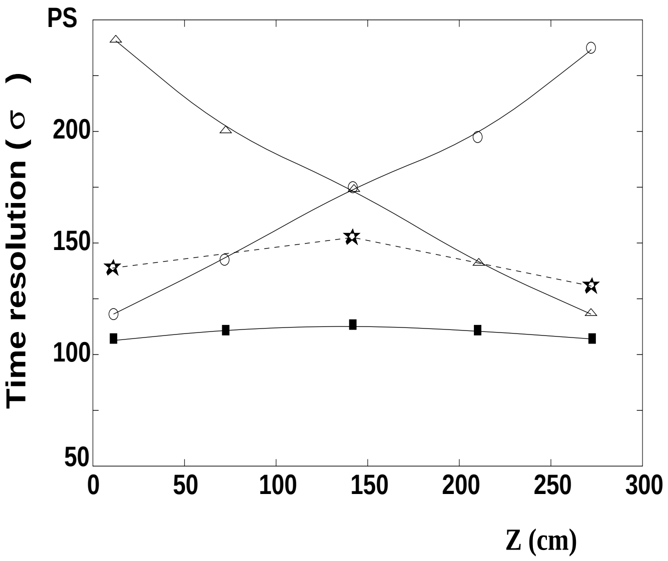

☆ Including 70ps of the time jitter of the start counter and 70ps position effect (~1.2 cm)

Testing for 48 counters

(a) testing the attenuation

S1 : Φ 50 x 10

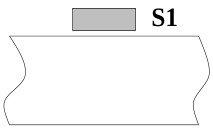

$$\log(Q1 / Q2) = -2Z / \lambda + L / \lambda$$

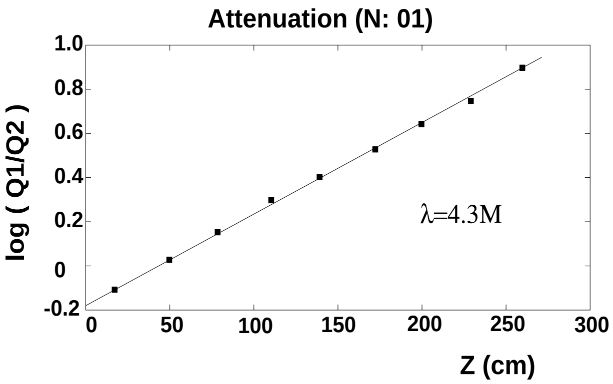

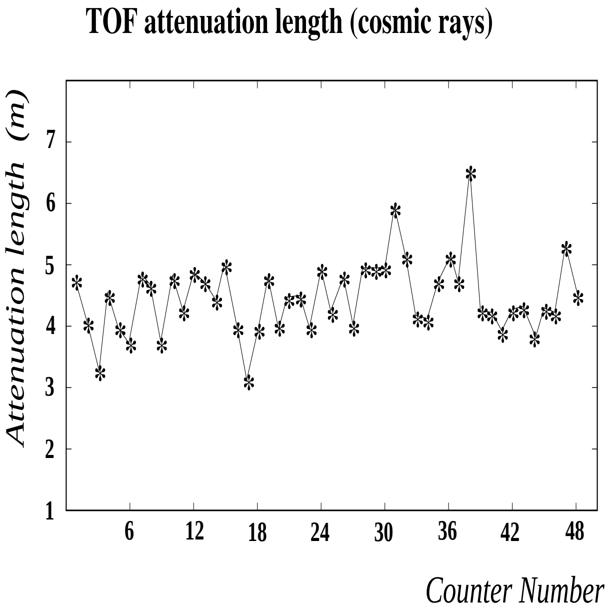

(b) Intrinsic time resolutions of 17 counters

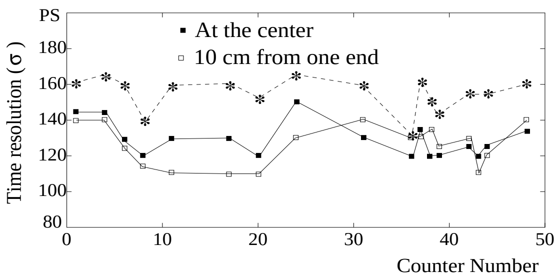

▪ σ_{S1} ~ 70 PS

□ : σ_Z ~ 180 PS (3 CM)

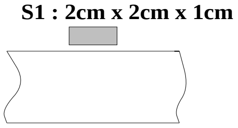

$$\sigma^2 = \frac{\sigma_E^2 * \sigma_W^2}{\sigma_E^2 + \sigma_W^2}$$

* At the center point ,including the time jitter of S1 counter

$$\sigma^2_{(Te+Tw)/2} = (\sigma^2_{Te} + \sigma^2_{Tw} + 4 * \sigma^2_{S1})/2$$

Figure 2: The Test of TOF Counter With Cosmic Rays

3. Laser monitor system

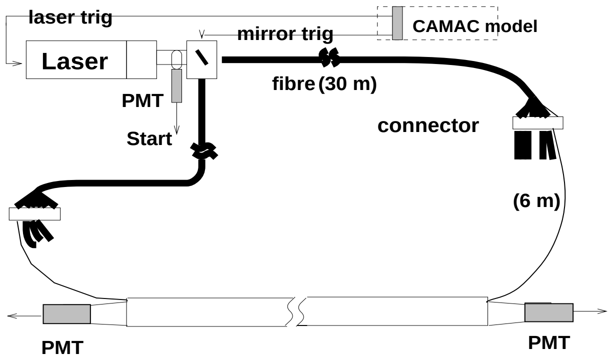

Schematic diagram for the laser monitor readout

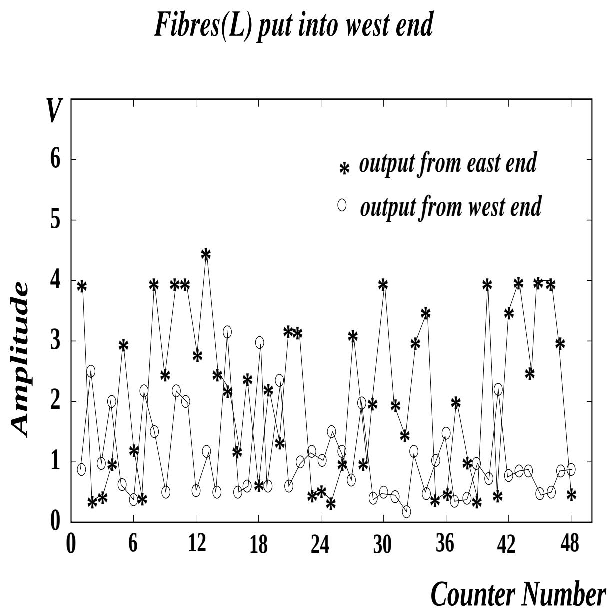

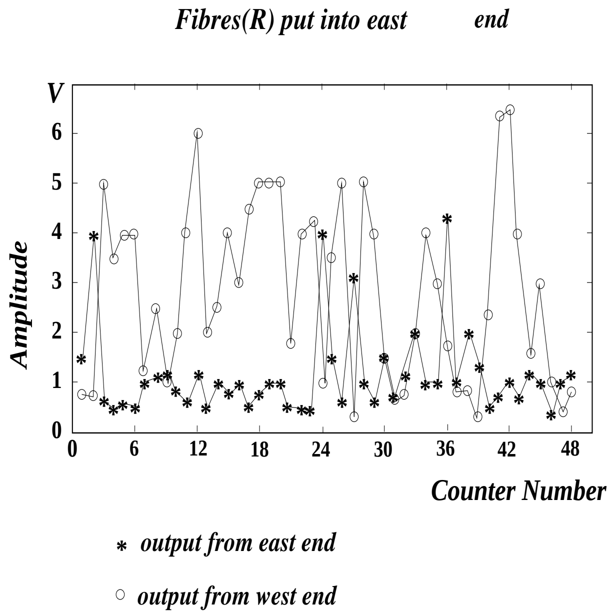

Figure 3: The Laser Monitor System

Circuit diagram of the voltage divider
of PMTs (R2490-05)

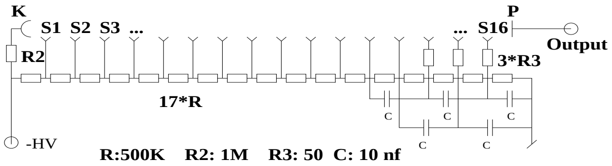

PMTs(R2490_05) have very high saturated current,
When $\bar{e}$ beam is injected into the storage ring ,PMTs
have output of 90 V at 50 Ω impedence.

output of a PMT for the Xe lamp pulse

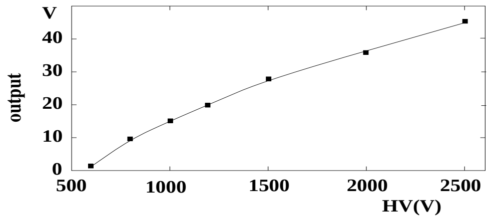

Gain of PMTs **(5 x10^6)**

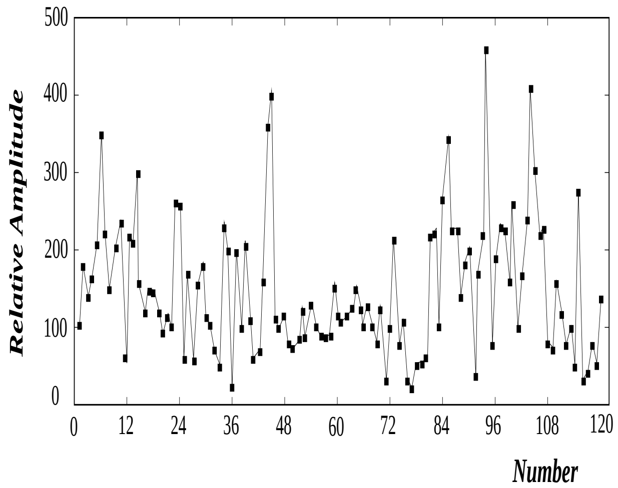

4. New TOF data

TOF attenuation length

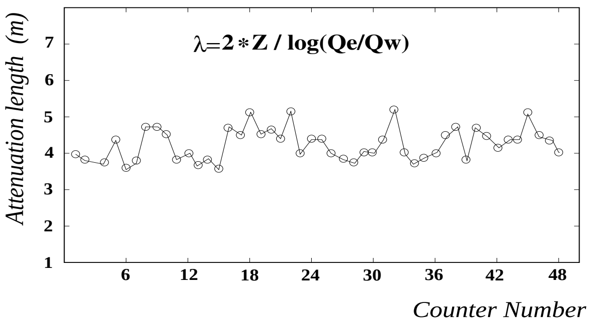

data: Run9042 raw data

including cosmic rays and good tracks

Z~ 15ps/ch. ∗(Te-Tw) /(2 ∗62.5ps/cm)

No Q correction in Te and Tw

Figure 4: New TOF Data and Runing

An Introduction of $BESII$ Gas System

Hansheng Sun,Yan Liu, Meng Zhao
Jingzhi Bai, Jianping Zheng, Xiaolan Luo
IHEP, Beijing, China

BES96, Zhangjiajie

1 Introduction

Among all the subdetectors used in Beijing Spectrometer ($BESII$), five are gas detectors. They are Vertex Chamber (VC), Main Drift Chamber (MDC), Barrel Shower Counter (BSC), Muon Counter ($MUON$), and End-cap Shower Counter (ESC). They require different components and ratios of the mixed gas, as well as different mixing accuracies and pressures. As the feature of the detectors have been improved, these detectors require increasingly higher quality of the gas supply. Therefore, gas system is an important component of $BESII$.

$BESII$ gas system includes three parts: The mass flow control system ($MFCS$) working under the normal pressure; BSC N-pentane system; and the vertex chamber gas supply system working under three atmospheres. Here is a brief introduction of above three systems.

2 Mass Flow Control System

2.1 Principle

A conceptual diagram of $MFCS$ is shown in Fig.1. The system includes five parts: pure gas supply part that provides pure gases for $MFCS$,$ex.$, Ar,CO_2,CH_4,$etc.$; mass flow control system, which is the essential component of the system, and control the ratios of various pure gases; storage and buffer, which allow the mixed gas entering it to mix extensively; back-up mixed gas supply system, which supplies mixed gas to the detector in case the $MFCS$ fails to work; the last part is the supplementary system including alarm, on-line data acquisition, analysis and monitor, as well as UPS.

The main idea of $MFCS$ is to use a mass flow meter and controller with high accuracy and fast response, as well as a electromagnetic valve to control the gas flow of various pure gas enabling them to mix under room temperature, and thus resulting in a dynamic gas mixing for the experiment.

Figure/Table to be sticked on

The key components of the $MFCS$ are a mass flowmeter and flow control— $1259B$, as well as 4 channel readout—$247C$. (Fig.2)

The feature of $1259B$:

- response time: $< 2sec$.
- accuracy:$\pm 0.5\%$ (FS).
- work pressure:150 PSI (max).
- environmental temperature:$(0 - 40)^o C$.
- zero point drift: < 500 $ppm/^o C$.
- work point drift:< 1000 $ppm/^o C$.

The functions of $247C$:

- control the mass flow going through $1259B$.
- $pre - setup$ of the mass flow of each pure gas.
- micro adjust the zero point of $1259B$.
- disply the real and setup mass flow of each pure gas.
- provide the interface for computer connection.

2.2 Characteristics of $MFCS$

- high accuracy of gas mixing $(< 1\% - - - seeTable1)$.
- great variety of mixing ratios of various gasses.
- long term stability (Fig. 3).
- low cost.
- high efficiency.
- suitable for gases with low saturation evaporating pressure.
- center pure gas supply $(Fig.2)$.
- liquid argon replacing gas argon, reducing transportation fees and increasing gas purity.

Figure/Table to be sticked on

Figure/Table to be sticked on

Table 1: **comparison of required and real feature**

Detector	Gas	$A(\%)^{\#}$	$\sigma(\%)^{\#}$	$(\sigma/A)^{\#}$	$A(\%)^{*}$	$\sigma(\%)^{*}$	$(\sigma/A)^{*}$
MDC	CO_2	10.0	0.5	5%	9.9	0.1	1.0%
MDC	CH_4	1.0	0.2	20%	0.99	0.05	5.1%
BSC	CO_2	20.0	1.0	5%	20.0	0.2	1.0%
ESC	CO_2	66.0	3.3	5%	65.9	0.6	0.9%
$MUON$	CH_4	10.0	0.5	5%	9.9	0.1	1.0%

Note: # — required value. *—real value.

3 N-pentane control system

3.1 The Operation principle

The system principle is shown in Fig.4. It consists of a feeder, an evaporator, a condenser, a mixer, a temperature controller and a monitor.

A gas mixture consisting $80\% Ar\ and\ 20\% CO_2$, coming from $MFCS$, passes through the evaporator and flows into the condenser. Thus a mixture of gas $Ar - CO_2 - C_5H_{12}$ is obtained for BSC usage.

3.2 The system structure

The structure is shown in Fig. 5.

1), Feeder

The feeder feeds gases in a sealed-off and semiautomatic manner.The N-pentane is fed into the evaporator via the feeder.The advantage of this system is the following:

a). avoid contamination of other materials like dust to enter the system.

b). decrease leakage of N-pentane during feeding, and increase system safety.

2), Storage and evaporator

The storage and evaporator are kept in a thermostat with a temperature ranging $(10 - -15)^oC$. There is a multi-layer network in the evaporator, thus it takes the $Ar - CO_2$ mixture a long time to pass through, so the effect of environmental temperature is decreased. In this way, it can help lighten the burden of the condenser.

3), Condenser

A two-stage condenser was placed in other thermostat to maintain the temperature inside the condenser at $(4 \pm 0.1)^oC$, the temperature at which $N - pentane$ obtains its saturating vapour pressure. There are also some wire nets in the condenser. Their function is to allow better mixture of the gas passing through them, and meanwhile to condense the extra $N - pentane$ into liquid. A pipe is used to connect the evaporator with the condenser, through which the condensed the $N - pentane$ will go back from the condenser to the evaporator automatically.

4), Mixer and Buffer

A big gas store tank was installed to the system. This will be advantageous in mixing

Figure/Table to be sticked on

Figure/Table to be sticked on

the $N-pentane$ vapour completely before entering to BSC. The comparison of the gas system before and after being upgraded is shown in table 2.

Table 2: **Comparison of the gas system before and after being upgraded**

Before upgrade	After upgrade
Open and manual feeding	Close and semi-automatic
Without thermostat evaporator	With themostat evaporator
One stage condenser	Two stage condenser
Temperature controller less effective	Improve the temperature Controller
Maximum flow speed (MFS) $0.18m^3/Hr$	Increased MFS $0.24m^3/Hr$
Range of C_5H_{12} concentration variation:$(25-35)\%$	$(27 \pm 0.5)\%$—Infrared Spectroscopic analysis and $(26.6-27.2)\%$— Chromatography

4 The Vertex Chamber(VC) gas system

4.1 The outline

- Operating gas: $50\%Ar + 50\%C_2H_6 + H_2O$.
- Gas pressure: 0.3 Mpa absolute.
- Pressure stability: (42.84 ± 0.01) $psi/40days$.
- Operating mode: filling up/exhausting gas, to allow fresh gas mixture to be used. automatic fill-up to maintain the chamber gas pressure at the pre-set point.
- Cycle period: once a day.
- Filling time: about 20 $min.$ (adjustable)
- Exhausting time: about 22 $min.$ (adjustable)
- Balance time: $< 30sec.$
- Gas leakage rate: $3.3liter/24hr.$

4.2 The design principle

- Safety and reliability.
- Gas pressure stability.
- Simple operation.
- Mixed gas automatic replenishment.
- Stable and even ratios of gas mixtures.

4.3 The construction of the VC gas system

- Chamber:70 liter, 3 atmospheres.
- Gas pipe:130m, 6 liter, easy to balance.
- Gas supply:high pressure gas mixture of $50\%Ar + 50\%C_2H_6$.
- Pressure limiter:two stage for safety.
- Pressure regulator:
  Controller ($Edwards1501B$)
  Transducer ($590A$)
  Servovalve ($DM20$)

4.4 Operation

1), Exhaust:
a),turn the function switch of $1501B$ from "Auto-mode" to "Close".
b),open the pressure limiter $valve3$ and adjust it to maintain the flows peed at $8liter/min$.
c), Close the pressure limiter $valve3$ when the gas pressure decreases to about 1 atmosphere.
2), Filling:Turn the function switch of $1501B$ from "Close" to "Auto-mode". It will work automatically.

4.5 Future work

- Use mass flow gas system to replace the gas mixture supply.
- Add water vapor to the gas mixture.
- Add mixer and buffer in to the system.

Trigger System of BESII

BES TRIGGER GROUP
IHEP, China

1 Introduction

The trigger of Beijing Spectrometer (BES) consists of 3 decision levels. The first level finishes its decision within one colliding period. The second and three levels spend four colliding periods to finish their decision. Trigger system use information from TOF, BSC, ESC, MDC, MU and VC detectors to select good events.[1] How to realize decision of each detector depends on its specific structure. BES is upgraded to become BESII. The Vertex Chamber (VC) is located the inner most of BESII instead of CDC .BESII has a new MDC, which differs from the old one in many aspects. For example the new MDC has totally 804 cells, while the old one has only 702 cells. Its geometry parameters are changed. The new trigger subsystems, VC trigger and MDC track finding system, are constructed for new detectors in upgrading. The main trigger is improved partially in new trigger system.

2 VC trigger-track combination

2.1 Geometry and electronics of VC

VC consists of 640 drift tubes arranged in eight concentric axial layers and four stereo layers. Layers 1-4 are axial layers with 40 straws in each layer, layers 5-8 are stereo layers with 40 straws in each layer, layers 9-12 are axial layers with 80 straws in each layer. The maximum drift distance in each tube of 4mm corresponds to a drift time of 80 ns.[2]

Vertex Chamber data acquisition is consists of front end electronics and TDCs. 1879TDCs installed at fastbus receive ECL signals from front end electronics and convert them to TTL level, then send these signals to auxiliary interface. Trigger logic can use them directly.

2.2 VC track combination

2.2.1 Cell selection and track combination

The particles coming from the interaction point pass VC and hit wires of each layer. These fired straws output wire signals and form good tracks. The inner and outer 4 layers(axial) are used for track combination logic, 5-8 stereo layers will be used for Z selection if it's necessary. The wire signals from inner or outer 4 layers are combined to form a cell hit. The signal from 1 layer or 2 layer is combined with one adjacent signal of layer 3 or 4(shown in Fig.1a). There are 40 basic cells in the inner layers and 80 cells in the outer layers. Because the radius of VC is 13cm. The track in the VC detector can be considered a straight line approximately. The inner cells can be coincided with relevant cells of the outer layers to determine a good track. The 640 ch of whole VC is separated by 40 fan sectors. In a sector all found good tracks are ORed to form a sector track signal(shown in Fig.1b).

Figure/Table to be sticked on

2.2.2 Scheme of VC trigger

Fig.2 shows Logic Block Diagram of VC Trigger. VC trigger consists of track combination, multi-logic selection and control signal fanout.

Figure/Table to be sticked on

2.2.3 Logic function

Track Combination logic realizes the gating, latch, cell combination, track combination . A switch can be used to turn off the inner layers and only outer layers cells are used for VC trigger . There are 5 modules plugged on the fastbus auxiliary interface to output 40 channels fan track signals to next logic.

Multi-logic Selection board(CAMAC board) has following function:

1. Logic discriminator gives VN1, VN2 signals to the main trigger.
2. Gives matching signals. The 3-4 VC sector signals are combined to match with a good track found in MDC trigger.
3. Read the distribution of VC track signal via CAMAC, to monitor the VC trigger status.

Fanout board Outputs 2 groups(gate and reset) and 8 channel fanout signals of per group to control VC track combination board. The gate signal is formed with width 100-120ns in this board.

2.3 Signal delay time of VC trigger

VC trigger condition must gives out decision in 420ns after collision. The delay time of VC trigger logic is limited for 70ns. The total signal delay time whish includes propagation time in logic and delay in cables is about 375ns, it is enough to catch level one trigger.

3 Tracking System of the New MDC

3.1 The 3/4 and good track combination

MDC trigger uses layer 2,4,6,8 to find charged track on the (r,() plan. MDC uses multi-sense-wire cells. There are four sense wires in one cell in the direction of r. The 3/4 logic is used to combine the four wire hits in one cell into cell hit. It requires that there are at least 3 wires were hit for one cell. There are totally 288 cells in layers 2, 4, 6, 8. Tracking logic is based on the position of hit cells. These cell signals are sent to track finding logic. In this logic those 'hit' cells are combined to see if they 'draw' a track which must satisfy:

1. Pass through the interaction point;

2. Its radius of curvature ¿83.3cm(transverse momentum greater than 100Mev/c) at 4.0kgs magnetic field.

Take layer 2 as basic layer, all of the good track combinations of layer 2,4,6,8 is calculated. The total number of combinations for good tracks is 287 in 1/8 of MDC. MDC track finding is used in level 2 trigger.

3.2 Schematic plot

It includes: ECL – TTL converter, 3/4 logic, tracking, matching, fan-out, track counting, veto and signal distribution. The inputs come from MDC layer 2, 4,6, 8, total 1152 pairs ECL differential signals. The outputs are good track number N (N¿=1, N¿=2, N¿=4), which goes to main trigger for second level trigger after 3/4, tracking, matching and track counting circuits. (Fig.3)

Figure/Table to be sticked on

3.3 Logic function

- Function of 3/4 logic modules is shown as following:

  1. Signal level transformation: ECl–TTL
  2. Signal register: controlled by GATE and RESET
  3. The 3/4 logic
  4. Overriding, to avoid the loss, caused by broken wires or dead cells.

- The track finding uses OR logic with 3 inputs. One of them is a found track from layer 2, 4, 6, others are from layers 2,4,8 and layers 2,6,8. Track logic is set as following: (layer 2 & 4 & 6).or.(layer 2 & 4 & 8).or.(layer 2 & 6 & 8)

Figure/Table to be sticked on

It has higher efficiency for track finding. Based on layers 2,4,6,8 and taken layer 2 as basic layer, by calculation we know corresponding cell numbers of layers 4, 6, 8 with one cell of layer 2: Layer 2, one cell:

layer 4, 4 cells

layer 6, 8 to 9 cells

layer 8, 15 to 16 cells

- Matching circuit (VC, MDC, TOF) MDC with hits in corresponding direction of VC and TOF to determine a good track. It is used to suppress background event. In matching, one track in MDC corresponds to 3 cells on VC and 7 cells in TOF(Fig.4). Four matching modes can be realized by CAMAC setting through on-line computer, these modes are shown as following.

    1. TOF matching: the tightest
    2. MDC, VC matching:
    3. MDC, TOF matching: moderate
    4. Only MDC: loose

Figure/Table to be sticked on

When data taking, we can get cell map of found track by CAMAC readout, it is helpful in data taking.

- Distribution boards

    One of Signal distribution boards receives cell signals from 3/4 logic and arranges them according requirement of track finding boards. There are overlaps between the outputs, so the design of the board is a very dedicated work. A small error can cause the tracking mal-function. Another signal distribution board is connected output of tracking and the input of matching circuit.

- Track counting circuit

  It counts the total charged track (after matching) N, gives out N¿=1, N¿=2 and N¿=4 as second level conditions. Additionally, a N0 cut is set in the circuit. When N¿=N0, this event was rejected as background event. Now, N0 is set to 16 or 12 tracks.

- VETO circuit

  In data taking, it was found that disturbance can cause wide area firing of MDC , and cause many fake tracks. This can increase the trigger rate, dead time and lose the effective luminosity. It is necessary to suppress this kind of background. When number of the adjacent track , which is one by one, is more than or equal to a pre-set value, a veto signal is generated by VETO circuit to suppress this kind of background.

  Now, 16 was set as the veto, that is to say when the adjacent track number is 16 or more, the veto is satisfied

- Font

  There are total 36 modules of 3/4 so 36 Gate and Reset signals are needed, so the font board receives Gate and Reset signal from main trigger and font 36 gate and reset signals for each of the 36 modules of 3/4.

4 Flexibility of VC ,MD. trigger

The trigger system should have following characteristic:

1. Good ability to suppress background

2. High efficiency–not lose good events

3. Flexibility–for different experiments

But these requirements are conflict each other, so it depends on the running conditions which one should be stressed. These requirements have been considered when the new trigger was designed.

There are several methods to suppress background:

1. Add VC trigger for level 1 to suppress cosmic ray which doesn't pass central point in (r,pi) plane and z direction and decrease events of pass 1.

2. Provide VN1, VN2 and Ntrk¿1, Ntrk¿2, Ntrk¿4 trigger conditions for the main trigger that can be selected according experiment requirement.

3. Use matching of VC, MDC and TOF to find a good track, there are 4 choices, which one of them should be used depends on the running and background condition.

4. When the total track number is greater than a preset value (for example 16), the event is vetoed. This veto is optional.

5. When there are sixteen or more adjacent tracks, the event is vetoed. This VETO is optional.

The several methods of increase efficiency is shown as following:

1. The 3 out of 4 logic avoid the random firing of wires, Moute-Carlo calculation appears that the efficiency of cell is enough to avoid the track-loss, which is caused by the finite wire efficiency.

2. Track finding logic uses (layer 2 & layer 4 & layer 6).or.(layer 2 & layer 4 & layer 8).or.(layer 2 & layer 6 & layer 8) logic, that can make up for finite cell efficiency of layers 4,6,8.

3. Set overriding register to avoid dead cell.

4. To set VC trigger to select that only outer layer cells are output as trigger condition, it increases VC trigger efficiency.

The main logic of new trigger use FPGA, this chip is field programmable to ensure the circuit flexibility. If necessary, it is unnecessary to change the circuit and connection to change logic(change the load EPROM).

5 Summary

There are 80 new boards of VC and MDC trigger to be completed and the trigger system has been installed. Each board had been adjusted carefully. The logic functions of VC and MDC trigger are separately tested and checked by computer to ensure them correct. After debugging of BES the TRGTBL(shown Table 1) is used for data taking successfully, the VN1 condition of VC trigger, only outer layers is set, is used for level 1, and Ntrk¿=1 is used for level 2.

Figure/Table to be sticked on

References

[1] Y.N. Guo et al., The Trigger of Beijing Spectrometer, High Energer Physics and Nuclear Physics, (1990)Vol 15, 01

[2] Vertex Chamber Group (Department of Physics, Colorado State University, USA),Geometry and Cabling of the BES Vertex Chamber, 1995

BES-II ONLINE SYSTEM

ZHANG Binyun, GUO Yanan, SUN Fang,YU Chuansong, ZHAO Weiren,
ZHANG Jiawen, LI Xiaonan, ZHAO Jingwei, YANG Changyou, ZHOU Xiaofan,
LUO Shuanqun, LI Fang, SHEN Hong, LU Hongyu
BES Online Group, IHEP, Beijing 100039

1 INTRODUCTION

The original online system of the BES took a dead-time of τ =24ms/event. At BES-II, the event rate will be 20Hz, the effective luminosity loss due to dead-time would exceed 40%. So the online system must be upgraded. The goal of the new online system is to reduce τ to 10ms/event.

2 HARDWARE CONFIGURATION

In contrast with the original BES DAQ cetralized in VAX-785, the new BES DAQ divided its task into ALPHA3600s host for background processes and front-end VME subsystem for data acquisition. They communicate with each other via Ethernet using TCP/IP protocol.

2.1 The Host

The configuration of ALPHA3600s is shown in Fig. 1. It is much more powerful than VAX-785. It can do more monitoring and online analysis during data-taking. We merged the touch pannel ammulator and the status and error message display into a single X-terminal. The X-terminal provides more comfortable user interface.

2.2 The Front-End VME Subsystem

In the BES-I online system, all data acquisition processes were done by single VAX-785 together with VCC and 8 CAMAC branches. Therefore, it is series in branch and parallel in BADCs. The new system are parallel throughout. The front-end data acquisition subsystem consists of not only CAMAC buses, but also VME and FASTBUS (Fig. 2). The two MVME162 single board conputers are the target elements executing data acquisition and logging tasks. Each CAMAC branch is interfaced to VME bus via a VCBD (CAMAC Branch Driver in VME crate). The VCBD is a double width VME

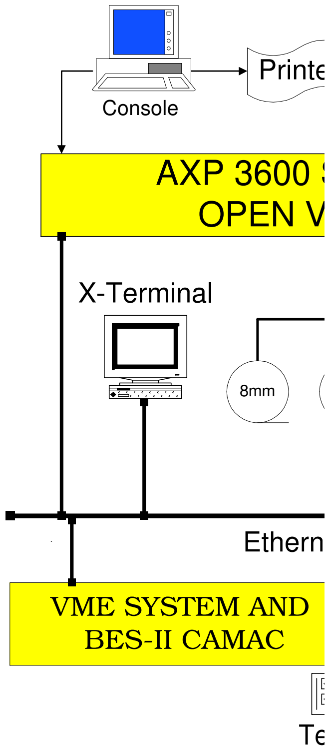

Figure 1: Configuration of the Host ALPHA 3600s

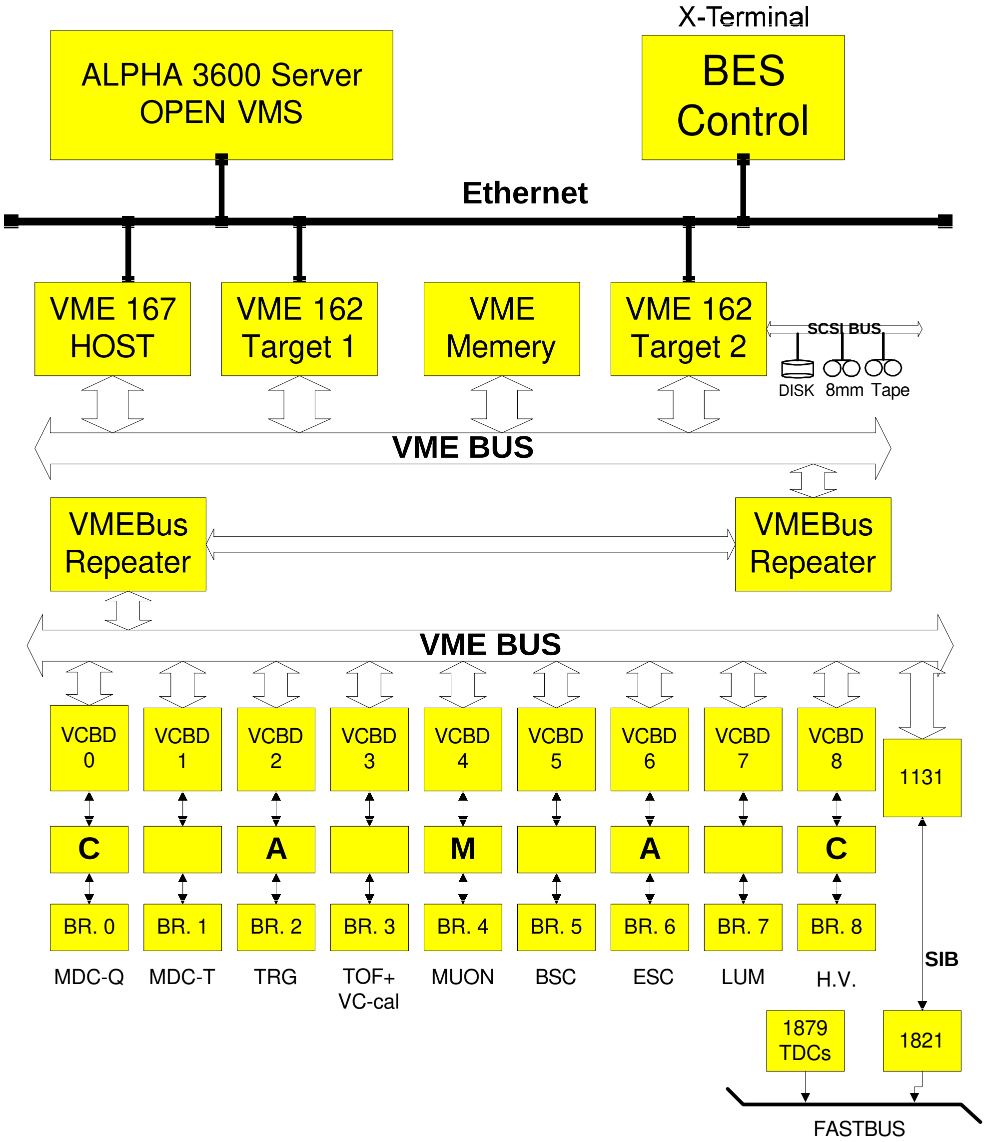

Figure 2: Hardware Configuration of the BES-II Online System

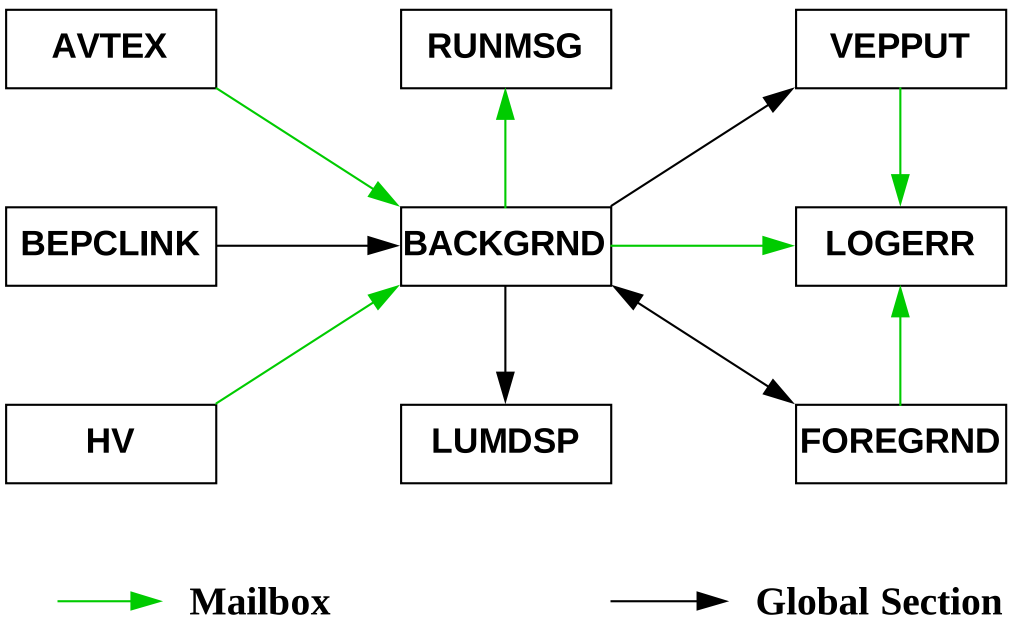

Figure 3: Data Communication between Host Processes

slave module. It has a 20MHz 68000CPU, 64KB program RAM and 64KB dual-port RAM, and CAMAC driver. The vertex chamber's readout electronics is provided by University of Washington. It uses 7 LRS1879 TDCs and a 1821 FASTBUS Segment Manager/Interface Module. The 1821 is linked to VME via LRS1131 VME-to-SIB Interface module. In the readout electronics, the number of BADCs for BSC and ESC are increased from 8 to 14, and the 2 BADCs for Muon Identifier work concurrently instead of seriesly, thus to reduce conversion time.

3 SOFTWARE ORGANIZATION

The software of BES-II online system is also divided into host part and front-end part.

3.1 The Host

In ALPHA3600s, we still use Open VMS operating system for inheritage. In transplanting the old VAX programs to ALPHA, we overcame several incompatibilities, e.g. the size of globe section, word alignment, subroutines written in MACRO, the NARGS and other problems. UGS and HANDYPACK were transplanted to ALPHA. We also wrote new code for Ethernet link, FOREGROUND, AVTEX and RUNMSG. Similar to the BES-I online software, there are 10 processes running in the host. They are:BACKGROUND, FOREGROUND, VEPPUT, AVTEX, RUNMSG, LOGERR, HV, LUMDSP, BEPCLINK and Calibration. The data communication between these processes are shown in Fig. 3. The Calibration process exchanges data with other processes via calibration data files. BACKGROUND is the core of the host software. With the help of event flags and priority assignment, it makes schduling between 7 group routines, including MAILHANDL, CONTROL, HIST$CONTROL, DEXEC, EVANAL, TIMERHNDL and MONITOR. FOREGROUND discharged data acqisition to VME front-end and has become maily the interface between host and VME. AVTEX accepts run commands from X-terminal touch pannel ammulator. RUNMSG displays run status and error message on X-terminal.. LOGERR accepts error massages from mailbox sent by other processes, logs them into file ERRLOG.DAT, and sends to RUNMSG. VEPPUT outputs various plots e.g. histograms and event display. LUMDSP displays luminosity and its S/N as a function of time on a graphic terminal. BEPCLINK wakes the process DATASEND on BEPC control computer and fetches BEPC status parameters, logs them onto tape, and displays them. HV is an interactive process. It can set state and parameters of high voltage power supply used in various detectors, read and regularly monitor them, display them, and log them onto tape.

3.2 The Software in the Front-End VME Subsystem

The programs of the front-end subsystem distribute in VCBD, 1821 and MVME162.

Programs in VCBD comprise CAMAC command driver and interrupt service routine for event data readout. CAMAC command driver interprets the CAMIO parameters of a CAMAC command sent by the host into C, N, A, F and issues a CAMAC cycle. They are mainly used in single CAMAC operations. and interrupt service routine for event data readout is an ecquivalent of VCC packet. The CAMAC commands needed for event data readout from BADCs of that branch is specified in file DATABASE.DAT of the host. When begin a run, they are converted and downloaded into corresponding VCBD. All these programs were written in C and ASM language.

The microcode of LRS1821 was developped on LIFT platform. (see LI Xiaonan, Fastbus Data Acquisition System for BES-II Vertex Chamber, This BES Annual Meeting)

Programs in MVME162s were developped on VMExec real-time operating system V3.1. MVME167 is the host of the fron-end subsystem. The two MVME162s are the target boards. There are 22 tasks in the first 162 and 6 in the second one. Communication between tasks are realized with message queue mechanism. These tasks respectively perform TCP/IP link with ALPHA3600s, data flow control, interrupt and exception handling, event building, interface to VCBD, sample data and message transferring to ALPHA, data logging, and other functions for BES/LUM running, PED/single foreground running, electronics tests, as well as HV control. Fig. 4 shows the data flow and control relations between these tasks.

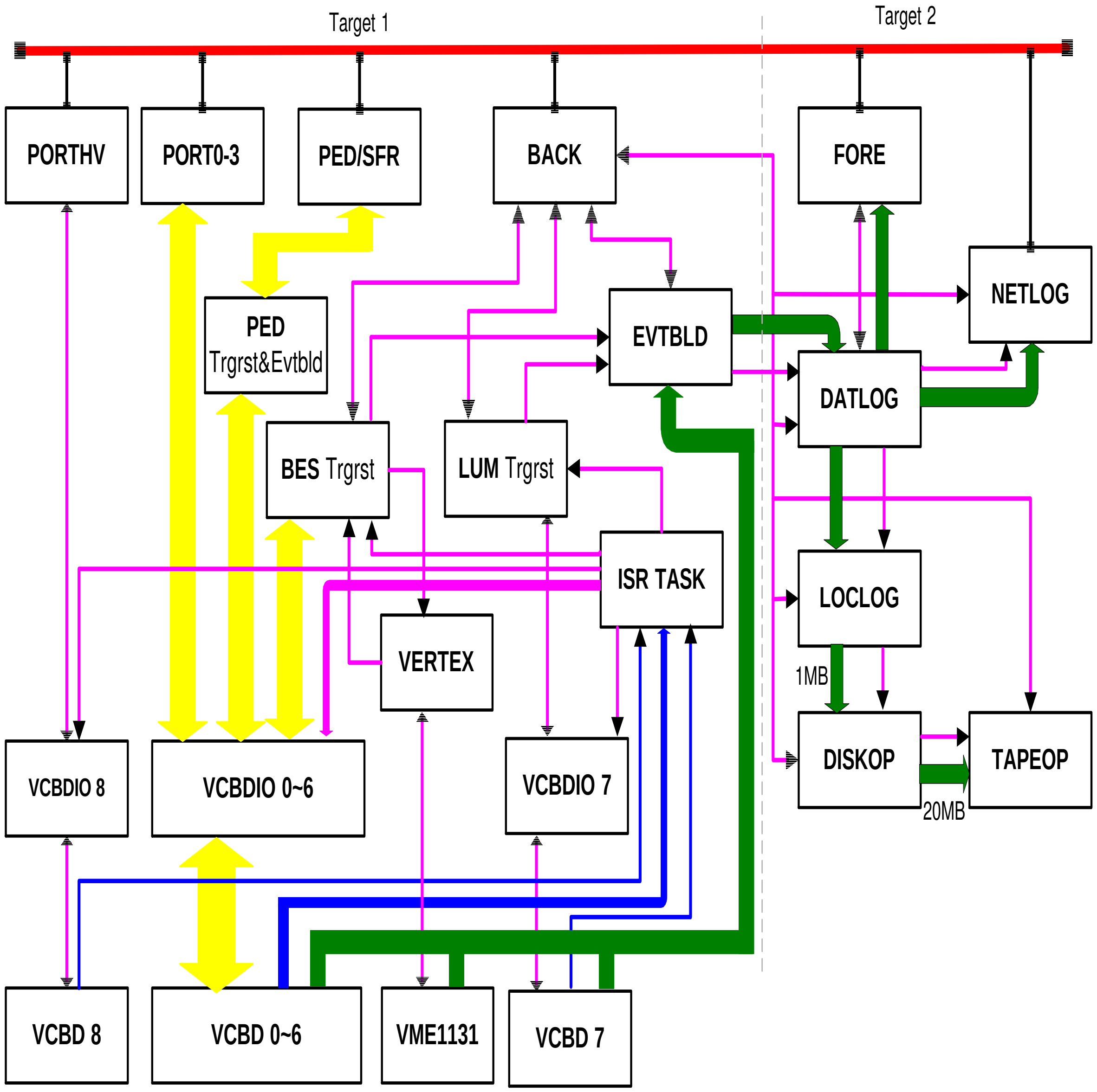

Figure 4: Data Flow and Control Relations between Tasks in VME162s

4 DATA TAKING PROCESS

When the trigger asserts a good event, it starts BADC conversion. Having finished its conversion and correction, each BADC sends a LAM signal to a new LAM Summary module after. When all BADCs in that subdetector finished, the LAM Summary module will interrupt the VCBD. The VCBD starts its interrupt service routine to collect event data from BADCs of that subdetector, and store them in the dual-port RAM for MVME162 to fetch them later. Then it interrupts MVME162 to inform that its data collection for that event has fnished. When interrupts from all VCBDs have arrived, the MVME162 send a CAMAC command to reset the whole electronics and the trigger, ready for accepting next event. This can be done before event building, because there is a data buffer for 2 events in each VCBD. So the reset can be done earlier.

The first MVME162 fetches segmants of event data from individual VCBDs and assenble them into a complete event data, and store it in the RAM module. When there accumulated 1MB event data, the task LOGLOG and DISKOP in the second 162 will store them in the hard disk. When 20MB accumulated in the disk, the task TAPEOP will transfer them into tape to minimize mechanical operation of the tape driver. The task NETLOG can transfer event data to a disk at the computer center via Ethernet for real-time filterring. Task FORE send sample event data to ALPH3600s on request.

5 RESULT

5.1 Dead-time

Fig.5 is the timing diagram of 2 consecutive events. The first row shows the 2 deadtimes are 8.40ms and 9.87ms respectively with an interval only 3.83ms. The spikes are the interrupt signals from LAM Summ arys to VCBDs. The time differences between rising edge of the TRIGD and spikes represent the BADC conversion times of individual subdetectors. The one of Muon Identifier dominants. The RESET signal was not connected. **The new online system has reached its goal.** The main sources of improvemant in terms of dead time are:

Shortening BADC conversion time by adding more BADCs and less channels per BADC;

Using real-time OS, the interrupt response time is only 80μs. The VMS interrupt response time of 8ms was eliminated;

Faster block data transfer and parallel data collection. In VCC, the data transfer speed was 6.5μs/word, while in the new VCBD, it is 3.9μs;

By buffering data in RAMs all over, the time for event building will not be counted in deadtime.

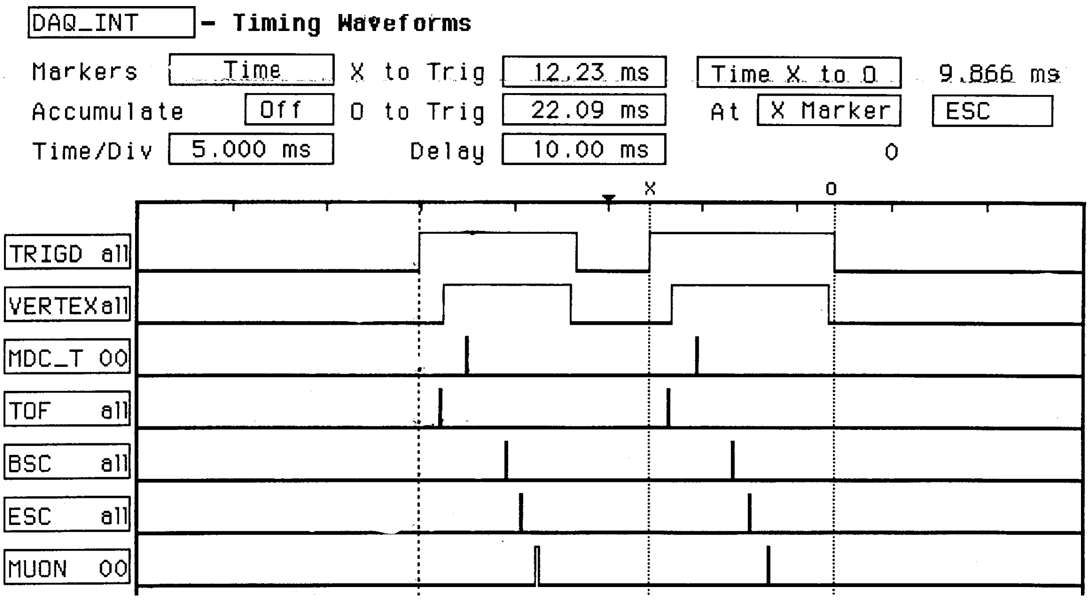

Figure 5: DAQ Timing of 2 consecutive events

5.2 Stability

Many bugs were found and corrected. Many measures were taken to avoid troubles. So far the Online system of BES-II can run stably for days without error reported.

5.3 Correctness

The data logged on disk were checked carefully, no mistake were found;

The event data were analyzed and displayed on screen. They look correct;

The data were processed offline, filterred and calibrated. Preliminary results have got. No error was found as far as data format is concernd.

In conclusion, we can state that the new online system of BES-II can be used in real data taking stably and correctly with dead-time less than 10ms/event.

Special thanks to Prof. GAO Cuishan for his valuable help.

Fastbus Data Acquisition System for BES-II Vertex Chamber

Li Xiaonan
Division 1, Institute of High Energy Physics, China

Abstract

Data acquisition system for BES-II Vertex Chamber (VC) is a part of data acquisition system of BES-II. The electronics system is based on Fast bus standard. This paper describes the hardware architecture and software of the system. The software is consist of microcode for Fast bus system and upper-layer control software. The total dead time of the subsystem is estimated to be 1.5 ms. But the dead time that is contributed by VC DAQ system to whole BES-II DAQ system is less than 0.5 ms.

1 Introduction

Vertex Chamber(VC) is a subdetector of BES-II. It is made of 12 layer straw tubes and has totally 640 electronics channels by single end readout way. It takes part in trigger to suppress background events far from interaction point. It is also useful to construct track with small angle or second vertex point. These can improve detecting efficiency of BES-II.

The task of VC DAQ is measurement the time information of VC. The electronics system is different from other subsystem in that it is based on Fast bus standard other than CAMAC standard. This subsystem is a part of BES-II DAQ system that uses VME system as front control computer [1]. The control procedure of data taking by VME system is similar with other subsystem. This paper describes the VC DAQ system. In section 2, the hardware architecture is covered. The software system is covered in section 3. The conclusion and discussion are in section 4.

2 Hardware architecture

The block diagram of VC DAQ hardware architecture is showed in Figure 1. It adopts Fast bus standard to measure time information. Fast bus has 32-bit address bus and data fields with high speed ECL backplane. The transfer rate of 32-bit data is up to

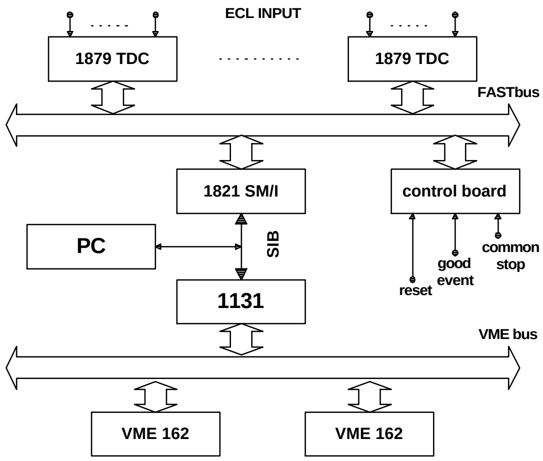

Figure 1: Hardware architecture of BES-II VC DAQ

10-30 MHz. The VME 162 processor boards control the VC DAQ system and other subsystems.

The electronics system is consist of seven 1879 TDCs [2] in a Fast bus crate with 1821 FB segment controller. Each of 1879 TDC has 96 channel ECL signal inputs. The 1879 provides multihit time-to-digital conversion for leading edge and trailing edge measurement. The conversion time is about 0.5 ms. It employs a 500 MHz, 512 element shift register to record history of time by pipeline mode. The shift is controlled by on-board crystal oscillator or by a external programmable oscillator in the CAT module. 1879 TDC range can be programmable to be 1, 2, 4,8 μs. Because drift time of VC is least than 80 ns, the 1879 TDC range is set as 1 μs. This implies that the least TDC bin is 2ns. Each readout of leading edge and trailing edge is a 32-bit word with 7-bit channel number, 5-bit slot address,and 9-bit TDC value and 1-bit clock phase lacth when common stop comes. The clock phase lacth can be used to improve least TDC count to be 1 ns.

FB system is controlled by 1821 FB segment controller [3]. 1821 provides complete FB operations. The operation on FB system is executed by the 64-bit instruction. One instruction can perform typically five operations. Execution is fast, nearly about 100 MIPs. Microcode program is loaded into program memory with 256 words deep. 1821 does not provide arithmetic operations on the data. 1821 has also 4k 32-bit data buffer memory.

Some types of interface are provided by 1821 to connect with intelligent hosts. In VC DAQ system, 1821 front panel SIB(Standard Interface Bus) 34-pin connector is connected to 60-pin connector of 1131 VME-SIB interface board [4] in the VME crate or to a PC to develop microcode program. Connection to 1131 is via a adapter card which interfaces the 34 conductor standard density cable used by 1821 to the 60 conductor standard density cable used by 1131. Using 7 registers, SIB communicates with 1821, initializing 1821, downloading microcode program, addressing data memory of 1821. 1131 is a 6U, A24/D16,D08 slave VME module. 1131 has 8k word data buffer memory and 8k word list memory. It can read data from 1821 by DMA way. All of control instruction for 1131 SIB are mapped to address of VME system.

1821 selects and reads 1879s by broadcast address mode and sparse data scan method. Only 1879 modules containing time data will be addressed and read out by 1821.

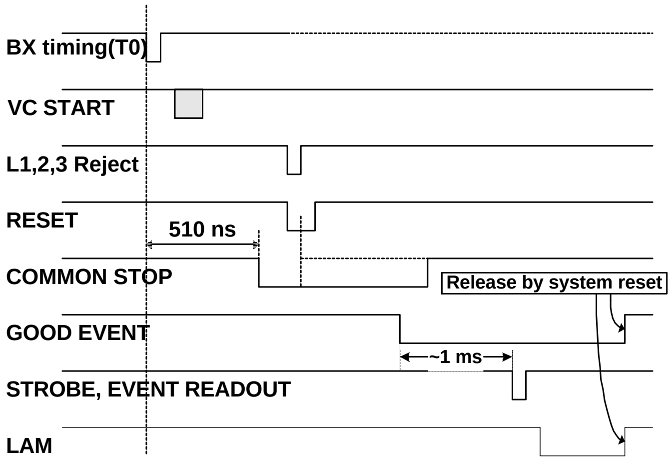

Figure 2: Time diagram of control signals

Three control signals, common stop, reset and good event, are provided by trigger system. Figure 2 shows time relation among them. common stop and reset are distributed to FB backplane by a FB control card, then sent to every 1879 module. common stop with 3.5 μs width is delayed 510 ns relate to beam cross time T0. The leading edge of common stop stops TDC to record history of time. The duration is waiting for trigger decision. The trailing edge will begin to convert time into TDC value if event passes three trigger decisions. In the mean time, trigger system provides good event signal after three periods of BEPC. This signal is delayed 1 ms to wait finishing of conversion and then produces a ECL strobe signal. The strobe is inputted to front panel IN1 connector of 1821. 1821 read out time data from 1879 if it detects strobe signal and sends interrupt signal LAM by front panel OUT2 connector. The 'AND' signal of FB LAM and TOF LAM by LAMSUM module is sent to VME system by VCBD of TOF branch because the conversion time of TOF subsystem is least in all of subsystems. If event does not pass the trigger decision, reset signal will reset TDC and common stop signal. It is required that the common stop must be deasserted within the reset pulse time to ensure that a conversion cycle is not started. Reset TDC before trailing edge of stop provides zero dead time.

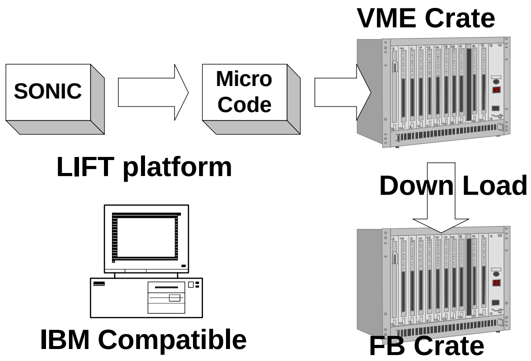

Figure 3: Developing procedure of microcode

3 Software System

The software for VC DAQ system is consist of two parts, microcode for 1821 and up-layer control software in VME system.

Because microcode is difficult to program, LeCroy provides assemble-type of SONIC language (Symbolic Macro Assembler). LIFT(LeCroy Interactive FASTBUS Toolkit) [5] that is installed on PC is used to develop microcode and test FB system. The developing procedure of microcode is shown in figure 3. SONIC program for VC DAQ is converted to microcode by LIFT. Microcodes are downloaded into program memory of 1821 by VME 162.

One part of microcodes initializes 1879 TDCs, TDC scale 1 μs, compact parameter 10 ns, and active time interval 512 bins. The initialization is done when each RUN begins. The another part of microcodes reads out time data of both edges of hit signal. It is downloaded when each RUN begins. After it is started, it tests strobe signal continually. When strobe exists, it read out 1879 data into 1821 data memory and sends LAM signal by front pannel OUT2 connector.

Up-layer control software in VME system is written by C language. It downloads 1821 microcode, controls procedure of data taking of VC and reads measured time data into data memory of 1131. Up-layer control task(VCDAQ) runs on a VME 162 target board. Figure 4 shows software architecture of VC DAQ and related parts of BES-II DAQ. The task VCDAQ is controlled by tasks of BES-II DAQ by way of message exchange. Message queue is a mechanics provided by real-time operating system of VME. The VCDAQ task waits the command packed in the message after task starts or each command is finished. Each command will make VCDAQ task to execute a series of operations. A acknowledge message should be sent back after a command is finished so that all of subsystem will work in coincidence. Some commands are shown in figure

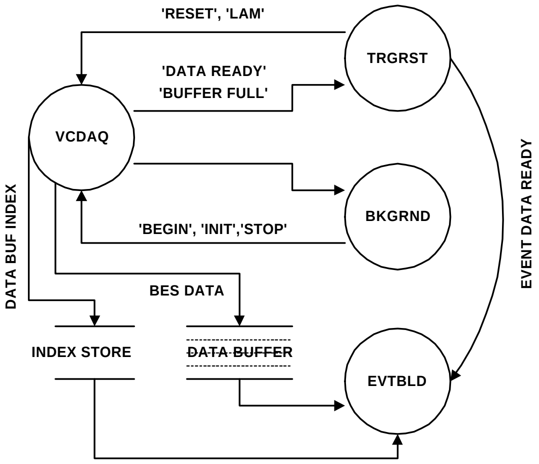

Figure 4: Software architecture of VC DAQ

4. 'BEGIN' sets index of event data buffer to be first buffer and cleans flag of event. 'INIT' makes initialization of 1879 TDC and downloads the microcode for 1879 readout. 'RESET' sets starting address of data memory of 1821 and starts up microcode. After main control task TRGRST receives interrupt signal from 1821(and TOF), a 'LAM' command is sent to VCDAQ to make it to read out TDC data from data memory of 1821 into 1131. SIB reads data memory of 1821 by two registers. Because only register for high 16-bit data provides DMA way to read out data, high 16-bit TDC data is read out by DMA way. Low 16-bit TDC data is read out word by word. After TDC data have been read into 1131, 'DATAREADY' is sent to TRGRST task. When TRGRST receives 'DATAREADY' from all of subsystem, it sends a command to task EVTBLD to build data from all of subsystem into a event data according to BES event data format. If length of VC data is larger than length of data buffer of 1131, a message 'BUFFER FULL' is sent. TRGRST will take this kind of phenomena into account.

1879 TDC data is 32-bit word. 1131 data memory is divided into high 16-bit and low 16-bit data memory due to way to read data. Each data memory is also divided into 4 data buffers with 1k word to store data of 4 events. The data buffer can store leading edge and trailing edge data of 511 hits. Both of edge data are read out at same time. It is separated into different subtype of BES event data by EVTBLD task. The first two words of data buffer are defined as data flag and data byte count that are used by EVTBLD task. The INDEX buffer to store the index number of data buffer makes EVTBLD task to build data of same event. During calibration of electronics, there is only one data buffer to store data of all of channels of VC electronics system. It is not necessary to buffer data during calibration because the whole system is reset after each event data is built, transmit and recorded.

4 Conclusion and Discussion

BES-II installs a new Vertex Chamber which DAQ is based on Fast bus system. The microcode for Fast bus system and uplayer control software for VC data acquisition are developed.

The dead time is a important feature for a DAQ system. The dead time of VC data acquisition procedure is contributed by three subprocedures: the first is 1879 TDC conversion time, 1 ms. The second is time to read 1879 TDC data by 1821. This contribution is negligible. The third is transmit time of data from 1821 to 1131. This is dependent on transmit rate of SIB and VME CPU. We measured the time to read data of all of channels of system, 1347 long word totally. It costs 1 ms to read high 16-bit data and 3.5 ms for low 16-bit data. Because there are only 10% channels to have hit, this contribution is only 0.5 ms. The first and second subprocedure are paralleled with other subsystems. The deadtime from these two subprocedures are much smaller than other subsystem. The third subprocedure is serial with TOF readout procedure. Therefore only third subprocedure has contribution to total deadtime of BES-II DAQ system, but less than 0.5 ms.

In order to decrease the deadtime, only the third subprocedure can be improved. Because 1821 SIB can not provide DMA transmit way for both high and low word, The personality card for 1821 ECLine bus connection and VME 1190 dual memory board [6] with ECL connector has to be adopted. The transmit rate of ECLine is as large as 64 Mb/s, it can improve transmit rate a lot.

This work is collaborated with HEP group of Washington University. American collaborators provide all of hardware and some basic microcode programs.

References

[1] Guo Yanan, BES-II Data Acquisition System, Report at this meeting.

[2] Operator's Manual, LeCroy Model 1879, Pipeline TDC, Revised December, 1985

[3] Operator's Manual, LeCroy Model 1821, Programmable Segment Manager/Interface, Revised March, 1987

[4] Operator's Manual, LeCroy Model 1131, VME to SIB Interface, April 1992

[5] Operator's Manual, LIFT, LeCroy Interactive FASTBUS Software Toolkit , Version 3.10, Revised May, 1991

[6] Operator's Manual, LeCroy Model 1190, VME Dual Port Memory, Revised august, 1994

The Current Status of BESII

Weiguo Li
IHEP, Beijing 100039

1 BES to BES II Upgrade

BES has been upgrated to BESII as shown in Fig. 1. Many systems are newly made. It includes a new VTC (Vertex Chamber), repaired from MarkIII straw chamber; a new MDC (Main Drift Chamber); new barrel TOF (Time of Flight) counters and its laser calibration system; new LUM (Luminosity Monitor) counters; new DAQ system based on VME-VCBD technique; new gas system using mass flow control. Other systems have been carefully repaired or modified. Here I will only touch on the main features of each sub-sytem, and mainly emphasize these sub-systems which are not covered by other speakers at this BES annual meeting.

VTC is composed of 640 straw tubes, read out by fastbus TDC 1879, with an expected wire resolution around 70 μm. Its Be beam pipe reduces the total material inside the MDC, so tracking combined with MDC and VTC informations will improve the recontructed momentum resoluition for charged particles. New MDC uses smaller cell compared with the old MDC and possesses a 90 degree symmetry, which enable the chamber to be operated at lower voltage and simplify the track reconstructions. The barrel TOF system uses new scintillators and new fine-meshed PMTs, so the PMTs can be operated inside the magnetic field, making it possible to use shorter light guide to increase the light collection. All these will improve the time resolution of the barrel TOF system. A resolution, including the beam length effect, around 200 ps is expected, down from 330 ps with the old system.

The Barrel Shower Counters (BSC) went through major repair and modifications. Before the upgrade, there are about 200 broken wires, affecting 253×2 readout channels, corresponding to 7.5% of the total 6720 channels. During the upgrade, these bad wires were treated differently depending on the accessibility of the wires. Some wires are replaced. These wires which are not accessible are disconnected, so the corresponding readout channels can be used again with other wires. In the total after the repair, only 37×2 channels are still dead, accounting for 1.1% of the total.

To make the gain more uniform, the high-voltage fanout are now grouped according to layers instead of phi sectors as in the previous operation. Since the layer width increases slightly radially from layer to layer, in the new arrangement, the high voltage applied to each layer can be finely tuned according to the pulse size seen. The expected voltage difference between inmost and outmost layers are 50 volts. Also, the high-voltage cables which are accessible without opening the steel plugs, have been increase by a factor of four, so in case some wires are shorted, less channels will be affected if one high voltage cable has to be disconnected. The remaining bad wires are carefully recorded so their effect can be simulated and corrected in the analyses. Other works done for BSC include the check of gas system, the repair of gas monitors, etc.

The repair for Endcap Shower Counters (ESC) involved the removal of 24 broken wires in the total of 8976, and the fix of some sparking problem, so almost all the readout channels are functional now. Also the number of high voltage cables are increased so the maximum number of wires affected by disconnecting one high voltage cable is 96. Also, the gas system was checked and the gas monitor counters were repaired.

A test was made for ESC to see which gas is better to be used in the system. After comparing different gases, a gas mixure of $A_r/CO_2/isobutane = 1 : 1.3 : 0.25$ is a better choice as compared with the gas mixure of $A_r/CO_2 = 34 : 66$ used so far. But the complication of introducing a new gas mixure makes this option less likely in a new future.

The muon chambers are fine as usual, only minor repairs are done, such as fixing a few broken cable connections and repairing some gas leakage.

To provent possible demage to detector during the beam injection when the detector is at working high voltage, the high voltage supplies are interlocked with a bending magnet at the end of linac which enables the beam injection. That means, if the detector high voltage is on, the beam can not be injected. Correspondingly all the high volatage suppliers are changed to CAEN.

To assist in reducing the beam background, two movable masks traveling in y direction are mounted betweem Q2 and separator, one at each side of the detector. Their mechanical control is tested and calibrated.

The solenoid power supplier was checked and repaired, the magnetic direction has been reversed by exchanging the leads to the coil.

New temperature probes are acquired and new readout is made for the enviromental parameters (temperature, pressure and magnet field).

2 BESII Debugging

BESII was completely assembled at the end of March. According to the schedule, April was devoted to machine study, requiring BESII to provide lum. measurement. Originally the whole month of May was allocated for BESII debugging with colliding beams, Because the request from machine people, the time period used by BESII was shortened to from 2nd of May to 22nd of May. Then the machine study is to be continued till the end of June, if the enviromental conditions permit to do so. According to this schedule, BESII debugging was divided to three phases. Firstly before May 12th, the task was to debugging the DAQ system, then three days were used for fixing the problems found in the first phase, at last one week was allocated to take some data at J/ψ.

Here I will emphasize the problems encountered during the debugging and how the problems were solved or to be solved. Then in the next section I will summarize the current status of BESII detector.

Before the start of BESII debugging, the online system was only tested partly. So a lot of efforts were devoted to read each sub-system out and then read the whole detector together.

At the beginning of April, after related VCBD hardware problems were fixed, both scalers and TDC/ADC of the luminosity monitors were successfully readout, Then the detector high voltage and the cable delays were adjusted. The time and pulse size distributions appeared to be reasonable. Although at the beginning, the ratio of signal to background was not good, because of bad vacuum conditions at the early stage of besm turn-on and at that time machine people were tunning the machine.

During the detector debugging, some of the front-end chips of TOF electronics were demaged because of unusual high input pulses from phototubes. It happened twice that significant fraction of the chips were demaged. The first was at the time of laser testing, the second happened probably at the time of beam injection. After the second time, signal from one phototube was checked using an oscilloscope, it was found that the pulse from the phototube during beam injection can be as high as 100 volts. It appears that the output from the new PMTs, using manufacture's recommended voltage setting, will not be saturated below 100 volts. On the contrast, the output from old PMTs will be saturated at about 20 volts. Based on this finding, the TOF electronics were modified to add more protection measures and the TOF high voltage power suppliers were interlocked with the beam injection. After this modifications, no more serious demage on TOF electronics happened again.

It was soon found that the readout of MDC was quite noisy, at the norminal threshold setting, a large percent of wires had hits and the hardware tracking rate was very high. Only after setting the threshold about 2.5 times of that used in the last run, the noise and tracking rate became managable.

Another problem developed later in April was that, some of the MDC high voltage channels drew too much current, so the high votage cables feeding these cells had to be disconnected. Those two problems related with MDC have not been solved yet, will be discussed in next section in more details.

One problem puzzled us for a few days was that, the readout of shower counters appeared to be noisy also. There were many hits in shower counters even no high voltage was applied to the counters. Soon it was noticed that, the reading value of each channel only changed a few ADC counts from event to event. Then it was traced to a bug in the online calibration that pedestals extracted from one BADC was downloaded to another BADC. The calibration program was modified to reflect the fact that the number of BADC was increased by a factor of two to reduce the readout time, a mistake in software was made in ordering the BADCs. The problem got fixed right away and the data from shower counters became reasonable.

Occasionally the DAQ system was blocked because the trigger system stoped to generate reset signal, this was solved by replacing the TR51 board, which is one of the control units in the trigger system.

For quite long, there was no VTC signals for event triggers. But there were hits for events triggered by VTC. At first, the timing was the suspect for the problem. Later it was realized that the signal from VTC in regular events may be too small to pass the TDC threshold, the hits seen in VTC triggers are caused by some forward tracks looping in VTC, which produce large pulses. So the voltage on VTC was increased from 3300 to 3600 - 3700 volts, and the threshold was lowered. Futher more, it was noticed that the gas pressure was set at 4 ATM absolute instead of 3 ATM, due to a misunderstanding about what gas pressure was used in MarkIII. After checking with the experts, the gas pressure was set to 3 ATM. The VTC data were seen beautifully after the above three measures were taken. The threshold reading is 2.2 now.

From the online histograms, some MDC channels had TDC hits without ADC hits. This happened before due to the cabling problem. After verifying it was the case, it was fixed by switching relevent cables. Also some bad channels in VTC readout was traced to bad cabling from main amplifier to the fastbus TDC, the problem was corrected by fixing the cables. Some bad electronics channels were replaced during the three day shut down period.

It was found that one HV supplier for barrel TOF was very unstable, changing the output reading by several dozen of volts. The problem was fixed by replacing the bad supplier.

The last problem in DAQ I want to mention is the fatal error caused by VME readout system. It happened that the DAQ system was stoped every few hours caused by fatal error in VME system. The problem was fixed by better handling the interrupts and add some capacitance on VME bus lines.

The main problems during detector debugging are mentioned above to keep the record and to provide some guidance for future problem trouble shooting.

3 Current Status of BESII

Right now the BESII DAQ system is working, all sub-systems work well except MDC. From online calibration, the number of bad electronics channels for MDC TDC, MDC ADC, BSC and ESC are 17, 11, 85 and 71 respectively, with no dead electronics channel in muon system.

Nice Bhabha and hardon events are seen, as well as some cosmic ray events. At J/ψ the hadron cross-section is about 1600 nb, calculated from online hadron selection and the luminosity from scalars. It is a reasonable number but somewhat smaller than expected, so it needs to be checked further. The maximum beam current during the run was 26 mA, and during BES annual meeting, the news is that the beam current has reached 39 mA. The luminosity is expected to be at least 1.5 times of that before BEPC upgrade.

The VTC works quite well with good efficiency, there is not much noise except cross talk between neighboring channels at a few percent level. The wire efficiency is more than 95% excluding dead channels, and the wire position resolution is estimated to be about 80 - 90 μm, both from the triplet histograms and from the position residure between the tracks and the hits. Right now there are 18 dead channels out of total 640 channels. The performance is much better than old central drift chamber.

MDC works but with above mentioned two problems. No wire has been broken so far among 22936 wires. The gas gain is quite uniform, pulse size distribution is quite the same from layer to layer at norminal voltage settings. The noise problem forces us to raise the threshold and will reduce the wire efficiency and hurt the position resolution, and the HV problem forces us to turn off some of the HV channels, so part of the channels become dead. Those two problems have to be solved in the Summar to make the new MDC a better chamber.

TOF is expected to work much better, with better detector and shorter beam length. The time resolution is expected to be at the level of 200 ps, compared with 330 ps with old BES detector. Some preliminary analyses show that the expected time resolution is achievable.

BSC data are better, in the sense that there are less dead channels and the gas gain is more uniform from layer to layer, and from one phi sector to the other. Most problems in ESC before upgrade were fixed and the hit distributions were fine. Muon data are also fine, with no noticible problems.

The luminosity monitor works. But from the online histograms and the preliminary offline analyses, the data appear not as good as before. In the ADC distribution, there are some overlap between the Bhabha peak and the background. One possible reason for this is that there are more material in front of lum. monitor now than before. This new geometry is forced by moving Q magnet inwards. Another possible reason is that at this stage of machine operation, the background is still higher than usual because the vacuum is still not good enough. Further study of lum. data is needed to understand what is happening.

The DAQ system work quite well with occasional minor problems. After fixing some hardware and software problems, the system works quite stable, although some minor problems may still show up in the future. The readout appears to be correct, checked both by online and offline histograms. Right now the average event readout time is below 10 ms, compared with more than 20 ms for old system. The trigger system also work well, including the VTC trigger, after replacing some problematic cards. The noise on shower triggers appears to be lower than before. The timing sequency controled by trigger system is fine, judged from the online time distributions of various sub-systems.

After the gas system was changed to mass flow control, there has not been much problems, the gas flow rate and the mixing ratio is quite stable. The temperature is better controled for C_2H_6 (BSC), using a new refrigerator system. Also the cost of gas has reduced.

The enviroment parameters are readout successfully by a PC. The NMR reading of the magnet is not as good as before. Part of the reason is the the probe has moved from about 0.7 m to more than 1 m from the interaction region in Z direction, the suspect is that the field around the probe is not as uniform as before. The temperature and pressure readings are reasonable, except the reading for a couple of temperature probes is suspected to be problematic. Those problems will be checked and be fixed in the Summer.

4 Summary

Overall BESII should be a better detector than BES in the following sense,

- Better mom. resolution is expected combining the MDC and VTC informations. There are less material in front of MDC, and the position resolution of VTC is much better than old CDC.

- Better barrel TOF system with expected time resolution of 200 ps, partly benificial from the shorten beam length. This will greatly improve the particle ID capability of BESII detector.

- Better shower courter energy resolution is expected after fixing bad chjannels and the gas gain is more uniform.

- The event readout time is reduced by more than a factor of 2, this is more significant as BEPC has increased the luminosity by a factor of 1.5. This improvement make the data taking more efficient.

- Because the VTC has 12 layers, it is possible to find tracks by VTC alone, making the track acceptance larger than before. For some physics analyses, it will make big difference.

The work to be done in Summar are as follows,

- To fix the two probelms related with MDC, the measures to be taken are: to put resistor filter right on the HV board at the endplate; to change the cables to coaxial type; to reduce the number of HV cables coming out; to pay attention to the grounding; to clean the HV parts, the HV distribution boards and the feedthroughs; to control the humidity by flowing dry air or nitrogen by endplates.

- To fix bad channels, either caused by HV, electronics or bad cables.

- To further tune the detector operating parameters, the HV setting, the threshold setting to achieve the best efficiencies and resolutions.

- To fix other problems found so far.

- Several tasks should be finished in the Summar, they are:
  1. Laser calibration system for barrel TOF.
  2. writing HV and enviromental paramaters on tapes.
  3. Writing data directly on disks at computer center through dedicated line.
  4. VTC electronics calibration and threshold setting circuit.
- Further offline data analyses to study the detector performance and to get some feedback for hardware problems.
- To take more data this run if possible.

It is estimated that another one month in the fall is needed to fully debug BESII detector. Also background at high current may be quite high, time is needed to understand and solve it if this is the case.

Codeman

Derrick Kong
University of Hawaii

1 Introduction

This report provides a review of the revised codeman system used by the BES Collaboration, concentrating on the primary server. It includes a summary of technical goals and tools used in implementing the system, a list of changes in the server, tips and hints on avoiding pitfalls of the system, and a look at some ideas for future developments in the codeman system.

2 Overview

A concise description of the codeman system is best provided by the introductory help file provided by the system itself:

> Codeman is the central component of a system aimed at synchronizing source code, parameterization files and documentation for the BES collaboration. Codeman is actually a system itself, consisting of a single master (primary) codeman and several servant (secondary) codeman executables, with one codeman secondary at each active BES site. Individual users communicate with the master codeman, which then communicates with and distributes files to the individual sites.[1]

The design goals behind the latest version of codeman are:

- Automated distribution of files to all sites.
- Prevention of user conflict over file control by implementing a control system similar to RCS or CVS.
- Assurance of successful code compilation on all platforms used in BES collaboration.

[1] From codeman.doc file, BES documentation distribution

- Maintain an archive of all code in case of accidental deletion or catastrophic failures.
- Inform members of collaboration of any changes in code.

Within these goals, a number of limitations are also present, partly due to programming feasibility and partly to compatibility restrictions with older sections of the system and user expectations:

- Inability to check for logic errors in code, only syntax errors.
- Maintenance requirements at all sites.
- Dependence on network connectivity and email reliability.
- Strict adherence to established syntax pattern for communication with primary and secondary servers.

3 Implementation

The current version of the codeman primary was rewritten from the ground up during the latter half of 1995. However, the secondary servers at each of the BES collaboration sites were not changed, as they already had advanced features which were not utilized by the old primary server.

This required the new primary to adhere to the existing communications protocol used by the secondaries: A set of keywords and specific syntax sent via email. This lowest common denominator was necessitated by the inhomogeneity among the computer systems in use by different collaboration sites, including Digital Vax (running VMS) and UNIX-based Alpha machines, HP workstations, and IBM RS6000 workstations. The details of this interface are described in detail below.

The above requirement, plus a desire to improve portability led to the choice of Perl (Practical Extraction and Report Language) as the language used for the codeman primary. Currently at version 5.001, Perl is a a powerful scripting language rapidly becoming standard on most UNIX systems. It has many advantages over other scripting tools including:

- Is platform independent across UNIX and is also available for VMS, DOS, and other operating systems, giving high portability factor.
- Is free and has extensive documentation and support network via Netnews, discussion groups, etc.
- Has a powerful regular expression and text parsing/manipulation routines, ideal for dealing with the established codeman communication methods.
- Has built-in debugging mechanisms and trace routines (like dbx).

Although written in Perl, the primary server also relies on the MH message handling system (version 6.8), common across UNIX platforms, to handle basic mail functions. This system was chosen because the interface is totally commandline driven, thus being suitable for inclusion in scripts.

The primary server actually consists of three main files: A short wrapper file, a local definition file, and the main script. The wrapper file is called every five minutes by a cron job, currently running on topaz.slac.stanford.edu, an IBM RS6000 workstation. It checks that the overall system is functioning (filesystems are present, etc), there is adequate disk space, and the codeman administrator has not halted the system for some reason.

The local definition file consists of a list of pathnames required by the primary to locate needed files and programs, plus email addresses for secondary sites, administrators, and an email newsgroup feed for notifications.

3.1 Packages

The actual files managed by codeman are divided into distinct groups called packages. Each package resides in a different directory and thus uses its own namespace; several packages may contain files with the same names, although the contents of the files may or may not be identical.

The main purpose behind the package name differentiation is to allow multiple versions of analysis code, with one stable "frozen" version, and one or more development versions. This allows users to continue analysis work while providing updates and changes to a later version. Over time, other packages have been added to codeman to provide for distribution and control over additional filetypes. The current packages supported by codeman are:

Package Name	Contents
BESCODE	Pre-upgrade analysis software (v87)
UPGRADE	Analysis software upgraded for BES-II (v100)
BESDOC	Documentation files
BESBIN	Utility scripts and executables
BESCONS	Constants files
BWFIT	Unbinned fitting package
BESLEX	Lexical converter code used in utilities
BESLUM	Code for BES-II luminosity monitor

Unfortunately, limitations in the secondary software on Vax computers make them unable to utilize most of the packages. Only the BESCODE and UPGRADE packages are available on Vax secondary machines.

4 Codeman User Interface

The internal codeman interface between the primary and secondary servers and vice versa is detailed in internal documentation and will not be covered here.[2]

The user interface consists of email messages sent to the primary server (secondary servers ignore all mail except from the primary). All user messages should have a blank subject line, followed by one or more directives in the body of the message. Allowed directives and their syntax are listed here:

Function	Syntax
Create new file	:NEW <filename> :PACKAGE <package> <comment>
Reserve file	:CO <filename> :PACKAGE <package> <comment>
Get file	:FETCH <filename> :PACKAGE <package> <comment>
Cancel reservation	:CANCEL <filename> :PACKAGE <package> <comment>
Delete file	:KILL <filename> :PACKAGE <package> <comment>
Check in file	:CI <filename> :PACKAGE <package> <comment>
Note that :CI must be followed by the code to be checked in, which is placed between the following two directives:	
Begin code section End code section	:BEGIN :END
Query by status Query on file name Query on jobs Query on users	:QUERY STATUS <status> Status = RESERVED, PENDING, NOT_RESERVED :QUERY NAME <filename1> <filename2> <etc.> :QUERY JOBS :QUERY USERID <username>
Get help	:HELP

5 Changes

As noted earlier, the current codeman primary interfaces with the preexisting secondary servers, so functional changes between the primary servers were limited.

The user-visible changes implemented during the primary server revision were:

- The :PACKAGE tag is now required for most commands. In the past version, such a tag was optional.
- Comments are required for most commands and only extend to end of the current line. Previously, comments could extend indefinitely.
- The primary is case-insensitive. Upper or lower case can be used in commands (However, programs are still case sensitive!).

[2]Design and Implementation of the Codeman UNIX Secondary Site System by Jim Panetta, April 1995 (internal BES memo).

In addition to the above changes, other additions and enhancements have been added over the past few months. These include:

- Addition of the BESLEX, BESLUM, and BWFIT packages.
- Synchronization of constants files across the collaboration and restriction of control over constants files to BESCONS package in codeman.
- Conversion to and from Vax format FORTRAN performed by the primary itself, removing reliance on a secondary code source.
- Minor command syntax changes, such as the format for :QUERY NAME.
- Improved formatting for user output.

6 Common Problems Using Codeman

When using codeman, the most problems stem from a few common errors. In most cases, such problems can be avoided by simply checking over a submission before sending it and remembering to group files properly.

- Not putting related files into a group. This is the biggest problem seen to date. Failure to group files can result in a huge number of submissions clogging the codeman queue, numerous compile failures as dependencies are improperly handled, and most dangerously, hidden logic errors in library code.
- Incorrect syntax. A simple check of the documentation can alleivate this problem.
- Improper code checkin: Failure to use :CI, :BEGIN, :END correctly. A number of checkin groups have been rejected because a submitter forgot to include the proper sequence of directives.
- Submitting too many requests at once. A huge backlog of requests to codeman can overtax the system. No more than a dozen directives should be in each message, and each person should have no more than 5 or 6 pending requests at a time.
- Failure to read codeman documentation. As changes and updates are made to the primary, the documentation is changed to reflect them. Users should stay up to date by reading the helpfile as well as the BES Coding Rules, available in the BESDOC package as bescode.tex or bescode.ps.

7 Future Plans

In general, it is expected that in a few years, the remaining Vax computers will be obsolete and people will generally move to UNIX machines. Computing power, cost, and support issues all point to that some time down the road. Until that happens, support will be maintained for the Vax machines as much as possible.

As for the primary itself, a number of possibilities were discussed during the rewriting of the code. Nothing has been actually decided upon, and it will likely be the poor programmer who actually must do the next version that gets to decide what will be done.

- Use of sockets/network communication rather than email. (Perhaps once all Vax machines are gone?)
- Conversion of code to native versions rather than having to use Vax format code for checkin. Requires rewriting of conversion utilities or a complex system to utilize current utilities.
- Addition of security features such as username and site checks.
- Other ideas?

8 Summary

- Latest version of codeman primary has been running since November 1995.
- Same basic functions and operations as previous versions.
- Packages supported: BESCODE, UPGRADE, BESBIN, BESCONS, BESDOC, BESLEX, BESLUM, BWFIT. Only BESCODE and UPGRADE available on Vax platforms.
- Latest version will continue to change and grow.

If you have further questions, comments, or suggestions, please feel free to contact me at:

`kong@uhheph.phys.hawaii.edu`

BES-II Software and Data Processing

Changchun Zhang[1,2]

Institute of High Energy Physics, Chinese Academy of Sciences, Beijing, 100039[1]

Abstract

The BES-II Software System and its code management have a good shape, and run successfully with new BES-II data. The BES computing environment on HP/UNIX system has been set up and palyed importmant role. Further studies of the BES-II detector performance and software improvement are necessary with existing BES-II data.

1 Introduction

In passed year, big progress in the BES-II upgrade have been obtained in both hardware and software respects. New Main Drift Chamber, TOF counter and Vertex Chamber are installed, and improvements in other subsystems is also achieved. An overall check-out and fine ajustment of BES-II system started with J/Ψ runs this May.

As scheduled, the BES-II reconstruction and calibration codes for MDC dEdx, VC, TOF, BSC, ESC and Muon counter are put into operation on HP/UNIX. The data production environment and jobs are successfully moved onto HP/UNIX and run well. Upgrade of Monte Calro simulation codes for BSC, MDC and VC has been made.

2 BES-II library and Upgraded Codeman

2.1 BES-II library v10.0 created

Temparary library v871 had been created at VAX/IHEP for quick moving of software upgrade since 1-Nov-1995 (Shaoqiang). IHEP people started to merge new VC/MDC reconstruction and MC simulation routines on VAX before upgraded codeman is ready, and debuging with v871 library.

New routines stored in v871 are all checked into upgrade library v10.0 soon after new codeman is ready. Then Synchrozied development of BES-II software can be performed

[1]Work supported in part by the National Natural Science Foundation of China

[2]E-mail: zhangcc@bepc5.ihep.ac.cn

on HP/UNIX. Problems, caused by difference between VAX/VMS and HP/UNIX, are solved at this phase.

2.2 Upgraded Codeman

The Codeman make us possible to develop the BES Software synchronizely through Wide Area Network. Contributions to the code developement can be auto-accepted and synchronized.

Secondary on UNIX is upgraded to maintain two libraries of BES-I and -II (mail/10-Aug-1995 from Jim). New primary on IBM/RS6000/AIX started to run from 28-Nov-1995 (see besnews/bescod/546 by Derrick). After upgrade, it can manage both BES-I and -II libraries parallelly. Packages supported by new codeman at UNIX system are (see Derrick's talk): BESCODE(v87, BES-I code),UPGRADE(v100, BES-II code), BESDOC(documentation), BESBIN(support scripts and executables) and BESCONS(constants files).

Since VAX at IHEP are going to be retied, no doc and no constant files will be maintained. Only BES-I and -II code libraries are linked with codeman. Not only BES-I and -II libraries but also doc and constant files on HP/UX at IHEP are updated through new codeman.

Codemen, Derrick, Jim, Pat, Ray, Shaoqiang and Sijun, who take care of codeman so successfully, should be appreciated. The BES collaboration is very grateful for their excellent cooperation and efficient work on codeman developement and software management.

3 BES-II Software Upgrade (v10.0)

3.1 Monte Carlo Simulation(Y.S. Zhu)

1. Barrel Shower Counter (B.S. Cheng)

Different values of SQS parameters for e,μ,h are used in order to improve the ADC and energy distributions for each layer. Magnetic field at BSC region is turned on. A compareson of MC events with J/Ψ,$\Psi\prime$ and Ds data has been made(see Fig. 1). Routines are ready and going to be checked in this summer.

Figure/Table to be sticked on

2. Main Drift Chamber (Q. Li)

This part of code are modified to fit new MDC configuration for both timing and dE/dx. Overflow problem caused by zero of drift time is found for both BES-I and -II code but not well studied yet.

3. Vertex Chamber (B.S. Cheng)

MC simulation codes for VC have been developed. Only TDC data on front edge of pulse are created. not well checked with new data yet.

4. MC events with MDC/VC

Upgraded MDC/VC routines have been checked into v10.0 library. MC events of $e^+e^- \to \mu^+\mu^-$ with combined new MDC and VC design can be produced (Mar 1996).

5. Endcap Shower Counter (J.C. Chen)

Simulation code is developed and well compared with old data in v8.6 on HP/UNIX. All routines are also linked with v10.0 library on HP/UNIX and will be checked in soon after the meeting.

6. MSBES (C.G. Li)

This new effort is try to develop a more friend interface between physicists and MC simulation code within GEANT package frame. Detector simulation part is adapted

from current BES-II MC code. Key benefit is to simulate hadron showers in our detector. More man power and working hours are needed.
7. Tune paremeters to fit real data is expected to be done later.

3.2 Reconstruction and Calibration(Rong Gang)

1. MDC Reconstruction codes(J. Liu)

JULIE routines for new MDC track reconstruction run first on VAX then on HP/UNIX with MC events of $e^+e^-, \mu^+\mu^-$ (Feb. 1996). Most of routines are stored into BES-II library (v10.0, May 1996). The code runs successfully with new BES-II data. A clear signal of $e^+e^-, \mu^+\mu^-$ from data were seen after global T0 is found (see Fig. 2). Survey file and wire position corrections need to be studied further. Fine tune and debug with improved calibration constants are required.

Figure/Table to be sticked on

2. MDC Calibration codes(Xie Yu)

Routines moved onto HP/UNIX, and results obtained on VAX can be repeated on HP/UNIX for BES-I data (J.F. Qiu, Jan 1996). Upgraded to BES-II has been done(Xie Yu, May 1996). A global T0 for all wires with Bhabha events was found (see Fig. 3). 160 T0 (40 layers and 4 parts for each layer) were calibrated with selected 4k Bhabha events. T0 for individual wires determined from hadron tracks with existing limited data sample will be studied later.

3. dE/dx (S.J. Sun, May 1996)

Mods for both Rec and Calib are finished and routines are stored into BES-II library (v10.0). A test is made to determine calibration constant with existing data sample.

4. VC (G.P. Chen)

Reconstruction codes for VC have been developed using JULIE technique on VAX and HP/UNIX. The codes are tested with MC events and checked into v10.0 libary. Calibration codes for VC is also developed and tested with MC events. Preliminary plots for spatial resolution found from the difference between fitted track and measured position are obtained with new data(see Fig. 4). Further test and optimization with real data need to be done. Alignment of VC from MDC is required.

Figure/Table to be sticked on

5. TOF Calibration (G. Rong)

Mods for TOF calibration codes moved from VAX/VMS to HP/UNIX and checks with BES-I data are done(Jan. 1996). From a careful study of new BES-II data, a TOF resolution of 200 ps in average is reached with preliminary and regular calibration procedure(see Fig. 5).

6. Calibration Constant files (G. Rong, D. Kong and C.C. Zhang)

Files in BESTEST/VAX are checked and compared carefully with files from calibarion account(offuse2 on VAX). Files on CIT/UH/IHEP/SLAC sites are also carefully compared. Useless files have been removed and missing files added. Because of long history, files for old J/Ψ data may not be completely included. For first time, same sets of calibration files are available for all sites. Derrick will turn on codeman for constants files checkin.

7. One event display (Schernau, - Mar 1996)

Mods are done for new MDC/VC configurations and related routines checked into v10.0 library.

4 BES Computing environment on HP/UNIX

4.1 Physics and Production jobs(X.Q. Hu)

1. HP Resource Allocated

In order to reduce network access to hpws0-1, HP master changed to hpws2 and new user disks (u01b, u01c) are added. hpws0-1 are allocated to Data Production Jobs while hpws2-7 to Physics Analysis Jobs. A software switch is designed in NQS (Network Queue System) so that jobs from individual users can be distributed to hpws0-1 or hpws2-7, respectively. The www or netscape access is not allowed on hpws0-1 during data production period.

2. Resource for physics analysis

4 GBytes disk space for each physics group Physics users are encouraged to run their jobs on one of hpws3-6 due to quick I/O of local disks. During data production period, physics analysis jobs are not allowed to run on hpws0-1.

3. Resource for data production

5x4 GBytes disk space are available for production jobs, and 4 GBytes disk for online data recording through network. hpws0-1 will fully work on data production jobs.

4.2 Production Jobs(X.Q. Hu and S.Q. Zhang)

1. Tape copy (Sun Yi, S.Q. Zhang and X.Q. Hu)

Multi-output files in one drunk job can be managed on HP with routines adapted from VAX. Tar copy is used for recording of filter/rec/prong data files, and tested on HP/UX. Software tool for tar copy on HP is adapted and improved.

2. Filter/BBsel/Rec (C.C. Zhang, X.Q. Hu, Y.Y. Shao, H.B. Lan)

Filter/BBsel routines are moved onto HP/UNIX and tested with BES-I data. They are much improved for selecting good Bhabha events. Careful comparisons on reconstruction codes between VAX and HP are done and improvement to reduce the difference is made.

3. Data Quality check job (Q.M. Zhu)

Job monitoring raw data quality, Mondst, moved onto HP and tested with BES-I data. DQ(Data Quality) job, checking data quality with selected physics events, is also adapted.

4. Run Mondst/Filter/BBsel with BES-II data (X.Q. Hu)

Interface routines from online format to offline format are developed. Debuging with BES-II data, improving Filter/BBsel codes for efficient selection of Bhabha events are all done. Quick data production of new data is performed well on HP. Tools to read/write 8mm tape are developed.

5 8mm Tape Copy

5.1 Why to make copy

1. VAX are going to be retired

The maintainance of VAX system and its peripheral devices are very expensive (1M rmb per year). Total cost of HP system with 4 times cpu and same disk space, comparing with VAX, is 2M rmb only.

2. Huge ammount of BES data

9M J/Ψ, 3.4M Ψ', 22.3 pb-1 Ds and τ data must be transfered from 6250 tapes onto 8 mm tapes.

5.2 Robot Auto-load Software

1. First Version (S.Q. Zhang and Q.H. Hu)

They have developed a tar copy command procedure to auto-load files from disk onto 8mm tape on VAX/VMS. 8mm tape drive suffered from slow data transfer through Ethernet Network and easy to be broken (15 tape copies/tape broken in average). No physical dismount operation is taken in the case of R/W hardware failure. Job is crashed but R/W head of tape drive is still moving.

2. Improved Version (Yu Xie, C.C Zhang)

Improved version of Auto-load software is developed in Oct 1995. Software wait technique is designed to deal with R/W hardware failure in order to avoid job crash. Local stage disk is added in copy procedur from disk to tape while network data transfer goes between disks only.

5.3 Tape Copy Jobs

1. What done (Q.M. Zhu, Z.Z. Du)

6x2 shifts per week for Tape Copy had arranged since October 1995. Jobs have been well organized. Most of DPG members participated. 50-60 tapes(6250 type) per day copied onto disk. Robot Library operates well since last December. Data on stage disk are auto-loaded onto 8mm tapes and then the disk is auto-emptied. Run462-3316 (incl 8M J/Ψ, τ, part od Ds data) have been copied in nearly 70 days. Later on 500 missing runs at UTD have been copied and sent to UTD. Run3579-3733 (1M J/Ψ) for IHEP and Ψ' missing runs at UH have also been copied.

2. Robot with 8mm tape drives is reliable

4 tape drives in Robot run well still after 147 8mm tapes in total have been copied using Robot library. Most of tapes recorded on two drives so that over 50 tapes in average done on one drive. 8mm tape drive runs much reliably than before (it was a broken per 15 tape copies) since software improved and local stage disk used.

3. What not done

Ds and Ψ' data, available at UTD and UH, will be copied at UTD and UH with US colleagues's help. Part of these data at UH have been copied and sent to IHEP. It is expected to finish 8mm tape copies of all existing BES-I data before the middle of September.

6 Future Tasks on software development

6.1 Fine Tune of existing codes

1. Careful tune of JULIE/MDC code : Lorentz angle effect; Magnetic Field Scale; Study with improved calibration constants; Momentum scale check using J/Ψ decay events; Reconstruction efficiency study.
2. Careful tune of JULIE/VC code.
3. TDC for tail edge of pulse in VC simulation should be added in.
4. MSBES is carried on to move forward.
5. Realization of MC code with new data : dead wires of current BSC status should be coded.

6.2 Developement of new codes

1. JULIE reconstruction code with Combined MDC/VC tracking information should be developed.
2. Matching VC/MDC track to ESC is intesting for extending solid angle of the detector.
3. TOF Calibration with Lasser Monitor data
4. Some of cpu consuming routines (Such as JULIE fitting routines) to be rewritten in C/C++ language.
5. New Windows NT platform (PC) will be studied at IHEP.

7 Summary

Codeman is upgraded well with its primary on UNIX and play satisfied role in the BES-II code management through Network. BES-II Software for both MC and Reconstruction have good shape, run successfully with new BES-II data. Excellent performance of TOF and MDC can be obtained by running the upgrdaded reconstruction and calibration codes. BES computing environment on HP/UNIX system become more importmant and efficient after optimizing effort. Robot auto-load system works well. 8mm tape copies of BES-I raw data went successfully. BES is ready to get part resources of VAX retired. It is necessary to make fine tune of existing codes and further development of new codes.

Measurement of the $D^{*+}(2010)$ Branching Fractions and D-meson Production Cross Section in e^+e^- Anihilation at $E_{c.m.}$=4.03 GeV

H.W. Zhao*, W.G.Yan, H.S. Mao
Institute of High Energy Physics, Beijing.

Abstract

D-meson production cross sections have been measured with neutral and charged D single tag events. And, D^{*+} branching fractions are determined by single tag D^+, D^0 events and double tag D^+D^- events both from production mode $e^+e^- \to \bar{D}D^*(D\bar{D}^*)$. This analysis is based on the data collected by BES detector at a center-of-mass energy 4.03 GeV, corresponding to an integrated luminosity of 22.3 pb^{-1}. We selected neutral and charged D meson from decay modes $K^{\mp}\pi^{\pm}, K^{\mp}\pi^{\pm}\pi^{\pm}\pi^{\mp}, K_s^0\pi^{\pm}\pi^{\mp}, K^{\mp}\pi^{\pm}\pi^{\pm}$, and $K_s^0\pi^{\pm}$. Single tag events of $K^{\mp}\pi^{\pm}, K^{\mp}\pi^{\pm}\pi^{\pm}$ and double tag events selected through ($K^-\pi^+\pi^+$ vs $K^+\pi^-\pi^-$), ($K^{\mp}\pi^{\pm}\pi^{\pm}$ vs $K_s^0\pi^{\mp}$), ($K_s^0\pi^{\pm}$ vs $K_s^0\pi^{\mp}$) are used to determine the results.

1 Introduction

D-meson production cross section between 3.7-4.3 GeV were predicted by coupled-channel model of charm[1], and were measured mainly by MARK II experiments[2]. More measurements are still required to make a test of this model.

Branching fractions for D^{*+} and D^{*0} decays have also been measured in a number of expriments[2,3,4,5]. The measurement result of $BR(D^{*+} \to D^+\gamma) = 17 \pm 5$ % given by MARK III [3] and the measurement result of $BR(D^{*+} \to D^+\gamma) = 1.1 \pm 1.4 \pm 1.6\%$ given by CLEO II [4] are quite diffrent. The former cannot be acoommodated by theretical models[1,6] without invoking a large anomalous charm quark magnetic moment[7], while the latter is in good agreement with theoretical predictions. Further independent measurements are called for and a clarification is also desireble because D^* branching fraction have a noticble impact on the measurements of the branching fraction of B meson decays.

In this paper, we report our measurement results of D-meson production cross section at 4.03 GeV and the D^{*+} decay branching fractions. The analysis is based on $22.3pb^{-1}$ of data from e^+e^- collisions at a centr-of-mass energy 4.03 GeV, taken with the BES detector during the 1992-1994 BEPC run.

Sec.II describes the measurement of D-meson production and Sec.III the measurement of D^{*+} branching fracrions by two different methods. A brief discussion is presented in Sec.IV.

2 Production cross section of D-meson at 4.03 GeV

In the 4-GeV region, three D production modes have been observed:
(1) $e^+e^- \rightarrow D\bar{D}$
(2) $e^+e^- \rightarrow D^*\bar{D}$ or $\bar{D}^*D$
(3) $e^+e^- \rightarrow D^*\bar{D}^*$
here D and D^* denote charged and neutral D meson and D^* meson respectively. Vector meson D^{*+} may decay to $D^+\gamma$, $D^+\pi^0$ or $D^0\pi^+$; D^{*0} may decay to $D^0\gamma$ or $D^0\pi^0$.

Monte Carlo studies show that the momentum of D meson relies on the production mode from which it comes. These three prodution modes can be well distingwished according to the momentum of D meson produced directly or from D^* decay. The momenta range for each mode is listed in Table I. One can determine from which production mode a D meson comes according to the momentum of D.

Table I. Momenta range for production modes

production mode	theoreticl momenta	experimental momenta
$e^+e^- \rightarrow D^*\bar{D}^*$	0.004-0.308 GeV	0.0-0.34 GeV
$e^+e^- \rightarrow D^*\bar{D}$ or $\bar{D}^*D$	0.368-0.664 GeV	0.34-0.70 GeV
$e^+e^- \rightarrow D\bar{D}$	P_{D^+}:0.752, P_{D^0}:0.764 GeV	0.70-0.85 GeV

$D^\pm$, D^0 and $\bar{D}^0$ are reconstructed from the decay modes as follows: $K^\mp\pi^\pm\pi^\pm$, $K^0\pi^\pm$ for charged D and $K^\mp\pi^\pm$, $K^\mp\pi^\pm\pi^\pm\pi^\mp$, $K^0\pi^\pm\pi^\mp$ for neutral D. Signals from these decay channels are observed. Well-reconstructed charged tracks (MFIT=2,-9,-19) were used to combine. Tracks (exclude K^0 channels)are required to come within 1 cm radialy and within ± 15 longitudinally of the measured beam crossing point. The polar angle of charged track are required to satisfy $|cos\theta| \leq 0.80$ to provide reliable tracking and barrel TOF information. The dE/dx and TOF information of a charged track are used to identify a particle. They are required to be consistent with the mass hypothesis assigned to the track. The confidence level of a track for each particle hypothesis (e, μ, π, K, P) can be calculated as $CL_i = 1 - Prob(\chi_i^2)$, where $Prob(\chi_i^2)$ is the probability of the χ^2) distribution for each partical hypothesis, $i = e, \mu, \pi, K, P$. χ_i^2 is the joint chi-square of the avilable dE/dx and TOF information for the track, defined as : $\chi_i^2 = \chi_i^2(TOF) + \chi_i^2(dE/dx)$, where $\chi_i^2(TOF) = (t - t_i)^2/\sigma_{TOF}^2$, t is the measured time of flight and t_i is expected time of flight for ith particle hypothsis. σ_{TOF}^2 is the resolution of TOF. Samillarly, $\chi_i^2(dE/dx)$ is defined as $\chi_i^2(dE/dx) = (dEdx - dEdX_i)^2/\sigma_{dE/dx}^2$. $CL_K > 0.01$ and $L_K/(L_K + L_\pi) > 0.5$ are required for K candidate and $CL_\pi > 0.01$ and $L_K/(L_K + L_\pi) \leq 0.5$ for π candidate, where $L_K = exp(-\chi_K^2(TOF)/2) \cdot$

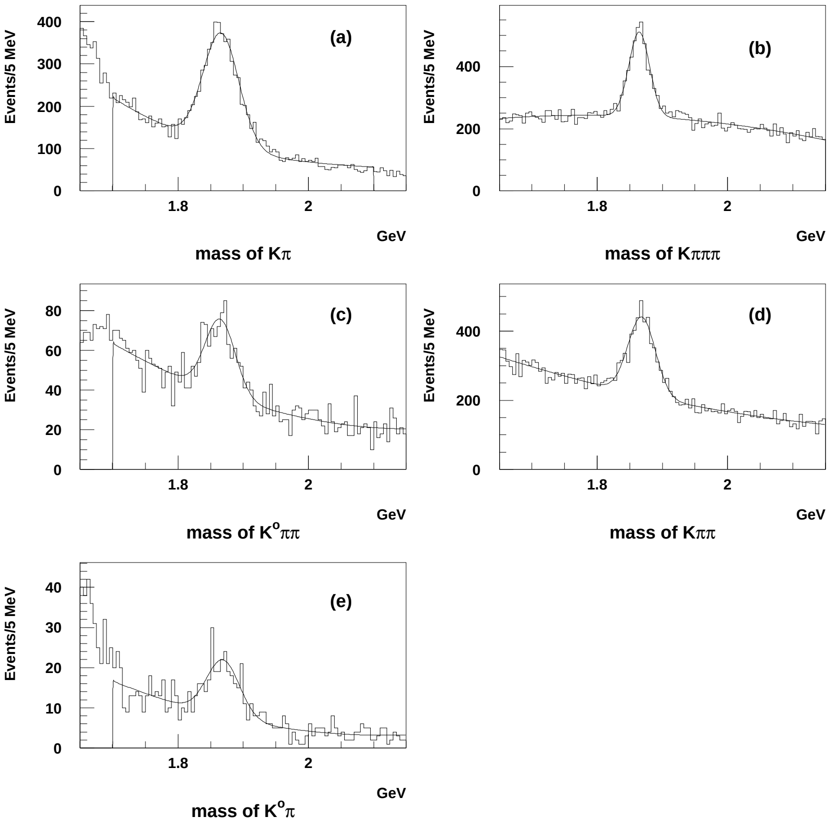

Figure 1: Invariarant mass distribution for (a). $D^0 \to K^-\pi^+$, (b). $D^0 \to K^-\pi^+\pi^+\pi^-$, (c). $D^0 \to K^0_s\pi^+\pi^-$,(d). $D^+ \to K^-\pi^+\pi^+$, (e).$D^+ \to K^0_s\pi^+$

$exp(-\chi^2_K(dE/dx)/2)$ and $L_\pi = exp(-\chi^2_\pi(TOF)/2) \cdot exp(-\chi^2_\pi(dE/dx)/2)$. Measured momentum of each charged track is corrected for dE/dx losses in material traversed before entering the MDC, and for a BES magnetic field shift. Tracks are combined to reconstruct $D^\pm$, D^0 and $\bar{D}^0$ through the given decay channels. For the channel of $K^\pm\pi^\mp\pi^\mp\pi^\pm$, at least one of the two possible $\pi^+\pi^-$ combinations must have a mass within ±150 MeV of the $\rho^0(770)$, and $K^\pm\pi^\mp$ a mass within ±50 MeV of the $K^{*0}(892)$, to decrease the combinational background. For the K^0 channels, the invariant mass of $\pi^+\pi^-$ is limited to be 498 ± 18 MeV and the decay length are required to be larger than 5 mm.

Fig.1 shows the invariant mass distributions of $K^\mp\pi^{pm}$, $K^\mp\pi^\pm\pi^\pm\pi^\mp$, $K^0\pi^\pm\pi^\mp$, $K^\mp\pi^\pm\pi^\pm$ and $K^0\pi^\pm$. Fig.2 shows the momenta distribution of $K^\mp\pi^\pm$ and $K^\mp\pi^\pm\pi^\pm$ under a cut of $|M_{K\pi} - 1.865| \leq 0.05$ GeV and $|M_{K\pi\pi} - 1.869| \leq 0.05$ GeV respectively.

The ammounts of tagged $D^\pm$, D^0 and $\bar{D}^0$ can be determined by fitting the invariant-mass distributions to Breit-Weigner function. The mean value of mass and width(σ) are obtained, as listed in Table II. Numbers of tagged $D^\pm$, $D^0(\bar{D}^0)$ produced from each

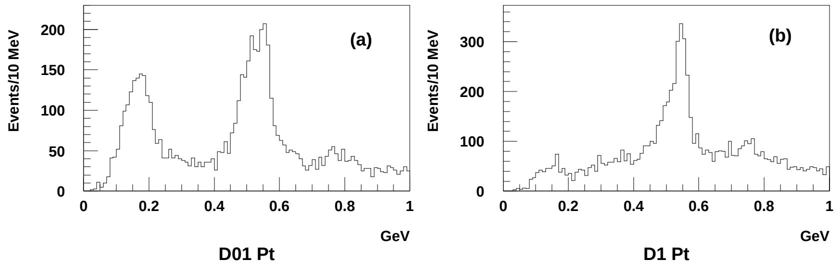

Figure 2: Momenta distribution for (a). $D^0 \to K^-\pi^+$ and (b). $D^+ \to K^-\pi^+\pi^+$

production mode are determined by fitting the inariant-mass distribution under cuts on momentum as listed in Table III.

Table II. Event number and mass for each tag Channel

Channel	mass(GeV)	width(MeV)
$D^0 \to K^-\pi^+$	1.8659±0.0007	27.6 ± 0.9
$D^0 \to K^-\pi^+\pi^+\pi^-$	1.8644±0.0007	15.9 ± 0.8
$D^0 \to K^0\pi^+\pi^-$	1.8649±0.0023	23.1 ± 2.3
$D^+ \to K^-\pi^+\pi^+$	1.8683±0.0009	21.0 ± 1.0
$D^+ \to K^0\pi^+$	1.8693±0.0034	25.3 ± 3.6

Table III. Events number for each production mode ($P_D : GeV$)

Channel		event number N_D		total
	$e^+e^- \to D^*\bar{D}^*$	$e^+e^- \to D^*\bar{D}(\bar{D}^*D)$	$e^+e^- \to D\bar{D}$	
	$p_D < 0.34$	$0.34 < P_D < 0.70$	$0.70 < P_D < 0.85$	
$D^0 \to K^-\pi^+$	$1809 \pm 63 \pm 53$	$2090 \pm 110 \pm 107$	112 ± 88	$3899 \pm 127 \pm 119$
$D^0 \to K^-\pi^+\pi^+\pi^-$	$898 \pm 43 \pm 9$	$1130 \pm 73 \pm 18$		$2028 \pm 85 \pm 20$
$D^0 \to K^0\pi^+\pi^-$	$192 \pm 26 \pm 5$	$268 \pm 41 \pm 20$		$460 \pm 49 \pm 21$
$D^+ \to K^-\pi^+\pi^+$	$428 \pm 43 \pm 7$	$1722 \pm 77 \pm 9$	< 95	$2150 \pm 88 \pm 11$
$D^+ \to K^0\pi^+$	< 20	$179 \pm 24 \pm 20$		

We obtained production cross sections via studies of $D^0 \to K^-\pi^+$ and $D^+ \to K^-\pi^+\pi^+$ channels. Efficences of reconstruction via $K^-\pi^+\pi^+$ and $K^-\pi^+$ for each event type, as listed in Table IV, are determined by Monte Carlo studies. They are used to calculate cross sections.

Table IV. Efficence for each event type

event type	efficiency (%)
$e^+e^- \to D^+D^-, directD$	$\varepsilon_1 = 0.289$
$e^+e^- \to D^+D^{*-}, directD$	$\varepsilon_2 = 0.265$
$e^+e^- \to D^-D^{*+}, D^{*+} \to D^+\gamma$	$\varepsilon_3 = 0.302$
$e^+e^- \to D^-D^{*+}, D^{*+} \to D^+\pi^0$	$\varepsilon_4 = 0.308$
$e^+e^- \to D^{*-}D^{*+}, D^{*+} \to D^+\gamma$	$\varepsilon_5 = 0.295$
$e^+e^- \to D^{*-}D^{*+}, D^{*+} \to D^+\pi^0$	$\varepsilon_6 = 0.312$
$e^+e^- \to D^0\bar{D}^0, directD^0$	$\varepsilon_1^0 = 0.354$
$e^+e^- \to D^0\bar{D}^{*0}, directD^0$	$\varepsilon_2^0 = 0.344$
$e^+e^- \to \bar{D}^0D^{*0}, D^{*0} \to D^0\gamma$	$\varepsilon_3^0 = 0.371$
$e^+e^- \to \bar{D}^0D^{*0}, D^{*0} \to D^0\pi^0$	$\varepsilon_4^0 = 0.375$
$e^+e^- \to D^-D^{*+}, D^{*+} \to D^0\pi^+$	$\varepsilon_5^0 = 0.357$
$e^+e^- \to \bar{D}^{*0}D^{*0}, D^{*0} \to D^0\gamma$	$\varepsilon_6^0 = 0.387$
$e^+e^- \to \bar{D}^{*0}D^{*0}, D^{*0} \to D^0\pi^0$	$\varepsilon_7^0 = 0.403$
$e^+e^- \to D^{*-}D^{*+}, D^{*+} \to D^0\pi^+$	$\varepsilon_8^0 = 0.394$

We denote $br^+ = BR(D^+ \to K^-\pi^+\pi^+)$, $br^0 = BR(D^0 \to K^-\pi^+)$, $b_1 = BR(D^{*+} \to D^+\gamma)$, $b_2 = BR(D^{*+} \to D^+\pi^0)$, $b_3 = BR(D^{*+} \to D^0\pi^+)$, $b_1^0 = BR(D^{*0} \to D^0\gamma)$ and $b_2^0 = BR(D^{*0} \to D^0\pi^0)$. From PDG 1994, we have $br^+ = 9.1 \pm 0.6\%$, $br^0 = 4.01 \pm 0.14\%$, $b_1 = 1.1 \pm 0.6\%$, $b_2 = 30.8 \pm 0.8\%$, $b_3 = 68.1 \pm 1.3\%$, $b_1^0 = 36.4 \pm 2.8\%$ and $b_1^0 = 63.6 \pm 2.8\%$.

In the case of $e^+e^- \to D\bar{D}$, the numbers of tagged D^+ and D^0 from $D^+ \to K^-\pi^+\pi^+$ and $D^0 \to K^-\pi^+$ can be written as follows:

$$N_{D^0} = L \cdot \sigma(D^0\bar{D}^0) \cdot \varepsilon_1^0 \cdot br^0 \tag{1}$$

$$N_{D^+} = L \cdot \sigma(D^+D^-) \cdot \varepsilon_1 \cdot br^+ \tag{2}$$

where the integreted luminosity $L = 22.3\ pb^{-1}$. $\sigma(D^+D^-)$ and $\sigma(D^0\bar{D}^0)$ are the exclusive production cross sections of $e^+e^- \to D^+D^-$ and $e^+e^- \to D^0\bar{D}^0$ respectively. ε_1 and ε_1^0 are efficiencies of associated event type, whose values are listed in Table IV. The inclusive production cross section of D^+ and D^0 come from this mode can be calculated as $\sigma(D^0) = \sigma(D^0\bar{D}^0)$ and $\sigma(D^+) = \sigma(D^+D^-)$.

In the case of $e^+e^- \to DD^*$ or $\bar{D}D^*$, we have

$$N_{D^+} = L \cdot \sigma(D^+D^{*-}) \cdot (\varepsilon_2 + \varepsilon_3 \cdot b_1 + \varepsilon_4 \cdot b_2) \cdot br^+ \tag{3}$$

$$N_{D^0} = L \cdot \sigma(D^0\bar{D}^{*0}) \cdot (\varepsilon_2^0 + \varepsilon_3^0 \cdot b_1^0 + \varepsilon_4^0 \cdot b_2^0) \cdot br^0 + L \cdot \sigma(D^+D^{*-}) \cdot \varepsilon_5^0 \cdot b_3 \cdot br^0 \tag{4}$$

and then there are $\sigma(D^+) = (1 + b_1 + b_2) \cdot \sigma(D^+D^{*-})$ and $\sigma(D^0) = b_3 \cdot \sigma(D^+D^{*-}) + 2 \cdot \sigma(D^0\bar{D}^{*0})$

In the case of $e^+e^- \to D^*\bar{D}^*$, we have

$$N_{D^+} = L \cdot \sigma(D^{*+}D^{*-}) \cdot (\varepsilon_5 \cdot b_1 + \varepsilon_6 \cdot b_2) \cdot br^+ \tag{5}$$

$$N_{D^0} = L \cdot \sigma(\bar{D}^{*0}D^{*0}) \cdot (\varepsilon_6^0 \cdot b_1^0 + \varepsilon_7^0 \cdot b_2^0) \cdot br^0 + L \cdot \sigma(D^{*+}D^{*-}) \cdot \varepsilon_8^0 \cdot b_3 \cdot br^0 \tag{6}$$

then we get $\sigma(D^+) = (b_1 + b_2) \cdot \sigma(D^{*+}D^{*-})$ and $\sigma(D^0) = \sigma(D^{*0}\bar{D}^{*0}) + b_3 \cdot \sigma(D^{*+}D^{*-})$

Using the numbers of single tagged D^+ and D^0 (becaues of charge conjugation, $N_{D^+} = N_{D^\pm}/2$, and similarly for N_{D^0}) for each production mode, branching fraction values given by PDG 1994 and efficiencies listed in Table IV. Cross sections can be obtained from a calculation performance. We list the results in Table V and Table VI. The first item of error is statistic error caused by statistic uncertainty of ΔN_D. The second item of error is systimatic error due to the uncertainty of of br^+ and br^0, a variation of 2.5%L and the uncertainty of N_D via varying background function of fit.

Table V. Production cross sections of D^+ and D^0

production mode	$\sigma(D^0)$	$\sigma(D^+)$
$e^+e^- \to D^*\bar{D}^*$	$5.11 \pm 0.27 \pm 0.44\ nb$	$0.68 \pm 0.07 \pm 0.07\ nb$
$e^+e^- \to D\bar{D}^*$	$6.52 \pm 0.36 \pm 0.80\ nb$	$3.09 \pm 0.14 \pm 0.22\ nb$
$e^+e^- \to D\bar{D}$	$0.35 \pm 0.28 \pm 0.02\ nb$	$< 0.16\ nb$
Total(exclude $D\bar{D}$)	$11.63 \pm 0.45 \pm 0.91\ nb$	$3.77 \pm 0.15 \pm 0.23\ nb$

Table VI. Production cross section for each mode

production mode	cross section
$e^+e^- \to D^{*+}D^{*-}$	$\sigma(D^{*+}D^{*-}) = 1.06 \pm 0.11 \pm 0.10\ nb$
$e^+e^- \to D^{*0}\bar{D}^{*0}$	$\sigma(D^{*0}\bar{D}^{*0}) = 1.83 \pm 0.12 \pm 0.21\ nb$
$e^+e^- \to D^\pm D^{*\mp}$	$\sigma(D^\pm D^{*\mp}) = 2.34 \pm 0.10 \pm 0.17\ nb$
$e^+e^- \to \bar{D}^0 D^{*0}$ or $D^0\bar{D}^{*0}$	$\sigma(\bar{D}^0 D^{*0}\ \&\ D^0\bar{D}^{*0}) = 2.46 \pm 0.18 \pm 0.39\ nb$
$e^+e^- \to D^+D^-$	$\sigma(D^+D^-) \le 0.08\ nb$
$e^+e^- \to D^0\bar{D}^{*0}$	$\sigma(D^0\bar{D}^{*0}) = 0.18 \pm 0.14 \pm 0.01\ nb$

3 Branching Fractions of D^{*+}

At energy of 4.03 GeV, the momentum of the soft pion and photon which come from D^* decay are small (about 70 MeV for pion and 100 MeV for photon). It is difficult to reconstruct the D^* directly due to the low efficiency of pion reconstruction (smaller than 0.1) and high backgroud of photon. But, branching fractions can be determined from D^+ and D^0 single tag applying some theoretical constrains on branching ratio and cross sections.

Consider the mode $e^+e^- \to \bar{D}D^*$ or $D\bar{D}^*$, the numbers of single tagged D^+ and D^0 from $K^-\pi^+\pi^+$ and $K^-\pi^+$ can be written as follows

$$N_{D^+} = L \cdot \sigma(D^+D^{*-}) \cdot (\varepsilon_2 + \varepsilon_3 \cdot b_1 + \varepsilon_4 \cdot b_2) \cdot br^+ \tag{7}$$

$$N_{D^0} = L \cdot \sigma(D^0\bar{D}^{*0}) \cdot (\varepsilon_2^0 + \varepsilon_3^0 \cdot b_1^0 + \varepsilon_4^0 \cdot b_2^0) \cdot br^0 + L \cdot \sigma(D^+D^{*-}) \cdot \varepsilon_5^0 \cdot b_3 \cdot br^0 \tag{8}$$

where D^* branching fractions b_1, b_2, b_3, b_1^0 and b_2^0 are unknown and need to be determined.

Isospin conservation and the P^3 dependence of P-wave widths are used to constrain the cross sections. At $E_{cm} = 4.03$ GeV, we have

$$\alpha = \frac{\Gamma(D^{*+} \to D^+\pi^0)}{\Gamma(D^{*+} \to D^0\pi^+)} = \frac{1}{2} \cdot (\frac{P_{D^+}}{P_{D^0}})^3 = 0.452 \tag{9}$$

$$\beta = \frac{\sigma(D^0\bar{D}^{*0})}{\sigma(D^+D^{*-})} = (\frac{P_{D^0}}{P_{D^+}})^3 = 1.077 \tag{10}$$

$$\gamma = \frac{\Gamma(D^{*0} \to D^0\pi^0)}{\Gamma(D^{*+} \to D^0\pi^+)} = \frac{1}{2}\cdot(\frac{P_{\pi^+}}{P_{\pi^0}})^3 = 0.710 \tag{11}$$

Consider the requirements of $b_1 + b_2 + b_3 = 1$, $b_1^0 + b_2^0 = 1$ and constrains of branching ratio $b_2/b_3 = \alpha$, $b_2^0/b_3 = \gamma$ which are derived from Eqs.(9)(11), branching fraction b_3 can be calculated from Eqs.(7)(8)(10) as follows:

$$b_3 = \frac{(\varepsilon_2 + \varepsilon_3)\cdot R - (\varepsilon_2^0 + \varepsilon_3^0)\cdot\beta}{[\varepsilon_3 + (\varepsilon_3 - \varepsilon_4)\cdot\alpha]\cdot R + \varepsilon_5^0 - (\varepsilon_3^0 - \varepsilon_4^0)\cdot\beta\cdot\gamma} \tag{12}$$

where $R = N_{D^0}\cdot br^+/(N_{D^+}\cdot br^0)$. Using the numbers of $N_{D^+} = 0.5\cdot(1722 \pm 77 \pm 9)$, $N_{D^0} = 0.5\cdot(2090 \pm 110 \pm 107)$ and ε's in Table IV, we obtain a result shown in Table VIII.

The first item of error is statistic error caused by statistic uncertainty of ΔN_D. The second item of error is systimatic error due to the uncertainty of of br^+ and br^0, a variation of 2.5%L and the uncertainty of N_D via varying background function of fit.

On the other hand, D^{*+} branching fraction are also determined via D^+D^- double tag. We selected double tag events through decay modes $K^-\pi^+\pi^+$ vs $K^+\pi^-\pi^-$, $K^\mp\pi^\pm\pi^\pm$ vs $K_s^0\pi^\pm$ and $K_s^0\pi^\mp$ vs $K_s^0\pi^\pm$ from the mode $e^+e^- \to D^\pm D^{*\mp}$, with $D^{*+} \to D^+\pi^0$ and $D^+\gamma$. The track selection criteria are the same as in Sec.II. The momentum of the reconstructed D^+ or D^- is required to be 340 MeV to 700 MeV to ensure it is producted from $e^+e^- \to D^\pm D^{*\mp}$. Invariant mass of $K^\pm\pi^\mp\pi^\mp$ are required to be $1870 \pm 67(3\sigma)$ MeV. Invariant mass of K_s^0 reconstructed via $\pi^+\pi^-$ are required to be $497.7 \pm 22.5(3\sigma)$ MeV, and the flight length of K_s^0 to be larger than 5 mm.

As the energy of photon from $D^{*+} \to D^+\gamma$ and $D^{*+} \to D^+\pi^0$, $\pi^0 \to 2\gamma$ is small. Impact of photon is estimated in background estimating. We observed 11 double tag events.Fig.3 show distributions of observed signals comparing with Monta Carlo signal.

The number of observed double tag event for ith decay mode (i = 1, 2, 3) can be written as:

$$N_{D^+D^-} = 2\cdot L\cdot\sigma(D^+D^{*-})\cdot br_i^+\cdot(1 - b_3)\cdot\varepsilon_{di} \tag{13}$$

where ε_{di} is the efficiency for the ith decay mode, b_3 is $BR(D^{*+} \to D^0\pi^+)$. bri^+ is the joint branching fractions for decay ($D^+ \to Hadrons$) vs ($D^- \to Hadrons$). From PDG 1994, we have $br_1^+ = BR(D^+ \to K^-\pi^+\pi^+) \times BR(D^- \to K^+\pi^-\pi^-) = 8.281 \times 10^{-3}$, $br_2^+ = BR(D^+ \to K^-\pi^+\pi^+) \times BR(D^- \to K_s^0\pi^-) \times BR(K_s^0 \to \pi^+\pi^-) = 8.554 \times 10^{-4}$ and $br_3^+ = (BR(D^+ \to K_s^0\pi^+) \times BR(K_s^0 \to \pi^+\pi^-))^2 = 8.836 \times 10^{-5}$.

Since there is a relation between cross section $\sigma(D^+D^{*-})$ and the number of single tagged D^+ in $e^+e^- \to D^\pm D^{*\mp}$, as described by Eqs.(7), for each double tag channel, we have

$$N_i = N_{i(D^+D^-)} = \frac{2\cdot N_{D^+}\cdot br_i^+\cdot(1 - b_3)\cdot\varepsilon_{di}}{(\varepsilon_2 + \varepsilon_3\cdot(1 - b_3 - \alpha\cdot b_3) + \varepsilon_4\cdot\alpha\cdot b_3)\cdot br^+} \tag{14}$$

where N_i is the number of double tag events via decay channel i. N_{D^+} is the number of single tagged D^+. For each double tag channel of $(Hadrons$ vs $Hadrons)_i$ (i = 1,

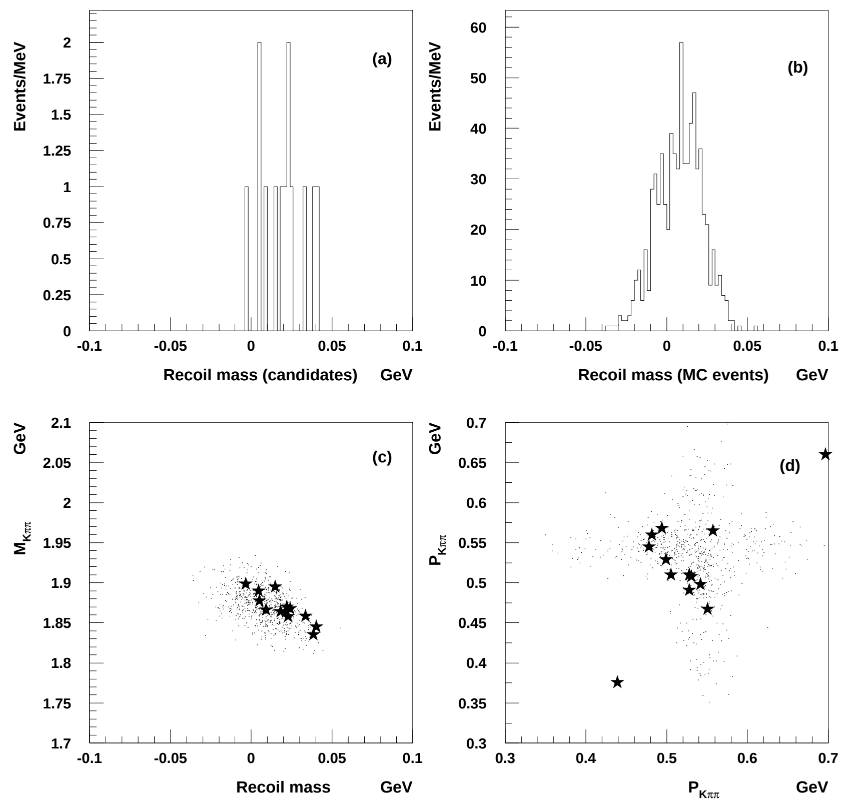

Figure 3: (a). Recoil mass of double tag candidates. (b).Recoil mass of D^+D^- from $e^+e^- \to \bar{D}D^*(D\bar{D}^*)$ (Monte Carlo events). (c). Mass of $K^+\pi^-\pi^-$ vs Recoil mass, compared with MC events (dots: MC events, star: candidates). (d). Momenta of $K^+\pi^-\pi^-$ vs Momenta of $K^-\pi^+\pi^+$, compared with $e^+e^- \to D^{\mp}D^{*\pm}, D^{*\pm} \to D^{\pm}\gamma, D^{\pm}\pi^0$ MC events (dots: MC events, star: candidates).

2, 3), the Poisson distribution function can be written as:

$$P_i(n_i, N_i + bg_i) = \frac{(N_i + bg_i)^{n_i}}{n_i!} \cdot e^{-(N_i+bg_i)} \tag{15}$$

where n_i is the number of observed events and N_i the expected number of event for decay mode i. bg_i is the background contribution for this decay mode.

Background contribution for each mode can be estimated by Monte Carlo simulation. bg_i can be calculated as

$$bg_i = \frac{N_i^{bg} \cdot 2 \cdot L \cdot \sigma(D^+D^{*-})}{N_{MC}} = \frac{N_i^{bg} \cdot 2 \cdot N_{D^+}}{N_{MC} \cdot (\varepsilon_2 + \varepsilon_3 \cdot (1 - b_3 - \alpha \cdot b_3) + \varepsilon_4 \cdot \alpha \cdot b_3) \cdot br^+} \tag{16}$$

where N_i^{bg} is the number of observed backgroud events from the ith tag mode in a total number N_{MC} of Monta Carlo $D^\pm D^{*\mp}$ events.

Table VII. D^+D^- double tag

i	tag mode	No. of Evt. n_i	efficiency ε_{di}	background level N_i^{bg}/N_{MC}
1	$K^-\pi^+\pi^+$ vs $K^+\pi^-\pi^-$	11	0.0729	$< 1. \times 10^{-5}$
2	$K^\pm\pi^\mp\pi^\mp$ vs $K_s^0\pi^\pm$	0	0.0678	$< 1.2 \times 10^{-5}$
3	$K_s^0\pi^\mp$ vs $K_s^0\pi^\pm$	0	0.0287	$< 1.2 \times 10^{-5}$

A joint liklihood function for three modes can be formed as follows:

$$Liklihood = \prod_{i=1}^{3} P_i(n_i, N_i + bg_i) \tag{17}$$

Using the result of double tag study in Table VII, we get a liklihood function:

$$Liklihood \propto \left(\frac{11.46 - 11.36 \times b_3}{0.567 - 0.3 \times b_3}\right)^{11} \times exp\left(-\frac{+13.18 - 12.49 \times b_3}{0.567 - 0.3 \times b_3}\right)$$

Fig.4 shows the liklihood function. The most probable value of b_3 are obtained. 32% of the area below and above this value gives a $\pm\sigma$ statistic error. We get $b_3 = 67.1^{+9.7}_{-23.1}\%$. Now b_1 and b_2 are calculated from $b_1 + b_2 + b_3 = 1$ and $b_2 = \alpha \cdot b_3$. the results are shown in Table VIII. The systematic errors are estimated by changing event selection criteria, a variation of estimated background level by 50% and a variety of $2L \cdot \sigma(D^+D^{*-})$ by 1 standard deviation.

Table VIII. Branching fractions of D^{*+}

decay mode		branching fraction (%) (D single tag)	(D double tag)
$D^{*+} \to D^+ + \gamma$	b_1	$3.2 \pm 8.5 \pm 11.2$	$0.1^{+35.1+8.0}_{-14.8-7.7}$
$D^{*+} \to D^+ + \pi^0$	b_2	$30.1 \pm 2.7 \pm 3.5$	$31.1^{+4.6+2.4}_{-10.9-2.9}$
$D^{*+} \to D^0 + \pi^+$	b_3	$66.7 \pm 5.9 \pm 7.7$	$68.8^{+10.2+5.3}_{-24.2-5.5}$

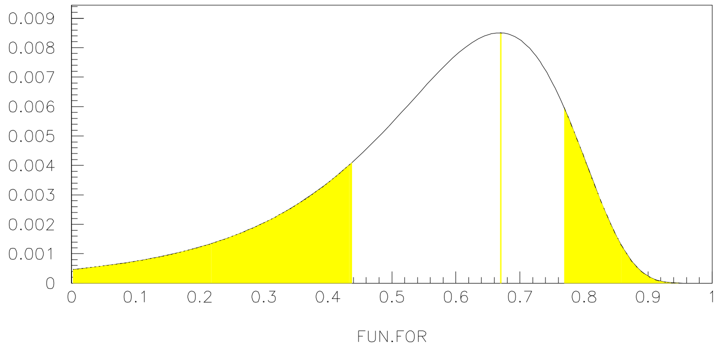

Figure 4: The variation of the normalized likelihood function with respect to b_3 ; the unshaded area under the curve denotes the 68% confidence interval.

4 Discussion

Coupled-channel model predicts the rate of charm production cross sections at $\Psi(4028)$ to be:
$R_{(D^{*0}\bar{D}^{*0})} : R_{(D^0\bar{D}^{*0}+\bar{D}^0 D^{*0})} : R_{(D^0\bar{D}^0)} = 1.0 : 1.35 : 0.005$
$R_{(D^{*+}D^{*-})} : R_{(D^+D^{*-}+D^-D^{*+})} : R_{(D^+D^-)} = 1.0 : 2.69 : 0.004$

SLAC-LBL gave a measurement at $\Psi(4028)$ that:
$R_{(D^{*0}\bar{D}^{*0})} : R_{(D^0\bar{D}^{*0}+\bar{D}^0 D^{*0})} : R_{(D^0\bar{D}^0)} = (1.0 \pm 0.10) : (0.85 \pm 0.09) : (0.10 \pm 0.06)$
The rates of charged D cross sections were not given.

In this experiment, we can give these rates as follows:
$R_{(D^{*0}\bar{D}^{*0})} : R_{(D^0\bar{D}^{*0}+\bar{D}^0 D^{*0})} : R_{(D^0\bar{D}^0)} = (1.00 \pm 0.13) : (1.35 \pm 0.23) : (0.10 \pm 0.08)$
$R_{(D^{*+}D^{*-})} : R_{(D^+D^{*-}+D^-D^{*+})} : R_{(D^+D^-)} = (1.00 \pm 0.14) : (2.20 \pm 0.18) : (0.08 - 0.08)$

In measurement of D^{*+} via single tag event, parameters α, β, γ are used. But the result are not sensitive to the value of γ very much. A variation of γ by $\pm 50\%$ leads to $\pm$ 0.1% variation on $BR(D^{*+} \to D^0\pi^+)$. So, it is not a good idea to calculate b_1^0, b_2^0 from b_3 and γ. In the method of double tag, only α is used (α is also used in MARK III and CLEO measurements). results from single tag and double tag agree well with each other and are consistent with the results of CLEO and theoretical predictions.

We would like to thank the staffs of the BEPC accelerator and the Computing Center at the Institute of High Energy Physics (Beijing).

References

[1] E. Eichten *et.al.*, Phys. Rev. D **21**, 227 (1980); E. Eichten *et.al.*, Phys. Rev. D **17**, 3090 (1978).

[2] G.Goldhaber *et. al.*, Phys. Lett. **69B**, 503 (1977); MarK II Collaboration, M. W. Coles *et. al.*, Phys. Rev. D **26**, 2190 (1982).

[3] Mark III collaboration. J.Adler *et. al.*, Phys. Lett. B **208**, 152(1988).

[4] CLEO collaboration, F. Butler *et. al.*, Phys. Rev. Lett. **69**, 2041(1992).

[5] ARGUS collaboration, H. Albrecht *et. al.*, ISSN 0418-9833 DESY 94-111.

[6] S.Ono, Phys. Rev. Lett. **37**, 655 (1976); W. Wilcox, O. V. Maxwell, and K. A. Milton, Phys. Rev. D **31**, 1081 (1985); R. L. Thews and A. N. Kamal, Phys. Rev. D **32**, 810 (1985); G. A. Miller and P. Singer, Phys. Rev. D **37** 2564 (1988); T. M. Yan, H. Y. Cheng *et. al.*, Phys. Rev. D **46**, 1148 (1992); T. M. Yan, H. Y. Cheng *et. al.*, Phys. Rev. D **47**, 1030 (1993).

[7] E. Angelos and G. P. Lepage, Phys. Rev. D **45**, 3021 (1992).

* Present address: Department of Tech. Phys., Beijing University.

Charmonium Physics in 1995/96 at BES

Yifan Gu
Institute of High Energy Physics,
Beijing 100039
for $\psi(2S)$ Group at IHEP

OUTLINE

1. **Introduction**
2. **Number of $\psi(2S)$ Events**
3. **Physics**
   (a) $^3S_1$
   (b) ^3P_J
   (c) $^1S_0$
4. **Summary**

1 INTRODUCTION

The BES has accumulated 3.6×10^6 $\psi(2S)$'s until April last year. Using this data sample, we are able to extend our study from $\psi(2S)$ to other charmonium states, and in the first place χ_c's.

2 Determination of the number of $\psi(2S)$ events

The number of $\psi(2S)$ events has been determined in three different ways. In the first, inclusive J/ψ production from $\pi^+\pi^- J/\psi$ was measured; PDG value for $B(\pi^+\pi^- J/\psi)$ was used. In the second, $\pi^+\pi^- J/\psi$, $J/\psi \to \mu^+\mu^-$ was detected and PDG values for $B(\pi^+\pi^- J/\psi)$ and $B(J/\psi \to \mu^+\mu^-)$ was used. The third method is to determine directly the number of $\psi(2S)$ events, which is still under investigation and yields only a very preliminary number for 1995 data set. The results obtained by all three methods are given in table 1.

Table 1: $N_{\psi(2S)}$ $(\times 10^6)$

method	1993/94	1995
$\pi^+\pi^- J/\psi$ inclusive	1.27 ± 0.11	2.28 ± 0.19
$\pi^+\pi^- J/\psi \to \pi^+\pi^-\mu^+\mu^-$	1.27 ± 0.11	2.28 ± 0.23
Direct Determination		2.34 ± 0.07

From this table we recommend the total number of $\psi(2S)$ events accumulated at BES as

$$N_{\psi(2S)} = 3.6(1 \pm 10\%) \times 10^6.$$

3 Physics

3.1 $^3S_1$ states

3.1.1 leptonic decays

The first measurement of the branching fraction of the $\psi(2S)$ decaying into $\tau^+\tau^-$ has been performed in 1994, using

$$B_{\tau^+\tau^-} = \frac{N_{\tau^+\tau^-} - \sigma_{QED} L}{N_\psi(2S)}$$

where $N_{\tau^+\tau^-}$ is the number of $\tau^+\tau^-$ events recorded on the $\psi(2S)$ resonance, which is a weighted average of six topologies including $e\mu$, $e\pi$, ee, $\mu\pi$, $e\rho$ and $\mu\rho$; σ_{QED} is the calculated QED τ-pair cross section including interference; L is accumulated luminosity at the resonance, which has been measured by recording wide angle Bhabha events in the BES detector, and $N_\psi(2S)$ is the number of $\psi(2S)$, which is determined to be $(1.27 \pm 0.11) \times 10^6$.

A check of $N_{\tau^+\tau^-}$ has been made recently using Hawaii unfiltered 93/94 $\psi(2S)$ data instead of filtered 93/94 data processed at IHEP, and D_s data with low threshold in MDC instead those data with both low and high thresholds.

A +3% correction has been given to the integrated luminosity of the D_s data set according to the recent refinement introduced by the D_s group at IHEP. in the analysis same event selection criteria were used except for a few minor modifications.

The value of $N_{\tau^+\tau^-}$ is thus found to be $9439 \pm 664 \pm 482$, compared with the previous $9524 \pm 776 \pm 498$. The resulting branching fraction is

$$B(\psi(2S) \to \tau^+\tau^-) = (3.47 \pm 0.52 \pm 0.62) \times 10^{-3},$$

which is well consistent with previous measurement of $(3.54 \pm 0.61 \pm 0.63) \times 10^{-3}$.

A draft titled *Measurement of the branching fraction of the decay* $\psi(2S) \to \tau^+\tau^-$ has been finished for submitting for publication.

Based on the analysis of $\psi(2S) \to \pi^+\pi^- J/\psi$, $J/\psi \to \ell^+\ell^-$ completed in 1994, a manuscript is also ready for publication which is titled *Precision Measurement of the* J/ψ *leptonic branching fraction* . Check by Hawaii colleagues using both 93/94 and 95 $\psi(2S)$ data are underway.

3.1.2 Hadronic decays of $\psi(2S)$

We have measured 26 decay channels for the $\psi(2S)$. Among them 15 channels are measured for the first time, and 11 are renewed data (Table 2). Thus the total decay modes from 34 in PDG listing increased to 49.

Substantial progress has been made on the study of the charmonium hadronic decay *puzzle.*

1. The measurement has extended from VP to VT, AP, VS, TP, VV, $B\bar{B}$ as well as radiative decays.

2. The *15% rule* from the PQCD prediction is observed for decay modes $\phi f_0(980)$, $b_1\pi$, $K^*(892)^0\bar{K}^*(892)^0$ $B\bar{B}$s and most of the more-than-two-particle decays.

3. Striking severe suppressions seen in VP final states $\rho\pi$ and K^*K:

$$B(\psi(2S) \to \rho\pi) < 0.29 \times 10^{-4} \quad (90\% \text{ C.L.})$$
$$B(\psi(2S) \to K^+\bar{K}^*(892)^- + c.c.) < 0.32 \times 10^{-4} \quad (90\% \text{ C.L.})$$
$$B(\psi(2S) \to K^0\bar{K}^*(892)^0 + c.c.) = (0.84 \pm 0.24 \pm 0.16) \times 10^{-4}$$

   We found a factor of > 64 relative to 15% for $\rho\pi$ and > 23 for $K^+\bar{K}^*(892)^- + c.c.$!

   What is the physics implication? There are mainly three proposals to explain this hadronic decay puzzle. the upper limit for $B(\psi(2S) \to \rho\pi)$ disagrees with Chaichian-Tornqvist model which predicts $B(\psi(2S) \to \rho\pi) = 7 \times 10^{-5}$ and Pinsky model, which predicts $B(\psi(2S) \to \rho\pi) = 4 \times 10^{-5}$.

Also, we see $b_1\pi$, $\phi f_0(980)$ and some other two-meson modes obeying the *15% rule*, which is in contradiction with the Chaichian-Tornqvist model.

Now the vector glueball model proposed by Brodsky, Lepage and Tuan is the only one left to explain the puzzle. Can it survive at all? (See 7 of this section).

Table 2: Branching fractions of $\psi(2S)$ decays

Decay Mode	$Br(\times 10^{-4})$
$\pi^+\pi^-K^+K^-$	$6.9 \pm 0.3 \pm 1.2$
$\pi^+\pi^-\pi^0$	$1.03 \pm 0.13 \pm 0.16$
$K\bar{K}\pi$	$1.30 \pm 0.20 \pm 0.25$
$K^*(892)^0K^-\pi^+ + c.c.$	$4.8 \pm 0.5 \pm 0.7$
$\phi\pi^+\pi^-$	$1.3 \pm 0.2 \pm 0.2$
$\omega\pi^+\pi^-$	$5.4 \pm 0.7 \pm 1.1$
$\rho^0\pi^+\pi^-$	$3.7 \pm 0.6 \pm 0.9$
$\rho\pi$	< 0.29 (90% C.L.)
$K^+K^*(892)^- + c.c$	< 0.32 (90% C.L.)
$K^0\bar{K}^*(892)^0 + c.c.$	$0.84 \pm 0.24 \pm 0.16$
$\omega f_2(1270)$	< 1.5 (90% C.L.)
$a_2\rho$	$3.1 \pm 1.5 \pm 1.1$
$K^*(892)^0\bar{K}_2^*(1430)^0 + c.c.$	< 1.79 (90% C.L.)
$K^*(892)^0\bar{K}_4^*(2045)^0 + c.c.$	$5.2 \pm 2.3 \pm 1.2$
$\phi f_0(980)$	$0.77 \pm 0.24 \pm 0.15$
$K^*(892)^0\bar{K}^*(892)^0$	$0.45 \pm 0.25 \pm 0.07$
$p\bar{p}$	$2.73 \pm 0.21 \pm 0.33$
$\Lambda\bar{\Lambda}$	$2.14 \pm 0.31 \pm 0.26$
$\Sigma\bar{\Sigma}$	$1.11 \pm 0.38 \pm 0.25$
$\Xi\bar{\Xi}$	$0.83 \pm 0.28 \pm 0.12$
$K_1(1270)\bar{K}$	$7.6 \pm 0.9 \pm 1.5$
$K_1(1400)\bar{K}$	< 2.7 (90% C.L.)
$a_2\pi$	< 0.83 (90% C.L.)
$b_1\pi$	$4.1 \pm 0.6 \pm 1.0$
$\gamma\eta'$	$1.45 \pm 0.37 \pm 0.36$
$\gamma f_2(1270)$	$2.46 \pm 0.41 \pm 0.67$

4. Significant suppressions are seen for the first time in VT final states: ωf_2, $K^{*0}\bar{K}_2^{*0}+c.c.$ and $a_2\rho$ (see table 3).

Table 3: VT modes results

Decay Mode (X)	Upper Limit or Br($\times 10^{-4}$)	$Q = \frac{B(\psi(2S)\to X)}{B(J/\psi\to X)}$ (%)
$\omega f_2(1270)$	< 1.5	< 3.5
$K^{*0}\bar{K}_2^{*0} + c.c.$	< 1.79	< 2.8
$a_2\rho$	$3.1 \pm 1.5 \pm 1.1$	2.8 ± 1.8

Let us investigate the physics implication of these findings. From the standpoint of PQCD, $\psi(2S)(J/\psi)\to VT$ are allowed by Hadron Helicity Conservation (HHC) Theorem, whereas $\psi(2S)(J/\psi)\to VP$ are forbidden by HHC. Thus it seems not easy to find a common explanation for both cases.

According to QCD, there is a power suppression due to higher orbital-angular-momentum states $(1/E_{cm}^2)^\ell$. Therefore, for tensor mesons, $\ell = 1$, the suppression is

$$\frac{B(\psi(2S))}{B(J/\psi)} = \frac{M_{J/\psi}^2}{M_{\psi(2S)}^2} \approx 0.71.$$

This is obviously not large enough to account for observed effects in VT final states.

It is also noted that the axial-vector meson b_1 is also a state of $\ell = 1$; nevertheless, $\psi(2S) \to b_1\pi$ relative to J/ψ observes the *15% rule*. This may serve as a collateral evidence that the anomaly revealed in VT modes is not due to the tensor mesons in higher orbital angular states.

5. Enhancement is first observed in decays of $\psi(2S)$ into $K_1(1270)\bar{K}$ relative to the J/ψ in the context of the *15% rule* (for detail see S.Olsen's presentation).

6. A program for study more VP decays is started by analyzing such channels as $\omega\pi^0$, $\omega\eta$, $\phi\eta$, etc.

   Why it is interesting to measure the branching fraction for $\psi(2S) \to \omega\pi^0$? Here an isospin changing process is involved, probably with the three-gluons exchange and replaced by a highly virtual photon. It has been pointed out that $B(J/\psi \to \omega\pi^0) \approx 3 \times B(J/\psi \to \pi^+\pi^-)$. For helicity theorem to be valid at the J/ψ mass scale, one need to invoke a nearby hybrid $q\bar{q}g$ state for this $I = 1$ transition in addition to a vector glueball, and the situation becomes clearly more contrived.

   It would be therefore quite interesting to measure the branching fraction for $\psi(2S) \to \omega\pi^0$ and $\psi(2S) \to \pi^+\pi^-$ as well. If both channels obey *15% rule*, they are likely to be purely electromagnetic decays, and this would imply the failure of Helicity Theorem at this energy scale. If, however, the $\omega\pi^0$ mode of $\psi(2S)$ is substantially suppressed than that given by *15% rule*, then it might have some peculiar hadronic nature. A preliminary result is obtained to be

   $$B(\psi(2S) \to \omega\pi^0) = (6.7 \pm 1.4) \times 10^{-5},$$

   which satisfies the *15% rule* quite well.

3080 3090 3100 3110

7. A refined analysis on $e^+e^- \to \rho\pi$ scan across the J/ψ resonance has been performed using a maximum likelyhood method to test the vector glueball model. In fitting the $\rho\pi$ cross section $\sigma_{\rho\pi}$ to the data, the mass and total width of the vector glueball O, M_o, Γ_o, and its mixing angle with J/ψ, θ, as well as other three parameters are treated as free parameters, where M_O and Γ_O were limited to vary as $|M_O - M_{J/\psi}| \leq 80$MeV and $\Gamma_O \leq 160$MeV. The fits yield an upper limit on the ratio of the cross section due to the vector glueball O and its interference with the J/ψ, σ_{o+I}, to that corresponding to the normal J/ψ resonance, $\sigma_{J/\psi}$,

$$\sigma_{o+I}/\sigma_{J/\psi} < 0.098 \ (90\% \, C.L.)$$

at $M_{J/\psi}$; while

$$\sigma_{o+I}/\sigma_{J/\psi} > 51.5$$

from the experimental limit of $B(\psi(2S) \to \rho\pi)/B(J/\psi \to \rho\pi)$ and the 15% relation for the $\sigma_{J/\psi}$ contribution.

As can be seen in Fig.1 and Fig.2, the existence of such a VG is definitely excluded.

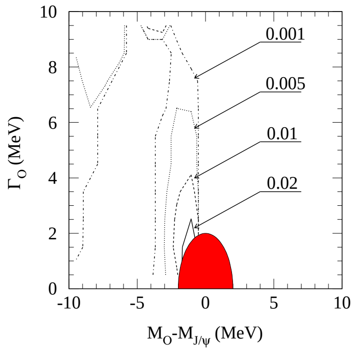

Fig.1: The contours of the fitted ratio $\sigma_{O+I}/\sigma_{J/\psi}$ for each pair of Γ_O and $M_O - M_{J/\psi}$ values. The shaded area is the insensitive region of this experiment. It is obvious that outside this region, the existence of the O to explain the anomalous $J/\psi \to \rho\pi$ can be ruled out.

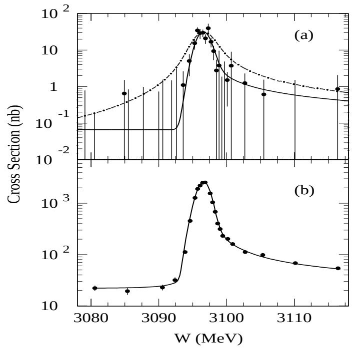

Fig.2: (a) The center-of-mass energy dependence of the $\rho\pi$ cross section resulting from the likelihood fit (solid curve), compared to the data corrected for the efficiency and background. The dotted-dashed curve is the expected cross section due to the O if its contribution is at the lower bound of relation (10) with $M_O = M_{J/\psi}$ and $\Gamma_O = 2$ MeV which corresponds to the limit of the experimental sensitivity. (b) The total cross section for $e^+e^- \to hadrons$.

A paper titled *Search for a vector glueball by a scan of the J/ψ resonance* has been submited to the Physical Review D and will appear soon.

Analyses on $\psi(2S) \to \pi^+\pi^-(\rho\pi)$ have also been made. It is yet to be decided if there is really some structure in $2 \sim 3\mathrm{GeV}/c^2$ $\rho\pi$ invariant mass region in this decay channel.

In conclusion, the experimental results from the BES show neither of the existing three models proposed to solve the $\rho\pi$ puzzle is satisfactory.

The puzzle thus remains big challenge to theoretical understanding in charmonium physics!

3.1.3 Radiative decays

Preliminary results on $B(\psi(2S) \to \gamma f_2(1270))$ and $B(\psi(2S) \to \gamma\eta')$ have been obtained (see table 4). It is interesting to note that a suppression relative to the *15% rule* occurs for the $\gamma\eta'$ channel, which is similar to $\rho\pi$ and $K^*\bar{K}$ (VP modes), but not for $\gamma f_2(1270)$ which is different from $\omega f_2(1270)$ (VT modes).

Table 4: Branching fractions of $\psi(2S)$ radiative decays

Decay Mode (X)	Branching fraction ($\times 10^{-4}$)	$Q = \frac{B(\psi(2S)\to X)}{B(J/\psi\to X)}$ (%)
$\gamma f_2(1270)$	$2.46 \pm 0.41 \pm 0.67$	17.8 ± 6.0
$\gamma\eta'$	$1.45 \pm 0.37 \pm 0.36$	3.4 ± 1.2

3.2 ^3P_J states

Although the charmonium P-wave states χ_c's were discovered soon after the J/ψ and $\psi(2S)$ in 1970's, the data on their decays are yet sparse. For a long time until 90's, only upper limits on their widths could be established, and very few decay modes for them could be studied.

Renewed interest in P-wave quarkonium states is aroused by recent development of NRQCD. New factorization method is derived for annihilation decay rates of S-wave, P-wave and higher orbital-angular-momentum states, which is the sum of a conventional term which takes into account the annihilation of the $Q\bar{Q}$ pair from a color siglet P-wave state and an additional term which involves the annihilation from a color octet S-wave state, and the infrared divergence countered in previous calculations are absorbed into the matrix element of this latter term. Therefore, P-wave quarkonium annihilations and productions provide new information on the nonperturbative part of QCD which is ignored to a great extent in the quark model description of the heavy quarkonia. One can use experimentally measured $\Gamma_{tot}(\chi_{c1})$ and $\Gamma_{tot}(\chi_{c2})$ to predict $\Gamma_{tot}(\chi_{c0})$, $\Gamma_{tot}(^1P_1)$. Precision measurement of $\Gamma_{tot}(\chi_{c0})$ thus provides stringent test of the theoretical prediction.

First measurement of χ_{c0} at the BES has been performed and yields interesting results as

$$\Gamma_{\chi_{c0}} = 15.0^{+3.2}_{-2.8} \text{ MeV},$$

and

$$B(\chi_{c0} \to p\bar{p}) = (14.5 \pm 3.9 \pm 3.1) \times 10^{-5}.$$

3.3 $^3S_0$ states

We have begun looking for η_c and $\eta_c(2S)$ in $\psi(2S)$ decays. the η_c signal is seen in $\psi(2S) \to \gamma\pi^+\pi^-\pi^+\pi^-$, $\psi(2S) \to \gamma\pi^+\pi^-K^+K^-$ and $\psi(2S) \to \gamma\pi^+\pi^-p\bar{p}$ (Fig.3).

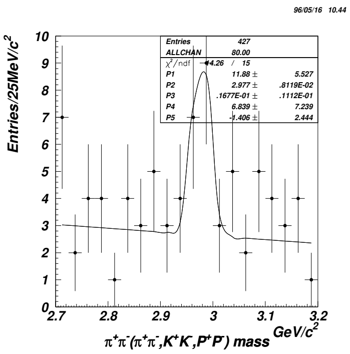

Fig.3: η_c signal

The following decay modes have been investigated for $\eta_c(2S)$ hunting: $\psi(2S) \to \gamma K\bar{K}\pi$, $\psi(2S) \to \gamma p\bar{p}$, $\psi(2S) \to \gamma\pi^+\pi^-\pi^+\pi^-$, $\psi(2S) \to \gamma\pi^+\pi^-K^+K^-$ and $\psi(2S) \to \gamma\pi^+\pi^-p\bar{p}$ (Fig.4).

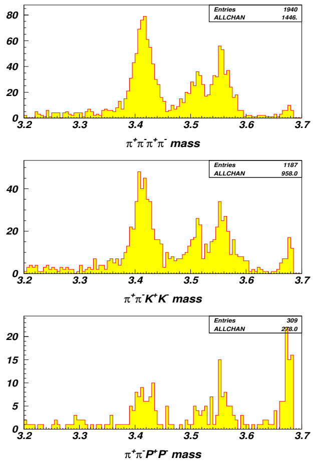

Fig.4: Hunting of the $\eta_c(2S)$

If CB observation is correct:

$$m = (3594 \pm 5)\mathrm{MeV},$$

$$\Gamma < 8\mathrm{MeV},$$

then one would see a shoulder-like effect in the higher mass side of the χ_{c2}. We are looking for such an effect.

4 Summary

- The number of $\psi(2S)$ is determined to be

$$3.6(1 \pm 10\%) \times 10^6.$$

- The knowledge of the charmonium hadronic decay puzzle has been greatly enriched
  - severe suppression in $\rho\pi$ and K^*K (VP)
  - significant suppression in ωf_2, $a_2\rho$ and $K^{*0}\bar{K}_2^{*0}$ + $c.c.$ (VT)
  - first enhancement in $K_1(1270)\bar{K}$
- All three models proposed to solve the $\rho\pi$ puzzle are disfavored, the puzzle remains open problem for theorists.
- First result on the width of χ_{c0} is presented, there is yet much to be done with χ_c's.
- Search for $\eta_c(2S)$ is underway; we would also keep an eye on the $^1P_1$.

Study of the P-wave charmonium state χ_{c0} in $\psi(2S)$ decays

Yuan Changzheng
Institute of High Energy Physics,
Beijing 100039

Abstract

$\gamma\pi^+\pi^-$, γK^+K^- and $\gamma p\bar{p}$ final states were studied with the $\psi(2S)$ data collected by BES/BEPC to measure the resonance parameters of the p-wave charmonium state χ_{c0}. The study gave the best estimate of the total width of χ_{c0} was $(15.0^{+3.2}_{-2.8})$MeV and the branching fractions of $\chi_{c0} \to p\bar{p}$ was $(14.5 \pm 3.9 \pm 3.1) \times 10^{-5}$. The branching fractions of $\chi_{cJ}(J = 0, 2)$ going to $\pi^+\pi^-$, K^+K^- and the branching fractions of $\chi_{cJ}(J = 1, 2)$ going to $p\bar{p}$ were measured too, the results were $B(\chi_{c0} \to \pi^+\pi^-) = (4.27 \pm 0.23 \pm 0.60) \times 10^{-3}$, $B(\chi_{c0} \to K^+K^-) = (3.44 \pm 0.21 \pm 0.47) \times 10^{-3}$, $B(\chi_{c2} \to \pi^+\pi^-) = (1.52 \pm 0.17 \pm 0.29) \times 10^{-3}$, $B(\chi_{c2} \to K^+K^-) = (5.2 \pm 1.1 \pm 1.8) \times 10^{-4}$, $B(\chi_{c1} \to p\bar{p}) = (8.3 \pm 2.9 \pm 2.7) \times 10^{-5}$ and $B(\chi_{c2} \to p\bar{p}) = (9.6 \pm 3.5 \pm 4.1) \times 10^{-5}$, where the first error was statistical and the second one systematic.

The charmonium p-wave triplet states $\chi_{cJ}(J = 0, 1, 2)$ were found in 1970's and most of their decay parameters were measured before 1980's. By studying the charmonium states formed directly in proton-antiproton annihilation, Fermilab experiment E-760 gave a precision measurement of the total widths of χ_{c1} and χ_{c2} in 1992 [1], but χ_{c0} was still not studied because of its small branching fraction of going to electromagnet final states and its large total width.

The only available data on the total width of χ_{c0} was reported by Crystal Ball (CBAL) [2], which was measured in two different ways – the inclusive process $\psi(2S) \to \gamma X$ (13-21MeV) and the exclusive process $\psi(2S) \to \gamma\pi^0\pi^0 \to 5\gamma$ $(8.8 \pm 1.3 \pm 1.5\text{MeV})$, agree within 2.2 standard deviations. By combining these two measurements, CBAL gave the best estimate of the natural linewidth of the χ_{c0} was $13.5 \pm 3.3 \pm 4.2$MeV. The decay of $\chi_{c0} \to p\bar{p}$ was forbidden by the massless helicity conservation law, the only measurement of its branching fraction is an upper limit, with 90% confidence level, $B(\chi_{c0} \to p\bar{p}) < 9.0 \times 10^{-4}$.

Beijing Spectrometer (BES) running at Beijing Electron Positron Collider (BEPC) collected $3.5(1 \pm 0.10)$ million $\psi(2S)$'s in its 1993/94 and 1995 running. In this paper we report a measurement of the total width of χ_{c0} and the branching fraction of $\chi_{c0} \to p\bar{p}$ with these data.

The BES is a conventional cylindrical detector that is described in detail in Ref. [3]. A four-layer central drift chamber (CDC) surrounding the beampipe provides trigger information. A forty-layer main drift chamber (MDC), located radially outside the CDC, provides trajectory and energy loss (dE/dx) information on charged tracks over 85% of the total solid angle. The momentum resolution is $\sigma_p/p = 0.017\sqrt{1+p^2}$ (p in GeV/c), and the dE/dx resolution for hadron tracks is $\sim 11\%$. An array of 48 scintillation counters surrounding the MDC measures the time-of-flight (TOF) of charged tracks with a resolution of ~ 450 ps for hadrons. Outside the TOF system, a 12 radiation length, lead-gas barrel shower counter (BSC), operating in self-quenching streamer mode, measures the energies of electrons and photons over $\sim 80\%$ of the total solid angle with an energy resolution of $\sigma_E/E = 22\%/\sqrt{E}$ (E in GeV), and spatial resolutions of $\sigma_\phi = 7.9$ mrad, $\sigma_z = 3.6$ cm. Surrounding the BSC is a solenoidal magnet coil that provides a 0.4 Tesla magnetic field throughout the central tracking region of the detector. Three double layers of muon counters instrument the magnet flux return and serve to identify muons of momentum greater than 0.5 GeV/c. Endcap time-of-flight and shower counters extend coverage to the forward and backward regions.

The most important techniques in determination of the total width of a resonance include two aspects: purely selected events and well determined mass resolution. The former make sure that the lineshape of the resonance is not distorted and the latter ensures that the width of the resonance determined is reliable.

To satisfy the above two requirements, the paired pseudoscalar mesonic decay modes of χ_{cJ} ($\pi^+\pi^-$ and K^+K^-) are used in our analysis, because it has the following advantages: 1. With four constrained kinematic fit, we can get relatively pure events. Although the cross contamination of the two channels we studied is inevitable, we can remove the contamination reliably according to Monte Carlo and the distributions got from data sample, so to get a pure distribution of each decay mode. 2. The Monte Carlo sometimes cannot describe the detector very well because the data taking procedure always going on for a long period of time and status of the detector changes much, while the Monte Carlo can only simulate the detector performance of some certain status. It will be risky to use the mass resolution completely determined from Monte Carlo. Instead in our analysis the mass resolution at χ_{c2} mass region was fitted out with the precisely measured width of χ_{c2} as input [4], and then it was used to calibrate the mass resolution function got from Monte Carlo simulation to give the mass resolution expected at χ_{c0} mass region, by fitting χ_{c0} with the mass resolution determined in this way, the reliable line width of χ_{c0} could be got. 3. The procedure of calibrating mass resolution function can not be used in some other decay modes of χ_{cJ}s although the branching fractions are larger, because χ_{c1} lies in the lower mass side of χ_{c2} and the possible existing η_c' lies in the higher mass side will fold together with χ_{c2} to make the procedure of getting the mass resolution χ_{c2} become very complicated. However, in the two modes selected, the J^Ps of χ_{c0} and χ_{c2} are $even^+$ while that of χ_{c1} and η_c' are 1^+ and 0^-, the decay of χ_{c1} and η_c' to 0^-0^- is forbidden by parity conservation, so we can get χ_{c0} and χ_{c2} resonances without any distortion due to the contamination from other resonances.

Events selection includes the identification of good photon, good charged tracks and separation of the events.

A neutral cluster is regarded as an photon candidate when its energy deposited in BSC greater than 50MeV and the cosine of the angle to the nearest charged track less than 0.96; the first hit of the cluster should be in the first three layers (about 3r.l.) of BSC and the hit cells at least in two layers. After identification, at least one and at most three photon candidates are allowed in one events. The candidate has the largest SC energy is considered to be the photon radiated from $\psi(2S)$.

The number of charged tracks in the events is required to be two with net charge zero and each track with high quality in track fitting; momentum of each track should greater than 1.0GeV/c and $|\cos\theta| < 0.8$, where θ is the polar angle relatives to the beam axis; to remove events with electron or with muon, we require at least one of the two tracks with $|\cos\theta| < 0.6$ and the total SC energy of the two charged tracks less than 1.4GeV and $Mustatus^+ + Mustatus^- < 3$ [5]; TOF and dE/dx information is used for charged particle identification. The probabilities of the particle to be identified as a pion, kaon and proton were assigned to each track ($Prob_\pi, Prob_K, Prob_p$), both tracks must have $Prob_\pi > 0.01$ (for $\pi^+\pi^-$) or $Prob_K > 0.01$ (for K^+K^-); define $umiss = Emiss - Pmiss$, the difference between missing energy and missing momenta of the charged tracks, we require it lies in $\pm 2.575\sigma$ ($Prob_\pi^{umiss} > 1\%$ for $\pi^+\pi^-$ or $Prob_K^{umiss} > 1\%$ for K^+K^-) of the expected distribution of $umiss$; do four constrained kinematic fit to $\psi(2S) \to \gamma\pi^+\pi^-$ and $\psi(2S) \to \gamma K^+K^-$ with the photon candidate and the two charged tracks, the probability of the fit P^{χ^2} should greater than 1%.

To separate $\gamma\pi^+\pi^-$ and γK^+K^- from each other, we define

$$Prob_{all}^{\pi^+\pi^-} = Prob_\pi^+ \cdot Prob_\pi^- \cdot Prob_\pi^{umiss} \cdot P_\pi^{\chi^2}$$

and

$$Prob_{all}^{K^+K^-} = Prob_K^+ \cdot Prob_K^- \cdot Prob_K^{umiss} \cdot P_K^{\chi^2}.$$

If $Prob_{all}^{\pi^+\pi^-} > 2 \cdot Prob_{all}^{K^+K^-}$ the event is regarded as a $\gamma\pi^+\pi^-$ event, and if $Prob_{all}^{K^+K^-} > 2 \cdot Prob_{all}^{\pi^+\pi^-}$ is a γK^+K^- event.

After posing all above selections to the data, fitting of the mass plots of $\pi^+\pi^-$ and K^+K^- with two Breit-Wigners folding a gaussian like mass resolution (all parameters free) shows that the mass of χ_{c0} and χ_{c2} in $\pi^+\pi^-$ mass plot is lower than the world average while that in K^+K^- mass plot is higher, which means that the events in our two samples are cross contaminated and the contaminated parts should be removed before fitting to get χ_c parameters.

We use Monte carlo simulation to get the probabilities of cross contamination of the two channels as well as the detection efficiencies and mass resolution. In the Monte carlo generator, the χ_{cJ}s are assumed to be generated via pure E1 transition of $\psi(2S)$ citee1, χ_{cJ} decaying to 0^-0^- meson pairs has only one independent helicity amplitude and so the whole process is determined. Events at different meson pair mass between 3.3 and 3.6GeV with a step of 10 to 30MeV and zero width were generated, assuming χ_{c1} is absolutely missing, the spin-parity of the resonance is assigned to 0^+

when mass less than 3.5GeV and to 2^+ when mass greater then 3.5GeV. After requiring the events satisfy the same selection criteria as for data, the detection efficiency, the probability of cross contamination and the mass resolution at each mass are got. Fitting all these values to the generated mass of meson pair, we get the detection efficiency, the probability of cross contamination and the mass resolution as a function of the mass of meson pair.

After selection, besides the $\pi^+\pi^-$ mass plot of $\gamma\pi^+\pi^-$ and K^+K^- mass plot of γK^+K^- events, we can also calculate the K^+K^- mass of $\gamma\pi^+\pi^-$ candidates and $\pi^+\pi^-$ mass of γK^+K^- candidates, the latter two plots show us the mass distribution of the cross contamination, subtract these two plots (after renormalized to the events may contaminate calculated from Monte Carlo) from the former ones, the distributions of pure events are got. Correct them with the detection efficiency functions, the produced forms of $\psi(2S) \to \gamma\chi_{cJ} \to \gamma\pi^+\pi^-$ or γK^+K^- are then obtained. The procedure can be expressed with the following formula:

$$X^{prod} = \frac{X^{obs} - \frac{Prob_X^Y}{\varepsilon_Y} Y_X^{obs}}{\varepsilon_X}$$

where X^{obs}, X^{prod} are observed and produced events of γX channel, Y_X^{obs} is the observed mass plots of γY channel but the mass is calculated using the meson mass of γX channel, ε_X is the detection efficiency of γX channel, and $Prob_X^Y$ is the probability of γY channel events misidentified as γX channel events, X and Y are $\pi^+\pi^-$ or K^+K^-. It should be noted that the operations in above formula is used for plots, or the events in each bin of the plots.

The resonance we observed in the experiment is a Breit-Wigner folds a gaussian like mass resolution, caused by detector resolution, event kinematic fit procedure etc.. In the plots got above, there are two obvious resonances with almost none background, we estimate the mass resolution of the process we studied to be proportion to the resolution got from Monte Carlo, namely $\sigma(m) = cons_\sigma \cdot \sigma^{MC}(m)$ and the background of the shape of a first order polynomial, the mass plots were fitted with the following function:

$$\begin{aligned} f(m) = \int_0^\infty dx \quad & \{(\frac{cons_{\chi_{c0}}\Gamma^2_{\chi_{c0}}}{(x-m_{\chi_{c0}})^2 - (\frac{\Gamma_{\chi_{c0}}}{2})^2} + \frac{cons_{\chi_{c2}}\Gamma^2_{\chi_{c2}}}{(x-m_{\chi_{c2}})^2 - (\frac{\Gamma_{\chi_{c2}}}{2})^2}) \\ & \cdot \frac{1}{\sigma(x)} e^{-\frac{1}{2}(\frac{m-x}{\sigma(x)})^2}\} + poly_0 + poly_1 \cdot m \end{aligned}$$

where $cons_{\chi_{c0}}$ and $cons_{\chi_{c2}}$, $m_{\chi_{c0}}$ and $m_{\chi_{c2}}$, $\Gamma_{\chi_{c0}}$ and $\Gamma_{\chi_{c2}}$ are the normalization factors, masses and widths of χ_{c0} and χ_{c2} respectively, $poly_0$ and $poly_1$ are the coefficients of the background polynomial and $cons_\sigma$ is the factor between the mass resolution of data and that of Monte Carlo.

Fix $\Gamma_{\chi_{c2}} = 2.00$MeV which was precisely measured by other experiments [4] and let other parameters free, fitting the plots with above function using maximum likelyhood method, we get $\Gamma_{\chi_{c0}} = 15.0 \pm 1.5$MeV from $\psi(2S) \to \gamma\pi^+\pi^-$, fit also gives $cons_\sigma = 1.21$

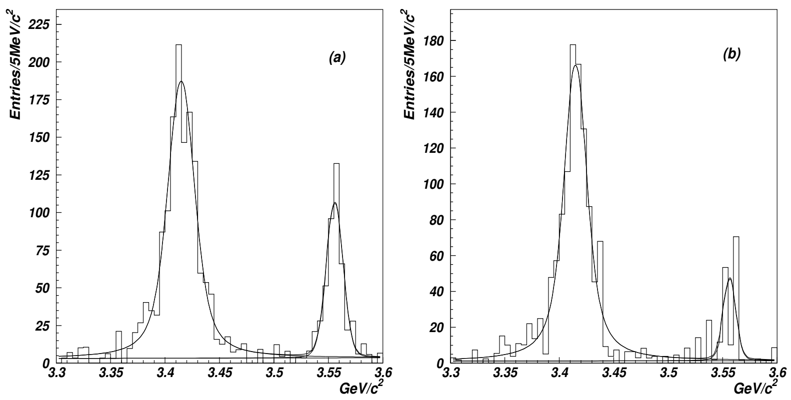

Figure 1: Fitted results of the mass plots, a) $\gamma\pi^+\pi^-$, b) γK^+K^-.

which means that the mass resolution estimated from Monte Carlo is about 20% smaller than the real one.

The results got from fitting K^+K^- mass plot of $\psi(2S) \to \gamma K^+K^-$ is not very reliable because of the limited statistics of $\psi(2S) \to \gamma\chi_{c2} \to \gamma K^+K^-$ (so we only use the $\Gamma_{\chi_{c0}}$ value fitted from $\pi^+\pi^-$ channel in the following discussion), but it in agreement with that got from $\pi^+\pi^-$ channel: $\Gamma_{\chi_{c0}} = 15.8 \pm 1.3$MeV and $cons_\sigma = 0.94$. The error quoted in $\Gamma_{\chi_{c0}}$ is from the fitting procedure only. The mass plots and fitted results are shown in figure 1 .

The events number of $\chi_{cJ} \to \pi^+\pi^-$ and K^+K^- are also fitted out for determination of the branching fractions of each channel. we got $n^{prod}_{\chi_{c0}\to\pi^+\pi^-} = 1390 \pm 74$, $n^{prod}_{\chi_{c0}\to K^+K^-} = 1121 \pm 70$, $n^{prod}_{\chi_{c2}\to\pi^+\pi^-} = 414 \pm 45$ and $n^{prod}_{\chi_{c2}\to K^+K^-} = 141 \pm 29$, where the error is statistical.

To select $\gamma p\bar{p}$ events, the same selection criteria are used for photon identification and charged tracks selection except that to remove radiative Bhabha and radiative dimu events we only require the SC energy of the positive track less than 0.7GeV or that of the negative track less than 0.8GeV and $Mustatus^+ + Mustatus^- < 3$; to identify the proton and anti-proton tracks, we require both tracks satisfy $prob_p > 0.05$ and at least one track $prob_p > prob_\pi$ and $prob_p > prob_K$. Do 4C-fit to $\psi(2S) \to \gamma p\bar{p}$ looping over all the photon candidates and the one combination with largest probability is kept and the χ^2 probability of the fit is required to be greater than 5%. After above selection, the invariant mass of proton and anti-proton is shown in figure 2, clear χ_c states can be seen in the plot, after background subtraction (from the lower and higher sides of the mass plot), 14.1 ± 3.8, 8.3 ± 2.9 and 7.5 ± 2.7 events are got for χ_{c0}, χ_{c1} and χ_{c2} respectively.

Assuming the χ_{cJ} states are got via pure E1 transition of $\psi(2S)$, and the independent helicity amplitudes of charmonium decays to $p\bar{p}$ are equal, detection efficiencies of the three channels are $\varepsilon_{\chi_{c0}} = 29.8\%$, $\varepsilon_{\chi_{c1}} = 32.8\%$ and $\varepsilon_{\chi_{c2}} = 28.5\%$.

The error of $\Gamma_{\chi_{c0}}$ may arise from the uncertainty of $\Gamma_{\chi_{c2}}$ which is used for mass resolution calibration, vary $\Gamma_{\chi_{c2}}$ a standard deviation from the nominal value, leads a deviation of $\Gamma_{\chi_{c0}}$ about 5%. Choosing of the bin width in the mass plot (from 5MeV to 2.5MeV or to 10MeV) cause a relative error of $+7\%$ or -1%, varying selection criteria

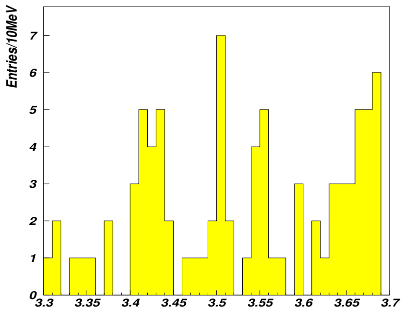

Figure 2: $p\bar{p}$ mass distribution of $\psi(2S) \to \gamma p\bar{p}$

Table 1: Branching ratios of $\chi_{cJ} \to p\bar{p}$

decay modes	Branching Fractions($\times 10^{-5}$)	Observed Events
$\chi_{c0} \to p\bar{p}$	$14.5 \pm 3.9 \pm 3.1$	14.1 ± 3.8
$\chi_{c1} \to p\bar{p}$	$8.3 \pm 2.9 \pm 2.7$	8.3 ± 2.9
$\chi_{c2} \to p\bar{p}$	$9.6 \pm 3.5 \pm 4.1$	7.5 ± 2.7

a standard deviation from the values used, contribute +17% or −15% totally. Add all these errors and the error caused by the fitting procedure in quadrature, the total percentage error of $\Gamma_{\chi_{c0}}$ is +21% in the upper side and −19% in the lower side.

The systematic errors of the branching fractions arise from selection criteria are 4.7%, 3.6%, 13% and 31% for $B(\chi_{c0} \to \pi^+\pi^-)$, $B(\chi_{c0} \to K^+K^-)$, $B(\chi_{c2} \to \pi^+\pi^-)$ and $B(\chi_{c2} \to K^+K^-)$, and 13%, 29% and 41% for $B(\chi_{c0} \to p\bar{p})$, $B(\chi_{c1} \to p\bar{p})$ and $B(\chi_{c2} \to p\bar{p})$; the errors caused by the uncertainty of total events number are 10% for all the channels; the uncertainty of $B(\psi(2S) \to \gamma\chi_{cJ})$ cause 8.6% error to χ_{c0} decay channels, 9.2% error to χ_{c1} decay channels and 10.3% error to χ_{c2} decay channels. Add all these errors in quadrature, the total percentage errors of $B(\chi_{c0} \to \pi^+\pi^-)$, $B(\chi_{c0} \to K^+K^-)$, $B(\chi_{c2} \to \pi^+\pi^-)$ and $B(\chi_{c2} \to K^+K^-)$ are 14%, 14%, 19% and 35% respectively, and those of $B(\chi_{c0} \to p\bar{p})$, $B(\chi_{c1} \to p\bar{p})$ and $B(\chi_{c2} \to p\bar{p})$ are 21%, 33% and 42% respectively.

Combining above analysis, we got

$$\Gamma_{\chi_{c0}} = 15.0^{+3.2}_{-2.8}\mathrm{MeV},$$

this result is consistent with the world average, but with high precision. Compared with the theoretical predictions, it is consistent with the expectation of Ref. [7] but has large discrepancy to that of Ref. [8].

The results of the branching fractions of χ_{cJ} decays are listed in table 1 and table 2.

The branching fractions of $\chi_{c1} \to p\bar{p}$ and $\chi_{c2} \to p\bar{p}$ are in agreement with the values

Table 2: Branching ratios of $\chi_{cJ} \to 0^-0^-$

decay modes	Branching Fractions($\times 10^{-3}$)	Observed Events
$\chi_{c0} \to \pi^+\pi^-$	$4.27 \pm 0.23 \pm 0.60$	350 ± 19
$\chi_{c0} \to K^+K^-$	$3.44 \pm 0.21 \pm 0.47$	258 ± 16
$\chi_{c2} \to \pi^+\pi^-$	$1.52 \pm 0.17 \pm 0.29$	84 ± 9
$\chi_{c2} \to K^+K^-$	$0.52 \pm 0.11 \pm 0.18$	24 ± 5

listed by PDG [4], which is got from $p\bar{p}$ experiment and with small error; $B(\chi_{c0} \to p\bar{p})$ is the first measurement in the world, which is consistent with the upper limit of PDG.

Backgrounds from $\psi(2S) \to \gamma\chi_{cJ} \to \gamma p\bar{p}$ are negligible according to Monte Carlo study. Backgrounds from $\psi(2S) \to \pi^+\pi^-\pi^0$ and $\psi(2S) \to K^+K^-\pi^0$ are estimated to be negligible according to their decay branching fractions.

References

[1] T.A.Armstrong et al., Phys.Rev.Lett. **68** (1992) 1468.

[2] J.E.Gaiser et al., Phys.Rev., **D34** (1986) 711.

[3] BES Collab., Nucl. Inst. Meth., **A344** (1994) 319.

[4] Particle Data Group, Phys.Rev., **D50** part I (1994) and references therein.

[5] BES Collab., High Ener. Phys. and nucl. Phys. (in Chinese), **20** (1996) 97.

[6] G.Karl, S.Meshkov and J.L.rosner, Phys.Rev., **D13** (1976) 1203;
W.Tanenbaum et al., Phys.Rev., **D17** (1978) 731;
M.Oreglia et al., Phys.Rev., **D25** (1982) 2259.

[7] W.Kwong, P.B.Mackenzie, R.Rosenfeld and J.L.Rosner, Phys.Rev., **D37** (1988) 3210.

[8] G.T.Bodwin, E.Braaten and G.P.Lepage, Phys.Rev., **D46** (1992) 1914.

Number of ψ' Events and Studies of $\psi' \to \pi^+\pi^- J/\psi$, $J/\psi \to l^+l^-$

F. A. Harris
Department of Physics and Astronomy
The University of Hawaii
2505 Correa Road
Honolulu, HI 96822
USA

Introduction

The number of ψ' events obtained by BES is important to all ψ' analyses. In this paper, the determination of the number of ψ' events found in both the 1993 and the 1995 ψ' data will be summarized. In addition, events from $\psi' \to \pi^+\pi^- J/\psi$, $J/\psi \to l^+l^-$ will be used to study the process $\psi' \to \pi^+\pi^- J/\psi$. This paper is an update of continuing work that was reported at the 1995 BES Annual Meeting[1].

Number of ψ'

The approach of IHEP[2] is followed. The idea is to use $\psi' \to \pi^+\pi^- J/\psi, J/\psi \to$ anything. The mass recoiling against the π's is plotted, and the J/ψ peak is used to determine the number of J/ψ events, $N_{J/\psi}$, and

$$N_{\psi'} = \frac{N_{J/\psi}/\epsilon}{B(\psi' \to \pi^+\pi^- J/\psi)}$$

ϵ is the acceptance for the π's in $\psi' \to \pi^+\pi^- J/\psi$, determined using a Monte Carlo[3], and B is the branching ratio for this process.

The data are reconstructed in Hawaii using version 8.6 of the BES software. Previously slightly different cuts from those at IHEP were used, but in the present analysis, the cuts are very similar to facilitate closer comparison of results. Also the efficiency has now been completely determined.

The analysis loops over all possible $\pi^+\pi^-$ combinations where the π's have:

1. good run (ppruns: status $>$ 0 or 1).

2. mfit = 2, -9, or -19.

3. $|\cos\theta| < 0.75$.

4. $p_\pi < 0.5GeV/c$. p_π is the π momentum.

5. $pxy_\pi > 0.1GeV/c$. pxy_π is the momentum transverse to the beam direction.

6. $\Sigma Hit_\pi^{dE/dx} > 13$. $\Sigma Hit_\pi^{dE/dx}$ is the number of hits used in the dE/dx calculation.

7. $|\chi_\pi^{dE/dx}| < 3.0$. $\chi_\pi^{dE/dx} = \frac{(dE/dx)_meas-(dE/dx)exp}{\sigma}$

8. $m_{\pi\pi} > 0.35GeV/c^2$ to eliminate gamma conversions.

The track momenta are corrected by the magnetic field correction (0.9970*p)[4] and the beam pipe correction. The invariant mass of the two π's, $m_{\pi\pi}$, is calculated, and $m_{\pi\pi}$ is required to be greater than $0.35GeV/c^2$ to eliminate γ conversions. The mass recoiling against the π's, $rcmass$, is calculated, and the $rcmass$ distribution is fitted using MinFit[5] to determine the amount of J/ψ signal and background, as shown in Fig. 1. The J/ψ line shape is determined from $\psi' \rightarrow \pi^+\pi^- J/\psi$ events, where $J/\psi \rightarrow l^+l^-$. A polynomial is used to describe the background.

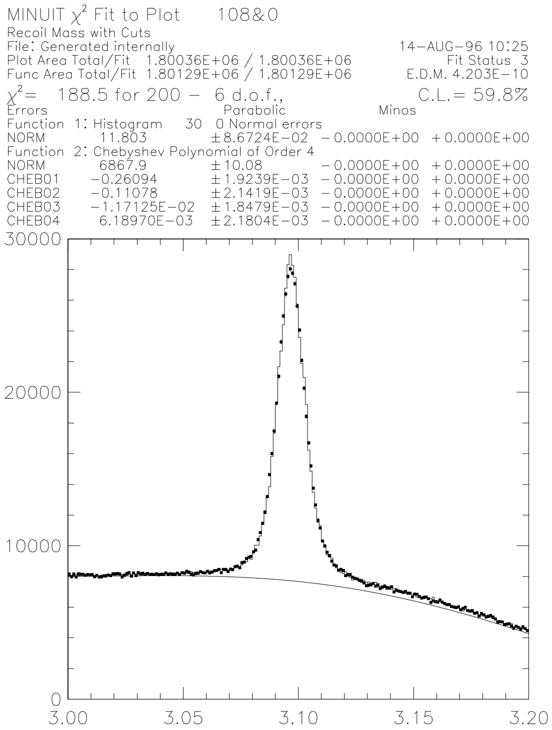

Figure 1: Number of events versus $rcmass$, the mass recoiling against the two π's. The points with error bars are the 1995 data, and the histogram is the sum of the line shape obtained from $\psi' \rightarrow \pi^+\pi^- J/\psi, J/\psi \rightarrow l^+l^-$ and a forth order polynomial to represent background. Note that Minfit allows fitting with histograms.

Results

Results for $N_{J/\psi}$, ϵ, and $N_{\psi'}$ are given in Table 1 for the 1994 and 1995 data sets and for $status > 0$ and $status > 1$. The dominant error is due to $B(\psi' \rightarrow \pi^+\pi^- J/\psi)$.

Table 1: $N_{J/\psi}$, ϵ, and $N_{\psi'}$ Results

Data	Status	ϵ	$N_{J/\psi}$	$N_{\psi'}$
1994	> 1	0.466	197541 ± 1567	$(1.30 \pm 0.01 \pm 0.13) \times 10^6$
1995	> 1	0.472	363036 ± 2728	$(2.36 \pm 0.02 \pm 0.22) \times 10^6$
1994	> 0	0.466	202893 ± 1586	$(1.34 \pm 0.01 \pm 0.13) \times 10^6$
1995	> 0	0.472	376966 ± 2789	$(2.45 \pm 0.02 \pm 0.23) \times 10^6$

Study of $\psi' \rightarrow \pi^+\pi^- J/\psi$, $J/\psi \rightarrow l^+l^-$

The $\psi' \rightarrow \pi^+\pi^- J/\psi$, $J/\psi \rightarrow l^+l^-$ sample is extremely important. As mentioned previously, it is used to determine the line shape of the J/ψ peak in the $rcmass$ distribution in the determination of the number of ψ' events. This sample can also be used to determine the J/ψ leptonic branching ratios, as well as study the physics of the $\psi' \rightarrow \pi^+\pi^- J/\psi$ process. The branching ratio $B(J/\psi \rightarrow ll) \simeq 6.0$ %.

An advantage of this channel is that the events are very clean. The π's in this process have low momentum, while the leptons have high momentum. The low energy tracks are used to determine "$rcmass$" (mass recoiling against the $\pi\pi$ system). The high energy tracks are used to determine "$ivmass$" (l^+l^- invariant mass). By cutting on both $rcmass$ and $ivmass$ and using particle identification (PID) for the leptons, a very clean sample of events is obtained.

In addition to the π cuts mentioned above, the following cuts are made in the event selection:

1. 4 prongs: 2 positive and 2 negative.
2. $|m_{J/\psi} - rcmass| < 0.1 GeV$.
3. $|m_{J/\psi} - ivmass| < 0.25 GeV$.
4. PID: For $\mu\mu$ decay, require $|\cos\theta| < 0.65$ and two muon layers be hit for at least one track. For ee decay, require $E > 0.8$ GeV for at least one track.

For the combined 94 and 95 data sets, 14481 e^+e^- and 17507 $\mu^+\mu^-$ events satisfy cuts.

The Monte Carlo generator used is PPGEN. A total of 100,000 (153 realization) plus 177,000 (154 realization) Monte Carlo events are generated each for e^+e^- and

$\mu^+\mu^-$. A total of 25725 (153) and 46019 (154) Monte Carlo $\mu^+\mu^-$ events satisfied cuts, while 21281 (153) and 37537 (154) Monte Carlo e^+e^- events satisfied cuts.

The Monte Carlo[6] assumes:

1. The orbital angular momentum between $\pi\pi$ system and J/ψ and between π's in the $\pi^+\pi^-$ system is 0.

2. The mass of the $\pi\pi$ system is weighted towards high mass.

$$\frac{d\sigma}{dm_{\pi\pi}} \propto \text{phase space} \times (M^2_{\pi\pi} - 4m^2_\pi)^2$$

3. Sequential 2-body decays: $\psi' \to X + J/\psi$, $X \to \pi^+\pi^-$, and $J/\psi \to l^+l^-$.

4. X and J/ψ are uniformly distributed.

5. π's are uniformly distributed in X rest frame.

6. Leptons have $1 + \cos^2\theta$ distribution in J/ψ rest frame.

7. J/ψ decay has α^3 order final state radiative correction in CMS of J/ψ.

Before comparing with Monte Carlo data, we correct the data distributions for detection efficiency. Monte Carlo events were used to determine a bin by bin efficiency correction, which was used to correct the data distributions.

Comparisons of the corrected $m_{\pi\pi}$ invariant mass distribution and various corrected angular distributions with Monte Carlo data are shown in Fig. 2. The excess at low $m_{\pi\pi}$ in Fig. 2a is due to gamma conversions. Fig. 2b shows the cosine of the angle between the e^+ and the beam direction in the rest frame of the J/ψ. The data agree well with the $1 + \cos^2\theta$ distribution assumed by the Monte Carlo. Fig. 2c shows the distribution of the cosine of the angle of the dipion system in the lab frame, and the data are consistent with being uniform in $\cos\theta$. Fig. 2d shows the distribution of the cosine of the angle between the π^+ and the J/ψ in the $\pi\pi$ rest frame. The agreement between the data and the Monte Carlo data here is not very good, indicating that the pions are not purely S wave.

We can use the $\cos\theta$ distribution in Fig. 2d and the $m_{\pi\pi}$ invariant mass distribution in Fig. 2a to test various Heavy Quarkonium Models, which were presented at the 1995 BES Annual Meeting [7]. Two non-perturbative models described were the Phenomenological Constituent Quark model of Tung-Mow Yan [8] and the Scale Anomaly model of Voloshin, Zakharov, Novikov, and Shifman [9]. The two models are the same at the level of second order color electric dipole transitions and can be shown to yield the following equations for the $m_{\pi\pi}$ invariant mass spectrum and the $\cos\theta$ distribution [7]:

$$f_1(q) \propto |\vec{q}|\sqrt{(q^2 - 4m^2_\pi)}\{[q^2 - \kappa(\Delta M)^2(1 + \frac{2m^2_\pi}{q^2})]^2$$

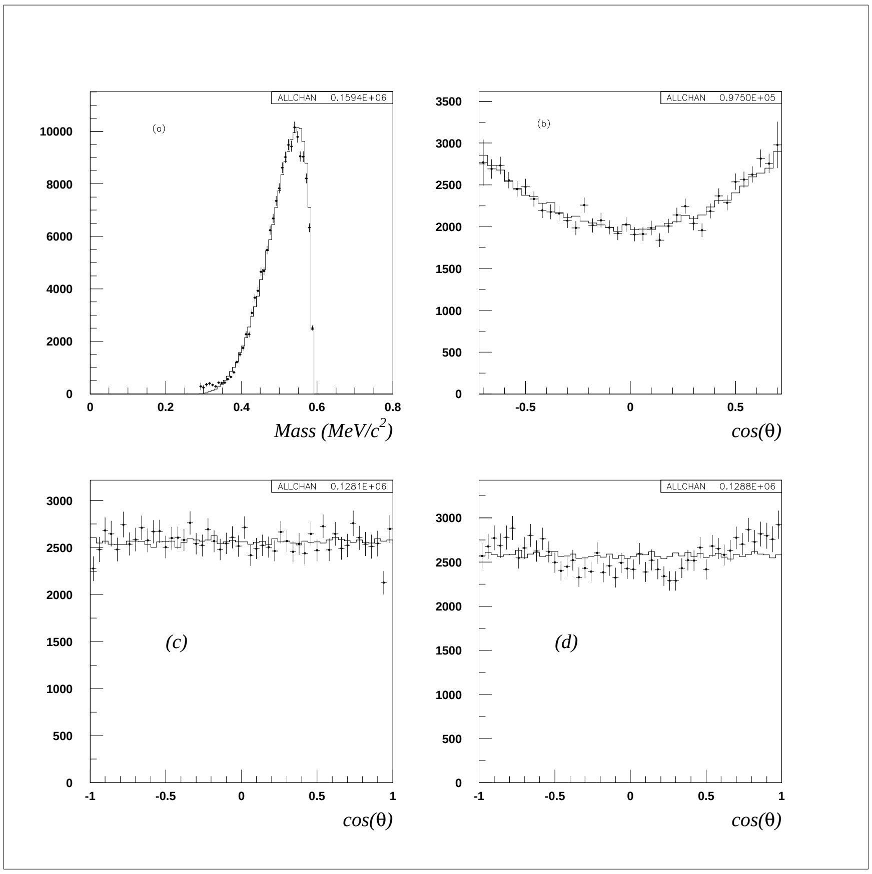

Figure 2: Distributions of $\psi' \to \pi^+\pi^- J/\psi, J/\psi \to l^+l^-$ events corrected for detection efficiency. Points with error bars correspond to data (1994 and 1995 combined); histogram corresponds to Monte Carlo data. **a)** Invariant mass of the dipion system. **b)** Cosine of the l^+ with respect to the beam direction in the J/ψ rest frame. **c)** Cosine of the dipion system in the lab. **d)** Cosine of the angle between the π^+ and the J/ψ in the dipion rest frame.

$$+0.2\kappa^2[(\Delta M)^2 - q^2]^2(1 - \frac{4m_\pi^2}{q^2})^2\}$$

$$g_1(\cos\theta) \propto \{0.9541 - 3.5276\kappa + 3.824\kappa^2 + 0.8451\kappa(\cos^2\theta - \frac{1}{3})$$

$$-1.9034\kappa^2(\cos^2\theta - \frac{1}{3}) + 0.2644\kappa^2(\cos^2\theta - \frac{1}{3})^2\}$$

where $\Delta M = M_{\psi'} - M_{J/\psi}$ and q is the four momentum of the dipion system. The fit to the first distribution is shown in Fig. 3a and yields $\kappa = 0.164 \pm 0.003$ and $\chi^2/DOF = 3.4$. The fit to the second distribution is shown in Fig. 3b and yields $\kappa = 0.135 \pm 0.019$ and $\chi^2/DOF = 0.84$. The fit is consistent a small D wave contribution in the decay. A fit to a flat $\cos\theta$ distribution gives a $\chi^2/DOF = 1.67$.

The χ^2 for the first fit is rather large. However, Cahn [10] points out that final state interactions affect the $m_{\pi\pi}$ distribution, so fitting this distribution without taking them into consideration may produce spurious results.

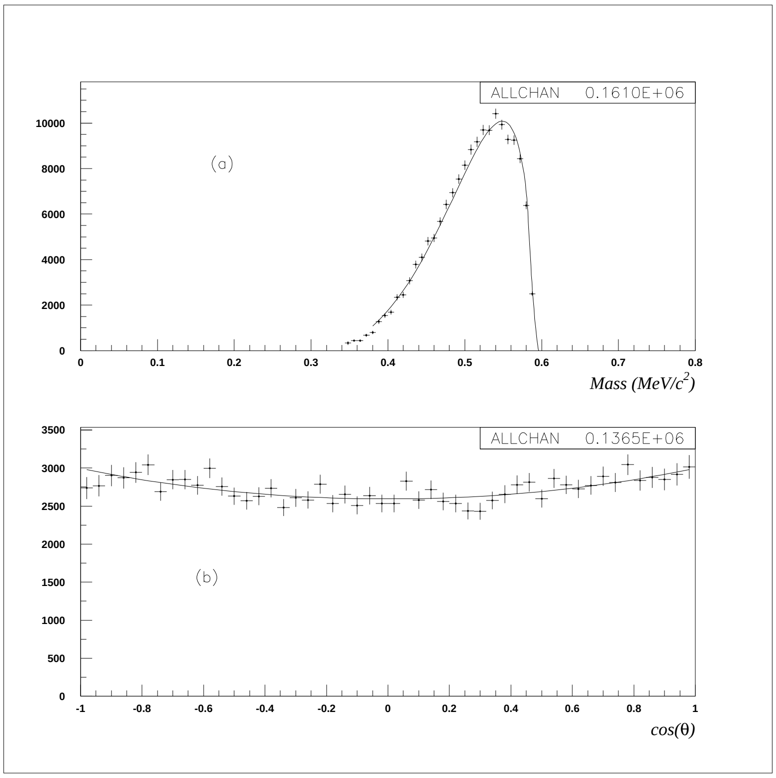

Figure 3: Distributions of $\psi' \to \pi^+\pi^- J/\psi$, $J/\psi \to l^+l^-$ events, which are corrected for detection efficiency. **a)** Invariant mass of the dipion system. **b)** Cosine of the angle between the π^+ and the J/ψ in the dipion rest frame. Points with error bars correspond to data (1994 and 1995 combined); smooth curve corresponds to the fits of $f_1(q)$ and $g_1(\cos\theta)$, respectively. The fit to the former excludes the reqion below $m_{\pi\pi} = 0.38$.

Summary

The current status of the determination of $N_{\psi'}$ has been given. Also $\psi' \to \pi^+\pi^- J/\psi$, $J/\psi \to l^+l^-$ events are used to investigate the process $\psi' \to \pi^+\pi^- J/\psi$. Some D wave contribution is indicated in the distribution of the cosine of the angle between the π^+ and the J/ψ in the $\pi\pi$ rest frame. Fits to this distribution and to the $m_{\pi\pi}$ distribution are made using non perturbative Heavy Quarkonium models. The results are preliminary.

References

[1] Harris, F. A., "Monte Carlo - Data Comparison of $\psi(2S) \rightarrow \pi^+\pi^- J/\psi$, $J/\psi \rightarrow l^+l^-$ and the Number of ψ' Events", BES95, 333 (1995).

[2] Li, Jin, "Recent Results on ψ' and J/ψ from the BES Experiment at BEPC", Submitted to Glasgow Meeting, July 1994. This method has also been described in the drafts of $\psi' \rightarrow \tau^+\tau^-$.

[3] The method used to determine the efficiency for $\psi' \rightarrow \pi^+\pi^- J/\psi$ is described in "Determination of the J/ψ Leptonic Branching Fraction via $\psi(2S) \rightarrow \pi^+\pi^- J/\psi$", draft of Oct. 94.

[4] This magnetic field correction was determined from the distribution for the mass recoiling against the $\pi\pi$ system ($rcmass$) for $\psi' \rightarrow \pi^+\pi^- J/\psi$, $J/\psi \rightarrow \mu^+\mu^-$. See http://www.phys.hawaii.edu/fah/www/fah for more detail.

[5] Brock, I. C., L3 Note 918, June 1994.

[6] BES Collaboration, "Determination of the J/ψ Leptonic Branching Fraction via $\psi(2S) \rightarrow \pi^+\pi^- J/\psi$", draft of Oct. 94.

[7] Jingyun Fan, Jin Li, Xiangzong Cui, Renchuan Wang, and Mulin Yan, "An Experiment Study of $\psi(2S) \rightarrow \pi^+\pi^- J/\psi$", April 1995.

[8] T. M. Yan, Phys. Rev. D22, 1652 (1980).
Yuping Kuang, T. M. Yan, Phys. Rev. D37, 1210 (1975).

[9] M. Voloshin, V. Zakharov, Phys. Rev. Lett. 45,688(1980).
M. A. Shifman, Usp. Fiz. Nauk 157,561(1989).
M. A. Shifman, Phys. Rep.22(1991).
V. A. Novikov, M. A. Shifman, Z. Phys. 37, 1210(1988).

[10] Cahn, R. N., Phys. Rev. D12, 3559 (1975).

ψ (2S) Decays to Baryon-Antibaryon Pairs

Lingjun Pan
University of Hawaii
Jim Panetta
Caltech

Abstract

A sample of over 3M ψ' decays registered in the BES detector are used to study final states containing pairs of octet and decuplet baryons. We report branching ratios for $\psi' \to p\overline{p}$, $\Lambda\overline{\Lambda}$, $\Sigma^0\overline{\Sigma}^0$, $\Xi^-\overline{\Xi}^+$, $\Delta^{++}\overline{\Delta}^{--}$, $\Sigma^+(1385)\overline{\Sigma}^-(1385)$, and upper limits for $\Xi^0(1530)\overline{\Xi}^0(1530)$, $\Omega^-\overline{\Omega}^+$. These results are compared to expectations based on flavor-$SU(3)$ symmetry.

1 Introduction

In the quarkonium model, the ψ' is the first radial excitation of the ^3S $c\overline{c}$ bound state. As such, its properties are expected to be relatively straight-forward to understand, at least in terms of those of the J/ψ ground state. Somewhat surprisingly, these expectations do not always hold. In particular, there are two rather dramatic anomalies associated with the ψ':

1. *The $\rho\pi$-puzzle.* One major puzzle in hadronic ψ decays is the large discrepancy between the decay widths for $J/\psi \to \rho\pi$ and K^*K and the corresponding widths for $\psi(2s)$ decays. These modes are expected to proceed via $\psi \to ggg$, with widths that are proportional to the square of the $c\overline{c}$ wave function at the origin, which is well determined from dilepton decays. The prediction, known as *"the 15% rule,"* is
$$\frac{\mathcal{B}(\psi' \to X_{had})}{\mathcal{B}(J/\psi \to X_{had})} = \frac{\mathcal{B}(\psi' \to e^+e^-)}{\mathcal{B}(J/\psi \to e^+e^-)} = 0.147 \pm 0.023,$$
where X_{had} designates any exclusive hadronic decay channel. Experimentally, the $\psi(2s) \to \rho\pi$ and K^*K are reduced by factor of sixty and twenty, respectively, from these naive expectations [1], [2].

2. *The ψ' anomaly.* The CDF group has reported a large anomaly in the charmonium production rate in high energy $p\overline{p}$ collisions [4]. It is expected that the J/ψ's are mainly decay products of χ states, which are expected to be copiously produced by gluon-gluon fusion. This channel is not expected to be available for

ψ' production, and these are expected to be primarily produced via B meson decays. Experimentally, the J/ψ production rate is a factor of two or three above expectations, while that for ψ''s exceeds expectations by as much as a factor of thirty.

These anomalies call into question the underlying assumption behind the theoretical predictions, namely that the ψ' is a pure $c\bar{c}$ state.

2 $\psi' \to B_i\overline{B_i}$

In the context of flavor $SU(3)$, a pure $c\bar{c}$ state is a flavor singlet and, in the limit of $SU(3)$-flavour symmetry, the phase-space-corrected reduced branching ratios to any baryon octet pair, $|M_i|^2$, where

$$|M_i|^2 = \frac{\mathcal{B}(\psi' \to B_i\overline{B_i})}{\pi p^*/\sqrt{s}}$$

(p^* is the momentum of the baryon in the ψ' rest frame), should be the same for every octet baryon, B_i. A similar relation holds among the decuplet baryons. Deviations from this rule would indicate non-SU(3)-singlet contributions to the decay amplitude. We consider the possibility of SU(3)-violating octet amplitudes, in which case the expression for M_i has the form [3]:

$$i = \begin{array}{ccl} p\overline{p} & = & a(1+\frac{1}{\sqrt{2}}\epsilon_1 - \sqrt{2}\epsilon_2)^2 \\ \Lambda\overline{\Lambda} & = & a(1-\frac{1}{\sqrt{2}}\epsilon_1 - \frac{1}{\sqrt{2}}\epsilon_2)^2 \\ \Sigma^0\overline{\Sigma^0} & = & a(1+\frac{1}{\sqrt{2}}\epsilon_1 + \frac{1}{\sqrt{2}}\epsilon_2)^2 \\ \Xi^-\overline{\Xi}^+ & = & a(1-\sqrt{2}\epsilon_1 + \frac{1}{\sqrt{2}}\epsilon_2)^2, \end{array}$$

where ϵ_1 and ϵ_2 are the symmetric and antisymmetric SU(3)-violating octet amplitudes relative to SU(3)-conserving singlet term.

The reduced branching fractions for $J/\psi \to B_i\overline{B_i}$ decays for the octet baryons, derived from the PDG values for the J/ψ branching fractions [8], are shown in Fig. 1. Fitting to the above formula, neglecting the possibility of complex relative phases between the amplitudes, gives $\epsilon_1 = 0.08 \pm 0.04$ and $\epsilon_2 = -0.06 \pm 0.04$ with $\chi^2 = 0.54$ (1 dof). (Fitting with a only singlet term gives a $\chi^2/dof = 5.0$.)

This relation has not been tested for the ψ', where the only relevant mode that has been measured is $p\overline{p}$, and that with rather poor precision [5],[6].

3 This experiment

We report preliminary results of measurements of the branching fractions for $\psi' \to B_i\overline{B_i}$, where $B_i = \{p, \Lambda, \Sigma^0, \Xi^-, \Delta^{++}, \Sigma^-(1385), \Xi^0(1530), \Omega^-\}$, using a sample of 3.44×10^6 ψ' events produced via e^+e^- annihilations at the BEPC collider and observed by the BES detector. The BES detector is described in ref. [7].

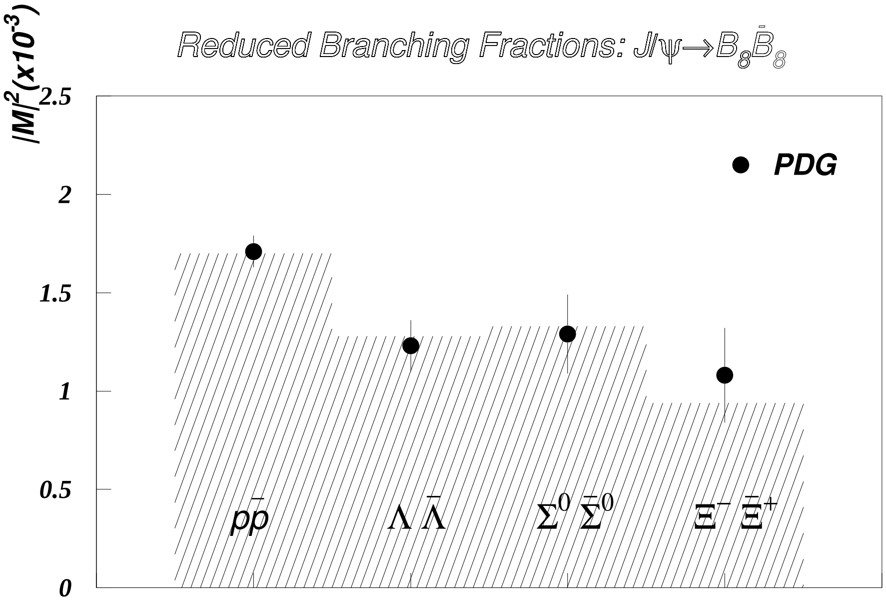

Figure 1: PDG values for the reduced branching fractions $|M_i|^2$ for $J/\psi \to B_i\overline{B_i}$, where $B_i = p, \Lambda, \Sigma^0, \Xi^-$. The shaded bars indicate results of a fit to an SU(3)-symmetry breaking model described in the text.

3.1 Event selection and constraints

We restrict our analysis to decays where all final state particles are reconstructed in the detector. For charged tracks we require that it not be positively identified as a lepton, $|cos\theta| < 0.8$, where θ is the polar angle, and $\Sigma Q_i = 0$, where Q is the charge of each track. For γ's we require $|cos\theta_\gamma| < 0.75$, $|cos\theta_{\gamma,trk}| < 0.9$, where $\theta_{\gamma,trk}$ is the angle between the γ and the nearest charged track, and $E_\gamma > 0.05$ GeV.

We subject each candidate event to kinematically constrained fits. For all modes we apply four constraints corresponding to energy and momentum conservation. We also use a beam constraint, e.g. $M_B = M_{\overline{B}}$, where appropriate. Charged track pairs that are $\Lambda \to \pi p$ candidates are passed through a secondary vertex-finding routine where the direction from the interaction point to the decay vertex is required to match the net momentum vector of the track pair. The specific requirements for each mode and the resulting number of events are listed in Table 1.

Mode	# charg	# γ	4-C	Beam-C	# events
$p\overline{p}$	2	0	yes	no	418± 21
$\Lambda\overline{\Lambda}$	4	0	yes	yes	85± 9.5
$\Sigma^0\overline{\Sigma}^0$	4	2	yes	yes	12± 4
$\Xi^-\overline{\Xi}^+$	6	0	yes	yes	18± 5
$\Delta^{++}\overline{\Delta}^{--}$	4	0	yes	no	100 ± 36
$\Sigma^{*-}\overline{\Sigma^*}^+$	6	0	yes	no	5± 2.5
$\Xi^{*0}\overline{\Xi^*}^0$	8	0	yes	no	0
$\Omega^-\overline{\Omega}^+$	6	0	yes	yes	0

Table 1: A summary of the event selection requirements for each mode.

3.2 Results

We plot our results for the branching fractions in Fig. 2, along with previous limits and results. The numerical values are summarized in Table 2. Our measured value for the $Br(\psi' \to p\overline{p})$ is higher than the value given in the PDG table, which comes from a DASP measurement based on 4 events [5] and a Mark I measurement with similar statistics [6]. The results for $\Lambda\overline{\Lambda}$ and $\Xi^-\overline{\Xi}^+$ are below the PDG upper limit values. Here we report first measurements for the $\Sigma^0\overline{\Sigma^0}$, $\Delta^{++}\overline{\Delta}^{--}$, $\Sigma^{*+}\overline{\Sigma^*}^-$ modes and 90% CL upper limits for $\Xi^{*0}\overline{\Xi^*}^0$ and $\Omega^-\overline{\Omega}^+$.

Decay Mode	Branching fraction
$p\overline{p}$	$(3.29 \pm 0.33 \pm 0.32) \times 10^{-4}$
$\Lambda\overline{\Lambda}$	$(2.03 \pm 0.27 \pm 0.20) \times 10^{-4}$
$\Sigma^0\overline{\Sigma}^0$	$(1.17 \pm 0.39 \pm 0.12) \times 10^{-4}$
$\Xi^-\overline{\Xi}^+$	$(1.03 \pm 0.35 \pm 0.13) \times 10^{-4}$
$\Delta^{++}\overline{\Delta}^{--}$	$(0.88 \pm 0.32 \pm 0.10) \times 10^{-4}$
$\Sigma^-(1385)\overline{\Sigma^*}^+$	$(0.46 \pm 0.46 \pm 0.13) \times 10^{-4}$
$\Xi^{*0}\overline{\Xi^*}^0$	$< 0.72 \times 10^{-4}$
$\Omega^-\overline{\Omega}^+$	$< 0.71 \times 10^{-4}$

Table 2: Measured $\psi' \to B\overline{B}$ branching ratio values.

4 Discussion

In Fig. 3, we plot the reduced branching fractions derived from our measurements for $\psi' \to B_8\overline{B_8}$. Fitting the data with the above described SU(3)-violating model gives $\epsilon_1 = 0.04 \pm 0.07$ and $\epsilon_2 = -0.22 \pm 0.07$ with $\chi^2 = 0.21$ (1 dof). (Fitting with a singlet term only gives a $\chi^2/dof = 4.3$.) The SU(3)-symmetry violation for the $\psi' \to B_8\overline{B_8}$ is more pronounced than for the J/ψ: an antisymmetric octet decay amplitude that $\sim 22\%$ that of the singlet amplitude is required to fit the data.

In Fig. 4, we plot the ratio of the reduced branching fractions derived from our measurements to 0.147 times that of the J/ψ. There is no PDG entry for J/ψ to $\Xi^0(1530)\overline{\Xi}^0(1530)$ and the J/ψ to $\Omega^-\overline{\Omega}^+$ mode is not kinematically accessible. For the $p\overline{p}$ and $\Lambda\overline{\Lambda}$ modes, there is good agreement with 15% rule expectations. Although the rule works less well for the heavier baryon states, there is no dramatic suppression as in the case for vector-pseudoscalar meson final states.

5 Acknowledgements

We acknowledge the strong efforts of the BEPC staff and the helpful assistance we received from the members of the IHEP computing center.

References

[1] M.E.B. Franklin et al. (Mark II Collaboration), Phys. Rev. Lett. **51**, 963 (1983).

[2] Y.F. Gu et al. (BES Collaboration), *Results on Hadronic $\psi(2S)$ Decays into VP and VT Final States*, contribution to this conference.

[3] Sandip Pakvasa, Private communication.

[4] M. Mangano (CDF collaboration), proceedings of the XXIX Rencontres de Moriond on QCD and High Energy Hadronic Interactions, Meribel, March 1994; and the XVIIth International Conference on High Energy Physics, Glasgow, July, 1994.

[5] R. Brandelick et al. (DASP Collaboration), Z. Phys. **C1**, 233 (1979).

[6] G. Feldman and M. Perl (Mark I Collaboration), Phys. Rep. **C33**, 285 (1977).

[7] J.Z. Bai et al. (BES Collaboration), Nucl. Inst. and Meth. **A344**, 319 (1994).

[8] L. Montanet et al. (Particle Data Group), *Review of Particle Properties,* Phys. Rev. **D50**, 1173 (1994).

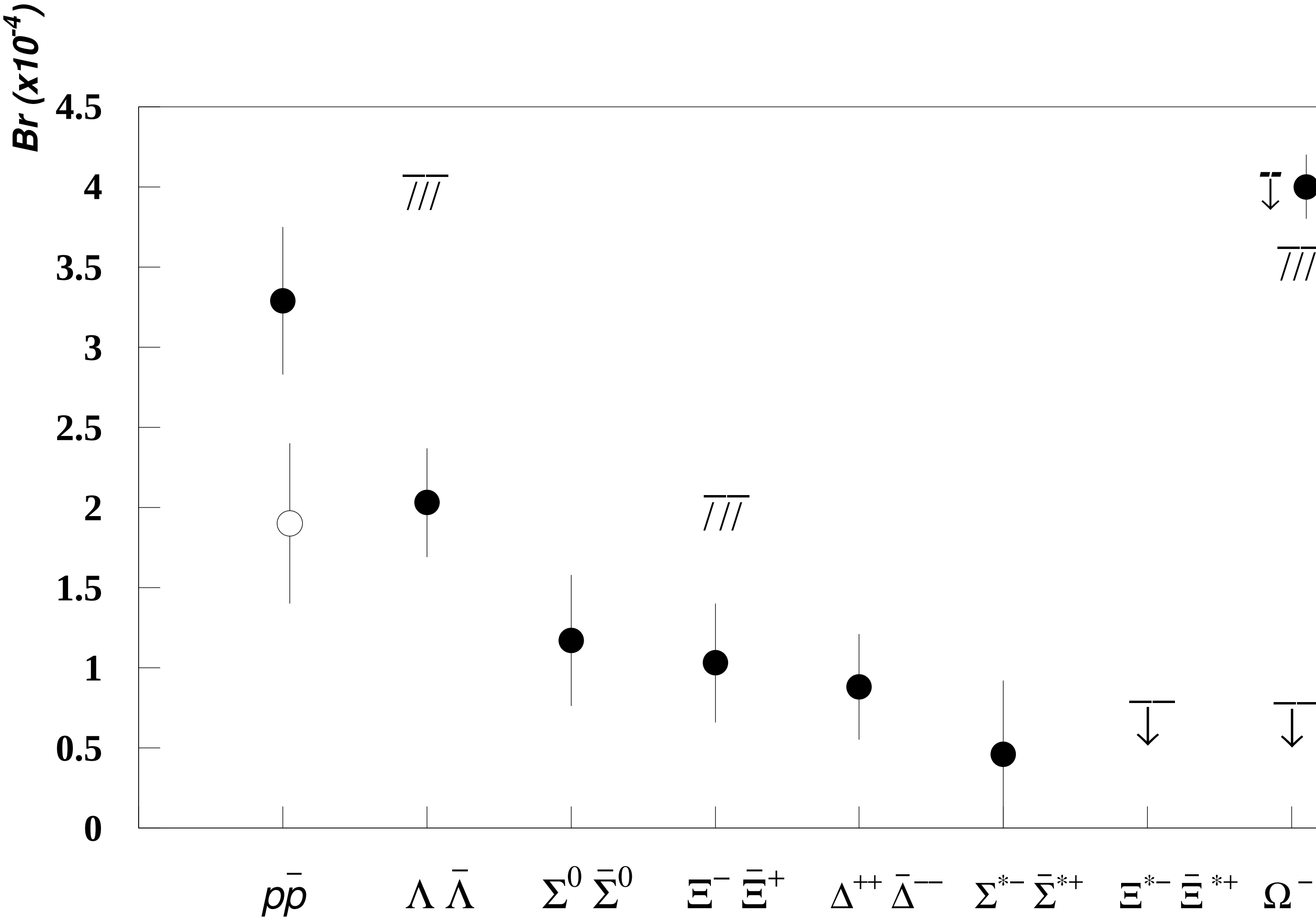

Figure 2: The measured branching fractions for $\psi' \rightarrow B_i\overline{B_i}$ decays. Previous measurements are indicated for comparison.

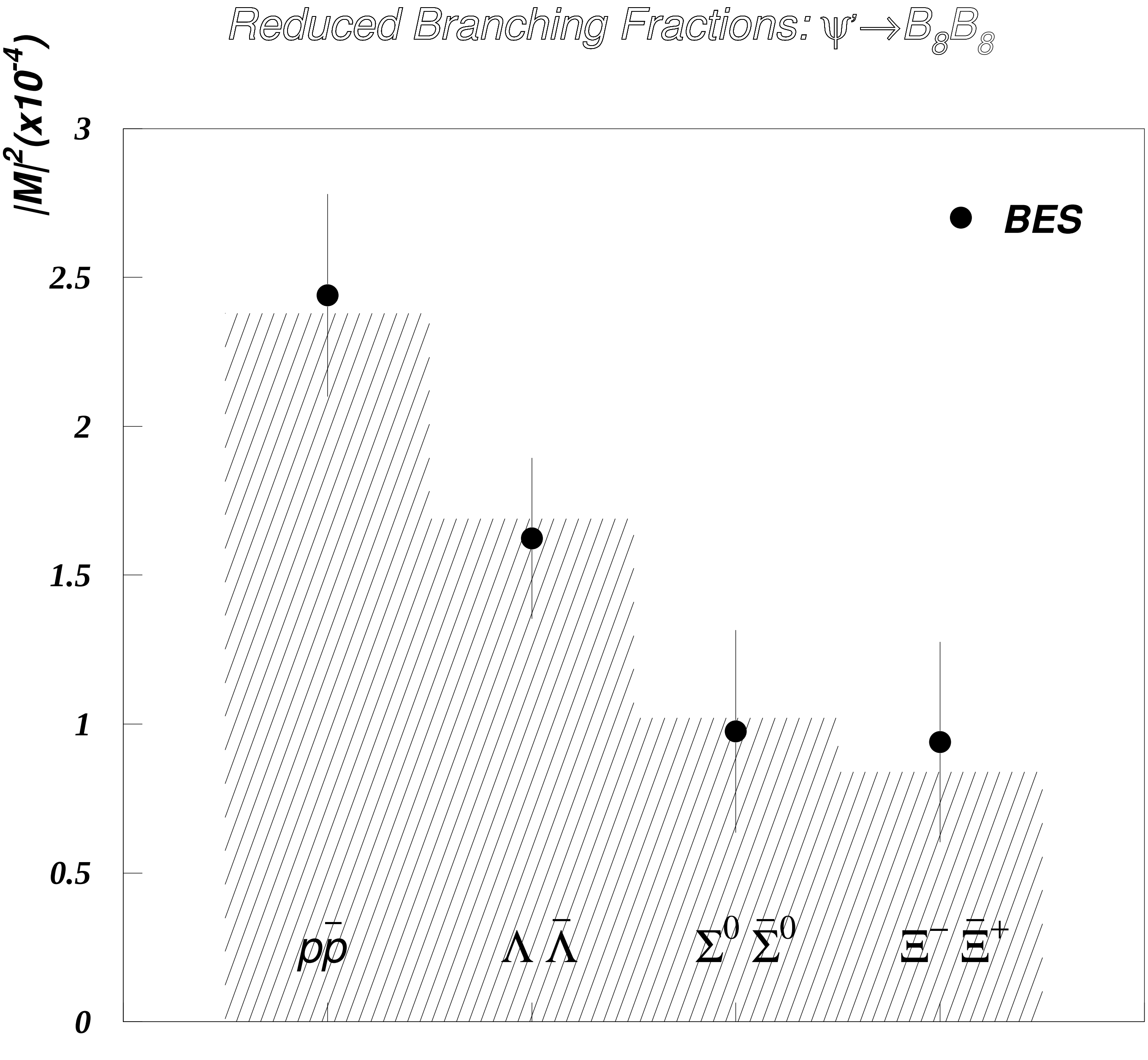

Figure 3: The reduced branching fractions $|M_i|^2$ for $\psi' \rightarrow B_8\overline{B_8}$ decays. The shaded bars indicate results of a fit to an SU(3)-symmetry breaking model with an antisymmetric-octet amplitude that is $\sim 22\%$ of the SU(3)-conserving singlet term.

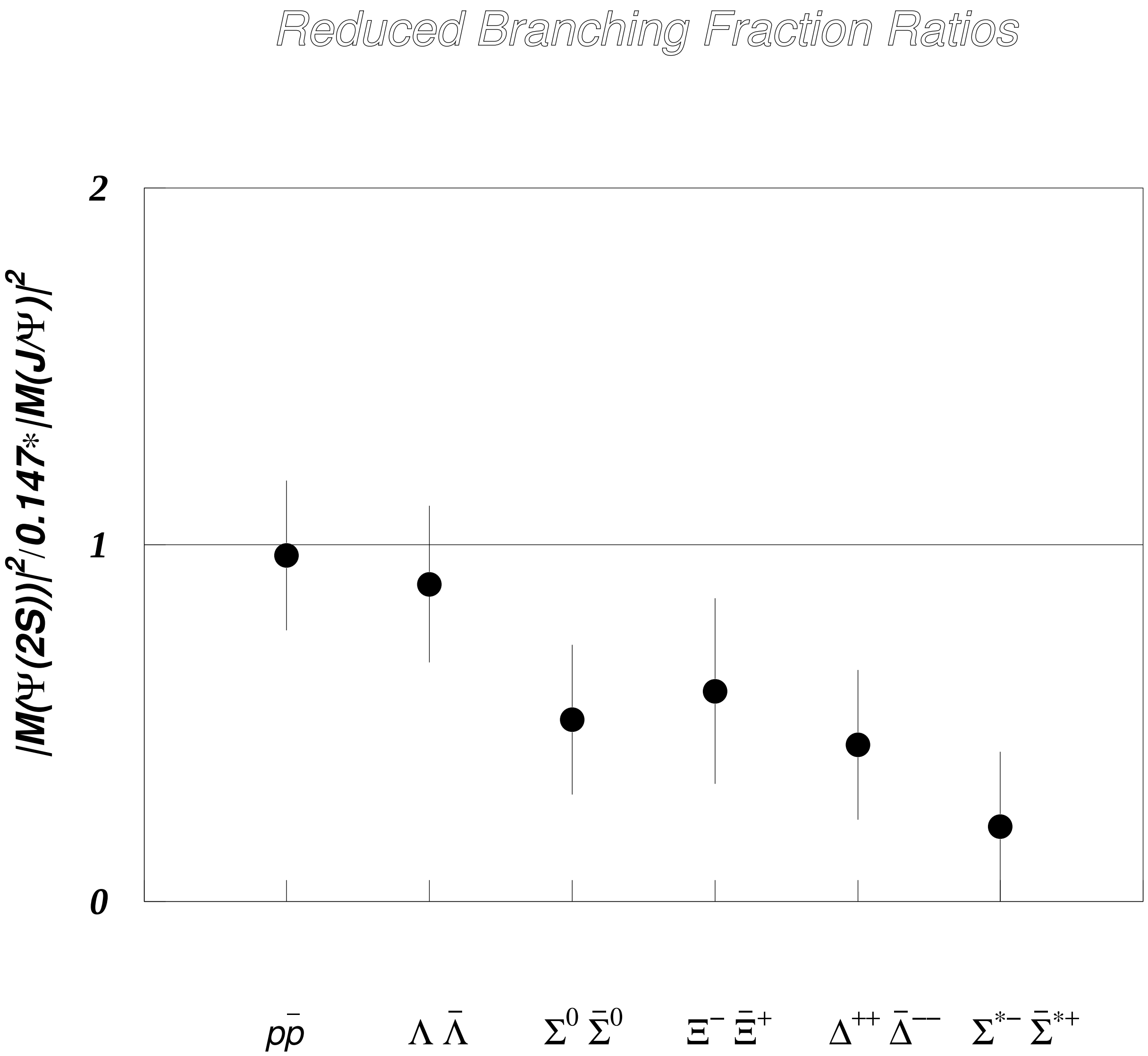

Figure 4: The ratio of the reduced branching fraction for $\psi' \to B_i\overline{B_i}$ to 0.147 times that for the J/ψ, for each baryon pair species measured here.

A Check of the Total Number of τ-pair Events Decayed from ψ' in the Measurement of the $Br(\psi' \rightarrow \tau^+\tau^-)$

Yu Chunxu, Luo Yong, Qi Nading, Cui Xiangzhong, Gu Yifan
Institute of the High Energy Physics
Academia Sinica
Beijing 100039, P. R. China

1 Introduction

1.1 The physics significance

Up to now, experimental evidence suggests that the τ particle is a conventional lepton, which behaves itself like other two charged leptons — electron and μ, obeying the rule of the $e-\mu-\tau$ universality hypothesis. In the $c\bar{c}$ system, the ψ' provides an unique opportunity to compare the three generation leptons by studying its leptonic decay. According to the theory, the relations between the branching ratios of the decay modes $\psi' \rightarrow e-, \mu-$ and $\tau - pair$, $Br_{ee}, Br_{\mu\mu}$ and $Br(\psi' \rightarrow \tau\tau)$ are given by

$$\frac{Br(\psi' \rightarrow \tau\tau)}{0.3885} \approx Br_{\mu\mu} \approx Br_{ee} \tag{18}$$

Previous experiments have yielded the measurements of Br_{ee} and $Br_{\mu\mu}$, but no $Br(\psi' \rightarrow \tau\tau)$. By use of the 93/94 ψ' data, we have measured the value of the $Br(\psi' \rightarrow \tau\tau)$, which was reported in the BES Annual Meeting, the HEP-Glasgow in 1994 and so on. But before formal publication, the measurement of the $Br_{\tau\tau}$ must be checked.

1.2 Our main task

This memo will clarify and solve some important problems as follows:

In the previous measurement of the total $\tau - pair$ event number $N_{\tau\tau}$, we used

a. the 93/94 ψ' filtered data collected by BES, which place a restriction on the tracks in the SC. We worry about that might result in the loss of the $N_{\tau\tau}$;

b. the 92 Ds data collected by BES, used as determining the detection efficiency ε_d, which are divided into two datasets, each with different threshold values set for the

MDC trigger(see Table 1). We are afraid that lead to the loss of the ε_d, namely the increasement of the $N_{\tau\tau}$.

Our way to deal with the above problems is

a. using the 93/94 ψ' unfiltered data reconstructed by USA instead of the filtered data;

b. using the 93 Ds low threshold data, instead of the previously used 92 Ds data(see Table 1).

Table 1 the different thresholds between these datasets

datasets	range	threshold (MDC)
92 Ds data	3097 — 3450	875
	3739 — 3966	625
93 Ds data	4489 — 4640	625
	4750 — 5698	
93/94 ψ' data	5738 — 6059	625

Certainly, in the course of checking, we also make some improvements on other conditions. For example, the isolated photon should be the same as that in the measurement of the τ-mass, that is, it has $Esc \geq 60MeV$, and is separated from the nearest charged track by $\theta_{open} > 12°$.

2 Formulae used in the measurement

2.1 The formula for measuring $Br(\psi' \to \tau\tau)$

$$Br(\psi' \to \tau\tau) = \frac{N_{\tau\tau} - \sigma_{Q+I} \bullet L}{N_{\psi'}} \tag{19}$$

where $N_{\tau\tau}$ is the total τ-pair event number; σ_{Q+I} is the sum of the cross section of the QED generating τ-pair and that of the interference part; L is the integrated luminosity at the ψ' resonance; $N_{\psi'}$ is the number of the produced ψ' events.

2.2 The formula for measuring $N_{\tau\tau}$

The $\tau\tau$ events are identified by means of the six topologies, $e\mu, e\pi, ee, \mu\pi, e\rho$ and $\mu\rho$. By using the observed event number n for each of the six topologies, $N_{\tau\tau}$ is expressed as

$$N_{\tau\tau} = \frac{n}{B \bullet \varepsilon_d \bullet \varepsilon_t} \tag{20}$$

where B is the branching ratio of the relevant $\tau\tau$ decay topology; ε_d and ε_t are respectively the detection and trigger efficiency of the relevant channel.

In fact, to evaluate ε_d we first measure the ε_d' at $\sqrt{s} = 4.03GeV$, which is expressed as

$$\varepsilon_d^{'} = \frac{n^{'}}{B \bullet \sigma_{QED}^{'} \bullet L^{'}} \tag{21}$$

where $n^{'}$ is the observed event number; $\sigma_{QED}^{'}$ is the cross section of the QED generating τ-pair at $\sqrt{s} = 4.03GeV$; $L^{'}$ is the accumulated luminosity at $\sqrt{s} = 4.03GeV$. Monte Carlo simulations of the BES detector have been made to determine the ratio $\lambda = \varepsilon_d/\varepsilon_d^{'}$, thus the above formula(3) will be simplified as follows:

$$N_{\tau\tau} = \frac{n \bullet \sigma_{QED}^{'} \bullet L^{'}}{n^{'} \bullet \lambda \bullet \varepsilon_t} \tag{22}$$

3 Analysis method

3.1 The preselection of $\tau^+\tau^-$ events

The six topologies are
6

$$\tau\tau \rightarrow e\mu, e\pi, ee, \mu\pi, e\rho \text{ and } \mu\rho$$

Each of these channels has two opposite charged tracks; for the decay modes $e\mu, e\pi, ee$ and $\mu\pi$, there should be no isolated photons, and for the $e\rho$ and $\mu\rho$ modes, there should be only two γs coming from π^0 which is decayed from $\rho^{\pm}$.

The preselection conditions are

- $|x| \leq 1.5cm, |y| \leq 1.5cm, |z| \leq 20cm$;
- $N_{chrg} = 2, \sum q_i = 0, M_{fit} = 2$; $N_{neu} \leq 20$;
- $2.5° \leq acol \leq 177.5°$; $acop \geq 6°$;
- if a neutral track in one event has $E_{sc} > 0.1GeV$, and is separated from the nearest charged track by $\theta_{open} > 20°$, the event is demanded $acol > 5°, acop > 10°$; $N_{neu} \geq 2, E_{sc} \geq 0.03GeV$ and $0.035GeV/C^2 \leq M_{\gamma\gamma} \leq 0.3GeV/C^2$.

3.2 The selection criteria of $\tau^+\tau^-$ events

We first introduce the criteria to identify the particles involved, that is, e, μ and π particles.

a. e

- $0.8 \leq \beta \leq 1.5$;
- $|\cos\theta| \leq 0.75$;

- no μ-hits;
- when $P \leq 350MeV, \beta \geq 1$ and $Esc/P \geq 0.7$;
- when $350MeV < P \leq 700MeV, \beta > 0.9$ and $idsh \geq -1$ and ($xspi \geq 2.5|xse|$ or $0 \leq xse \leq 10$);
- when $P > 700MeV$, ($Esc \geq 500MeV$ and $\beta \geq 0.9$ and $idsh \geq 1$) or ($Esc \geq 600MeV$ and $idsh \geq -3$).

b. μ

one layer μ-hit: $|Av| \leq 4$ and $|Az| \leq 6$.

first level μ-cut: having at least one layer μ-hit with two tube μ-hits;

second level μ-cut: having at least two layer μ-hits or the second layer and third layer having a μ-hit with two tube μ-hits.

- if a charged particle satisfies the second level μ-cut, it is identified as a μ;
- when $P_\pi lo \leq P \leq P_\pi hi$ or $\mu_{require} \leq 1$, if the charged particle satisfies the first level μ-cut and it has $Esc \leq 450MeV$, it is also identified as a μ.

c. π

- $|\cos\theta| \leq 0.75$;
- no μ-hits;
- when $P \leq 350MeV$, then $0.6 \leq \beta \leq 0.85$ and $Esc/P \leq 0.5$;
- when $350MeV < P \leq 700MeV$, $0.8 \leq \beta \leq 1.5$ and $idsh \leq -2$ and ($xspi \leq 0$ if $xse \leq 0$ or $|xse| \geq 2.5|xspi|$);
- when $P < 700MeV$, $0.85 \leq \beta \leq 1.5$ and $Esc \leq 400MeV$ and $idsh \leq -1$.

The selection criteria are divided into two parts.

The common conditions for selecting the six channels are:

- $|x| \leq 1.5cm, |y| \leq 1.5cm, |z| \leq 15cm$;
- the isolated photon is: $Esc \geq 60MeV$, the angle between it and the charged track nearest to it $\theta_{open} \geq 12°$;
- no isolated TOF. The isolated TOF means that there are some hits in the TOF, but they don't match any tracks in MDC. $T_{qual} = 1, 2$ or 7.

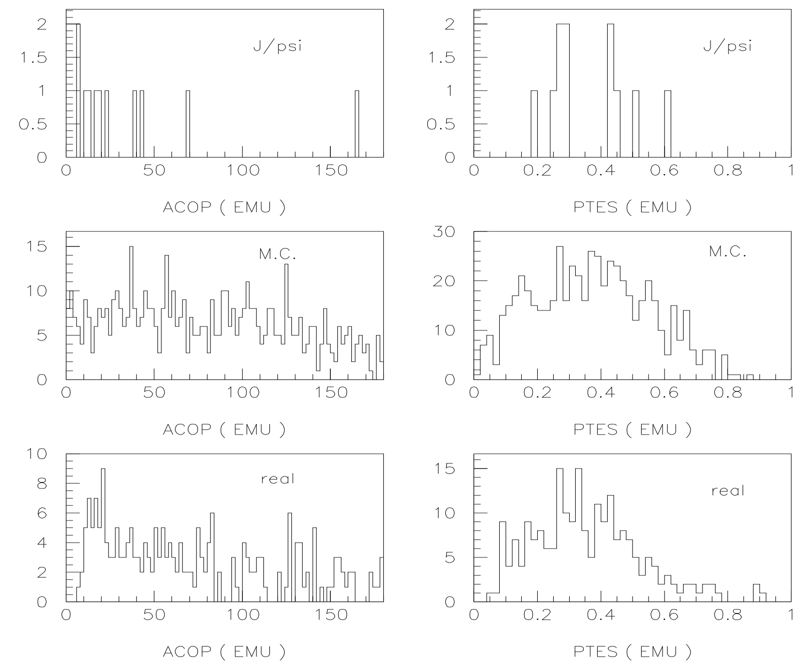

Figure 1: $e\mu$ channel

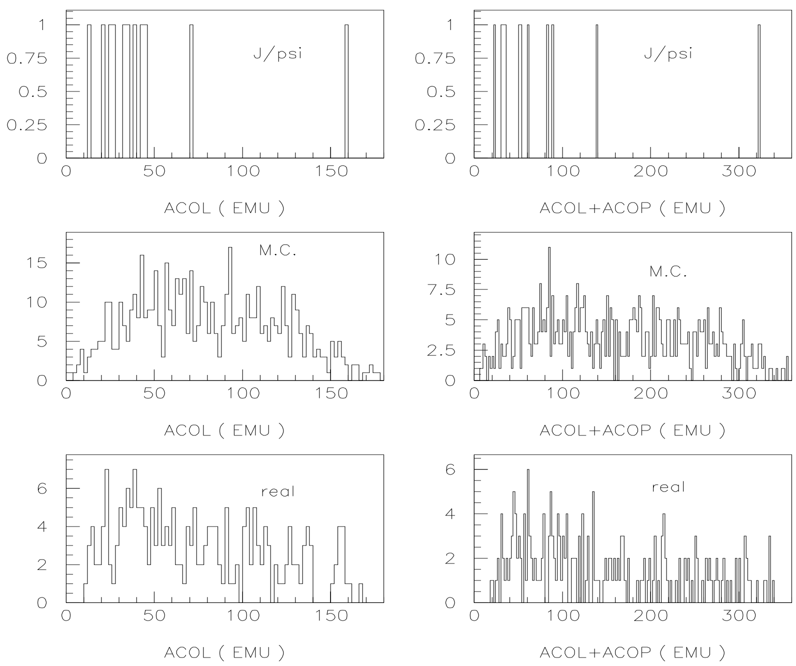

Figure 2: $e\mu$ channel

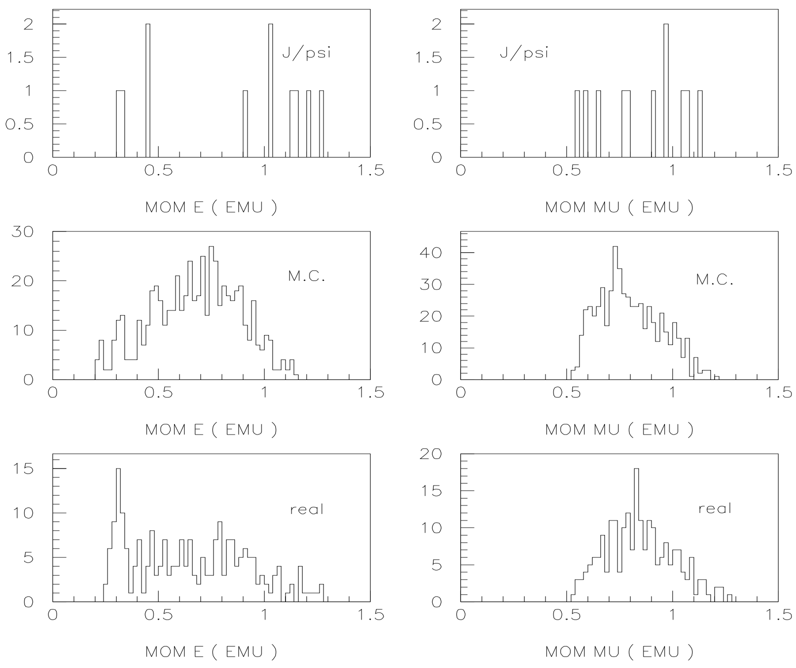

Figure 3: $e\mu$ channel

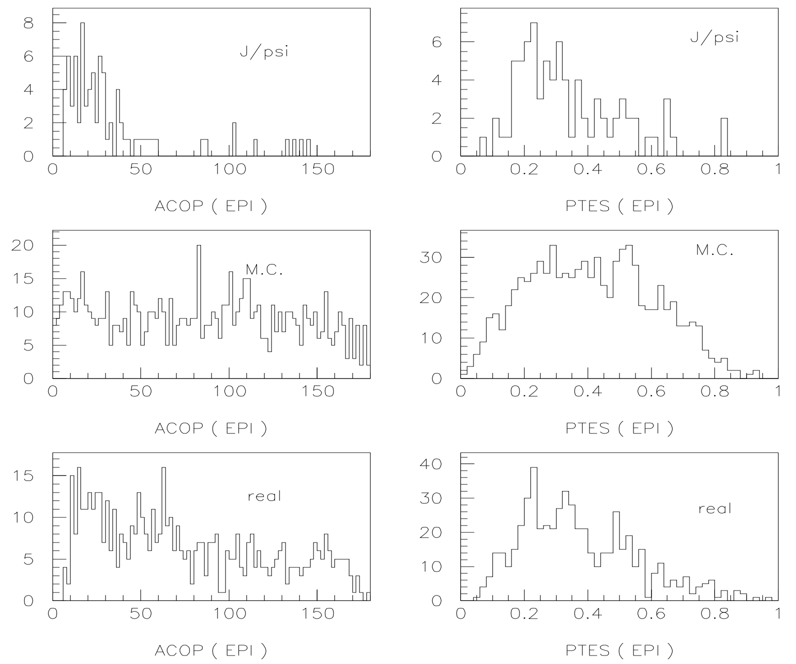

Figure 4: $e\pi$ channel

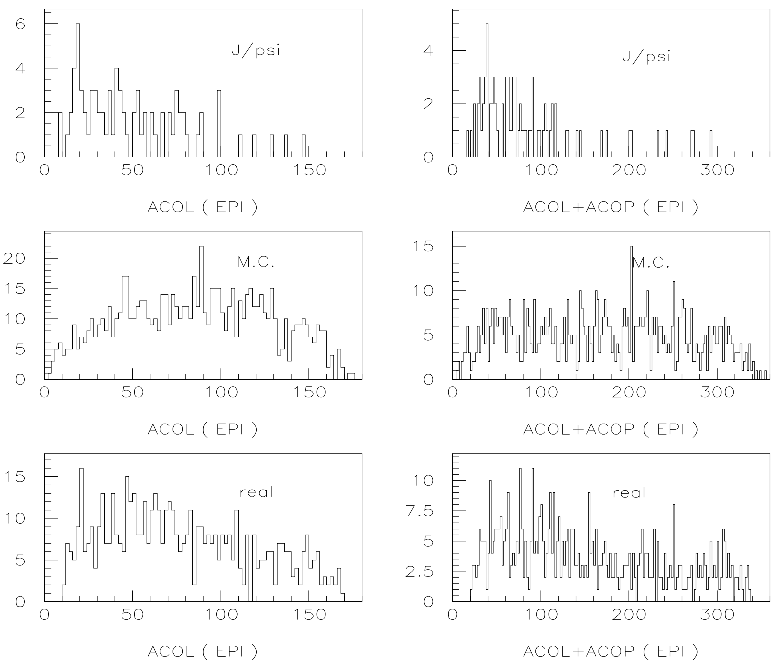

Figure 5: $e\pi$ channel

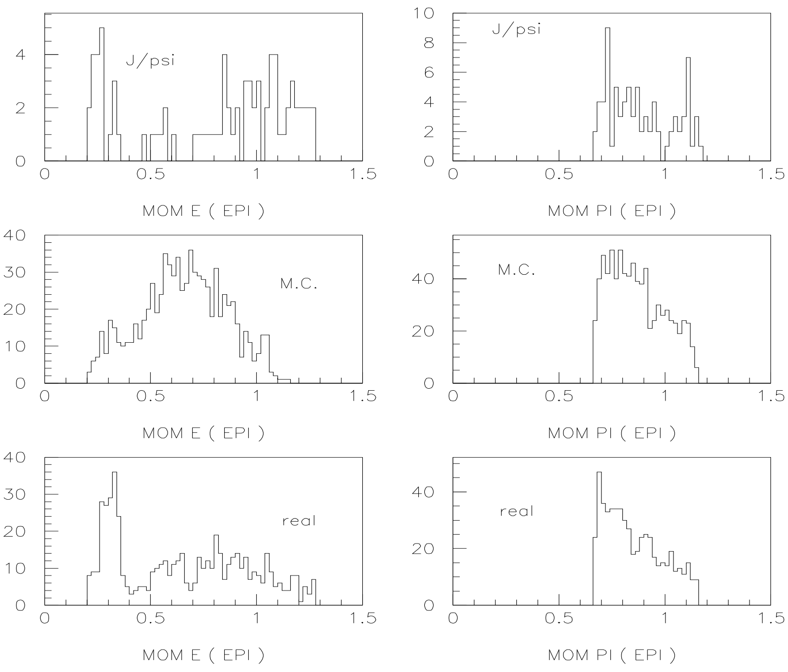

Figure 6: $e\pi$ channel

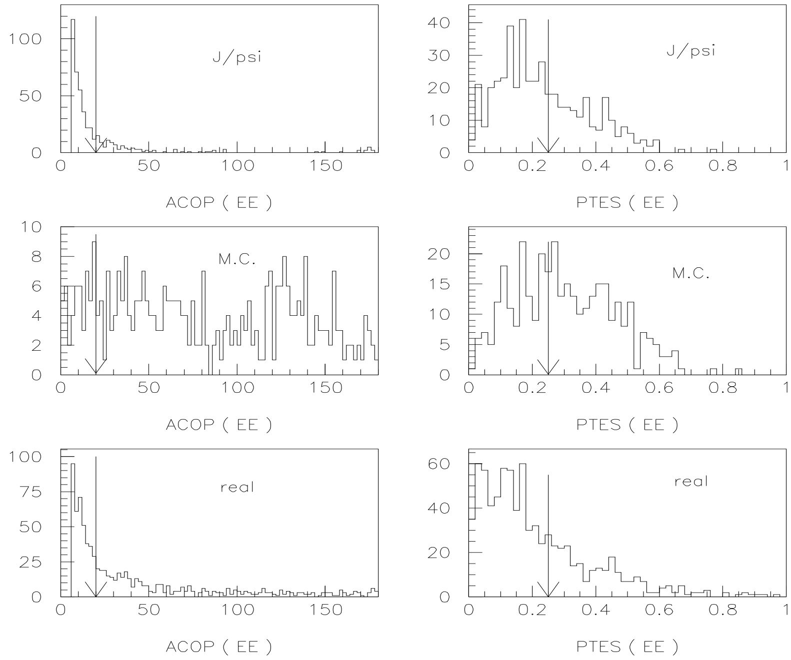

Figure 7: $\mu\pi$ channel

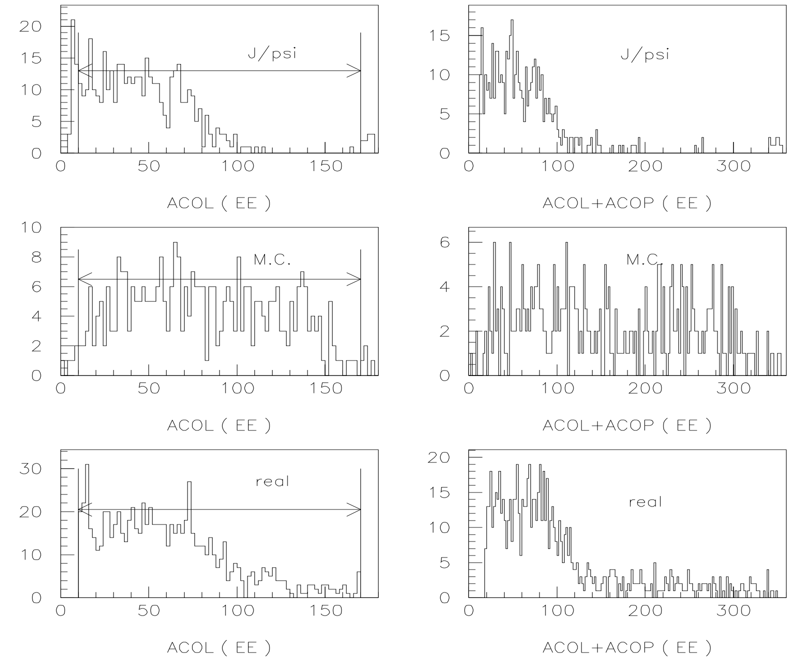

Figure 8: $\mu\pi$ channel

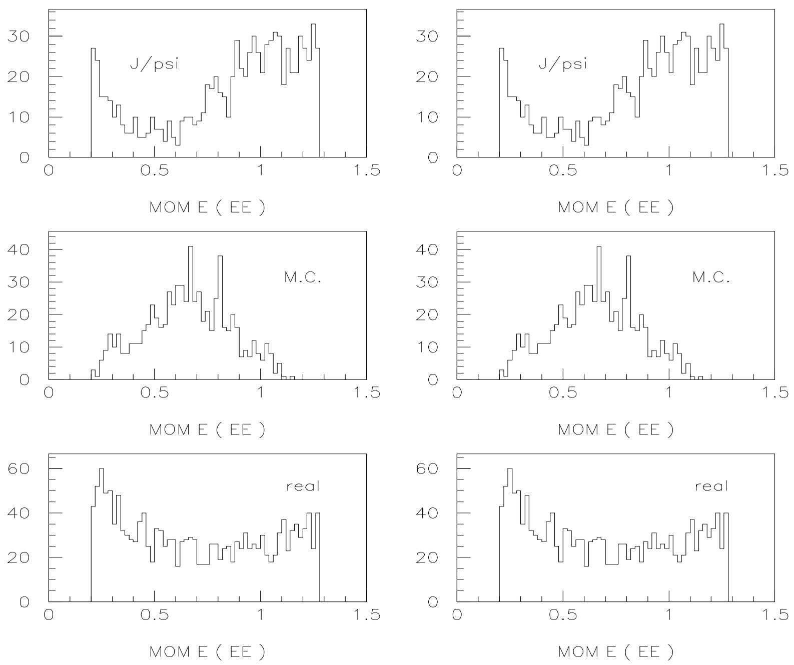

Figure 9: $\mu\pi$ channel

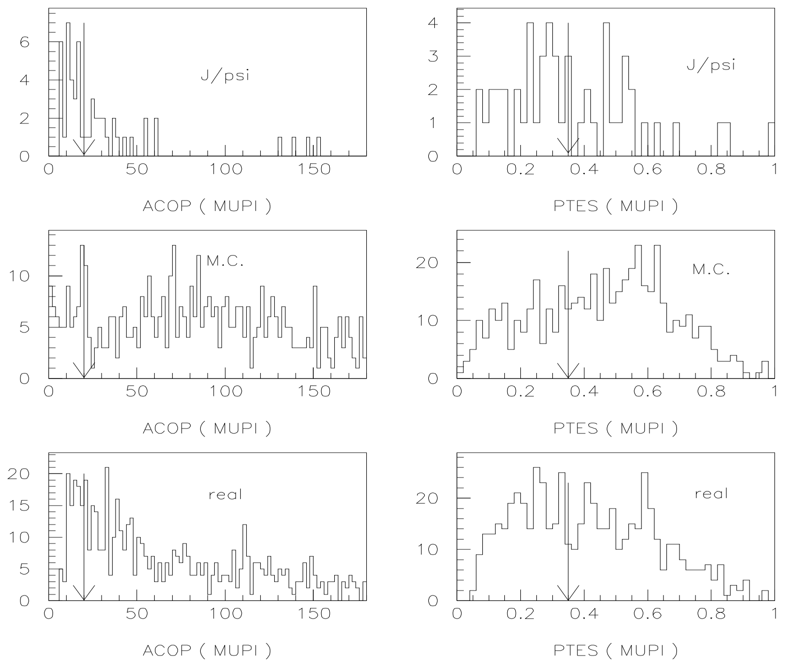

Figure 10: ee channel

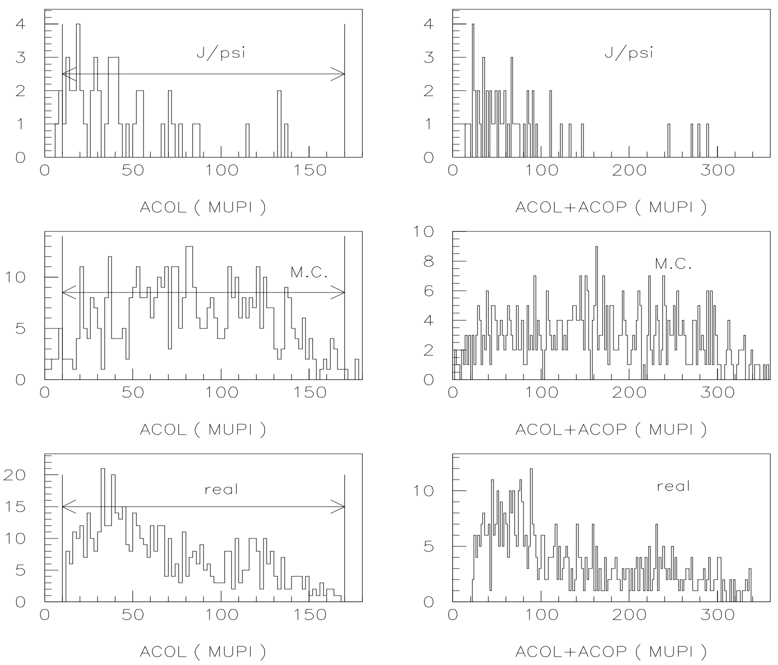

Figure 11: ee channel

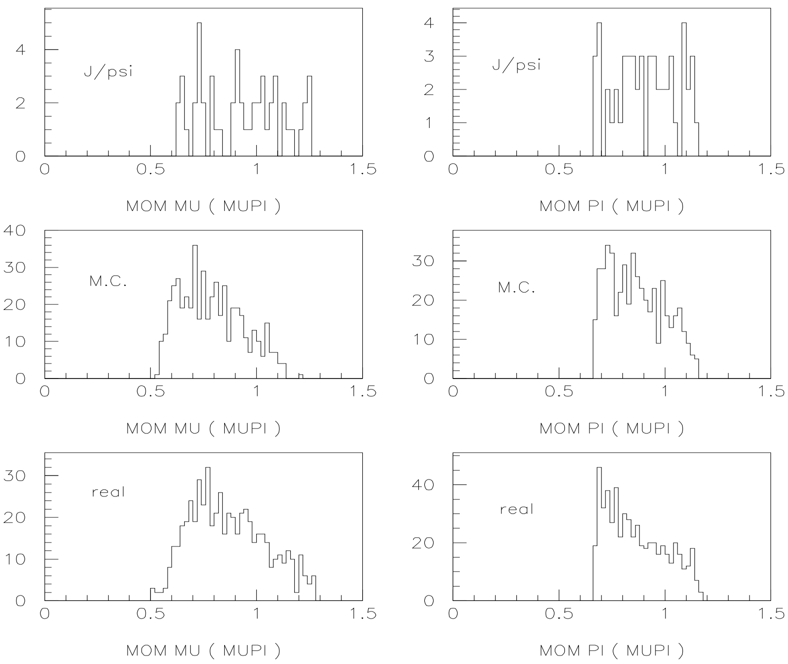

Figure 12: ee channel

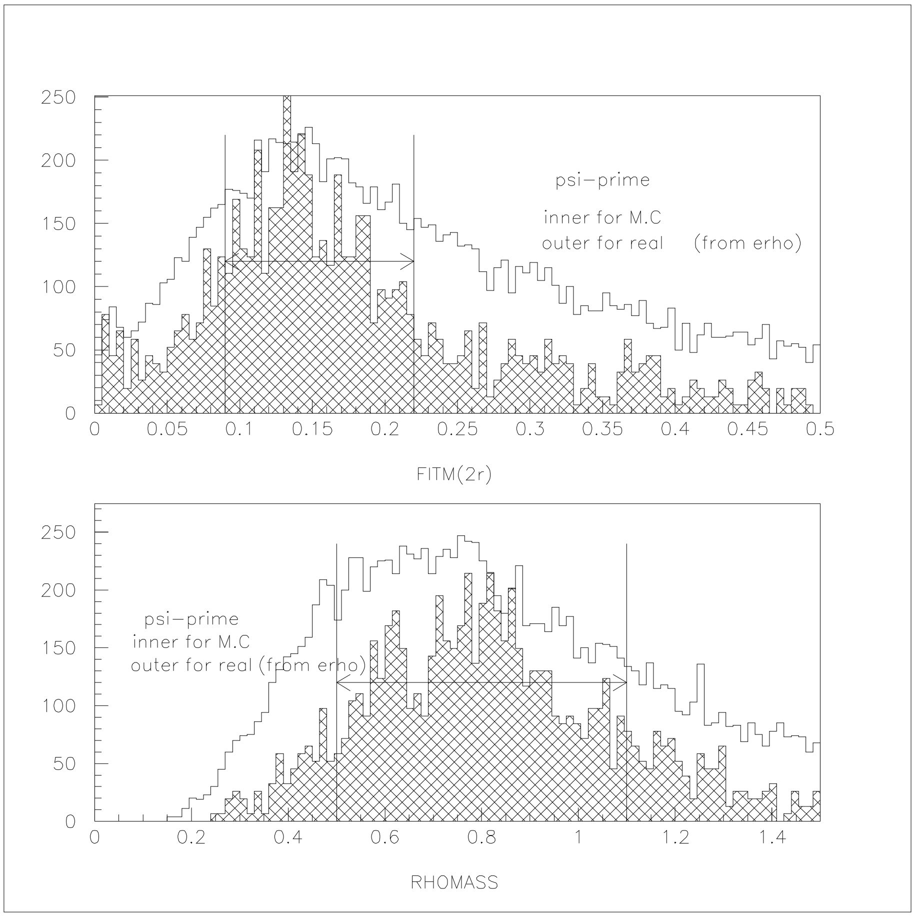

Figure 13: $e\rho$ channel, obtained after only a e, a π and two γs identitys

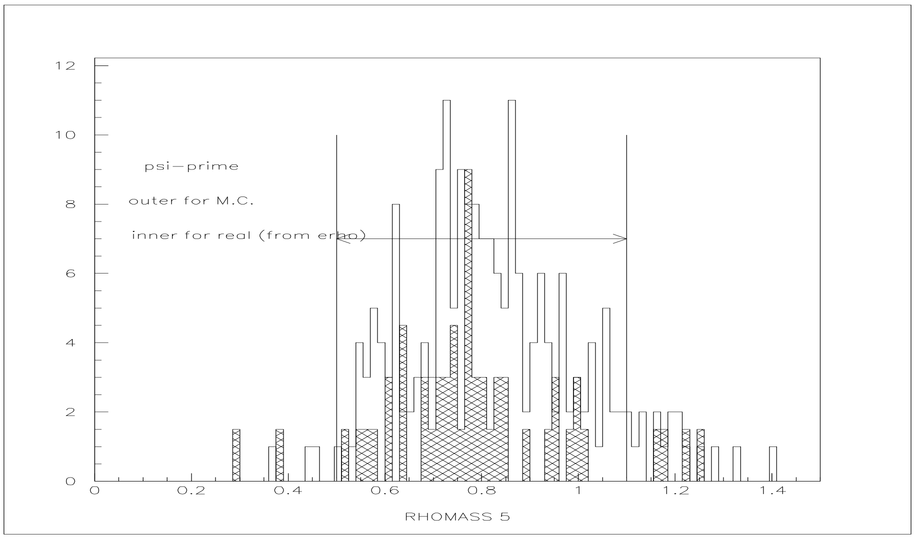

Figure 14: ρ_m, obtained after all cuts except for ρ_m cut(from $e\rho$ channel)

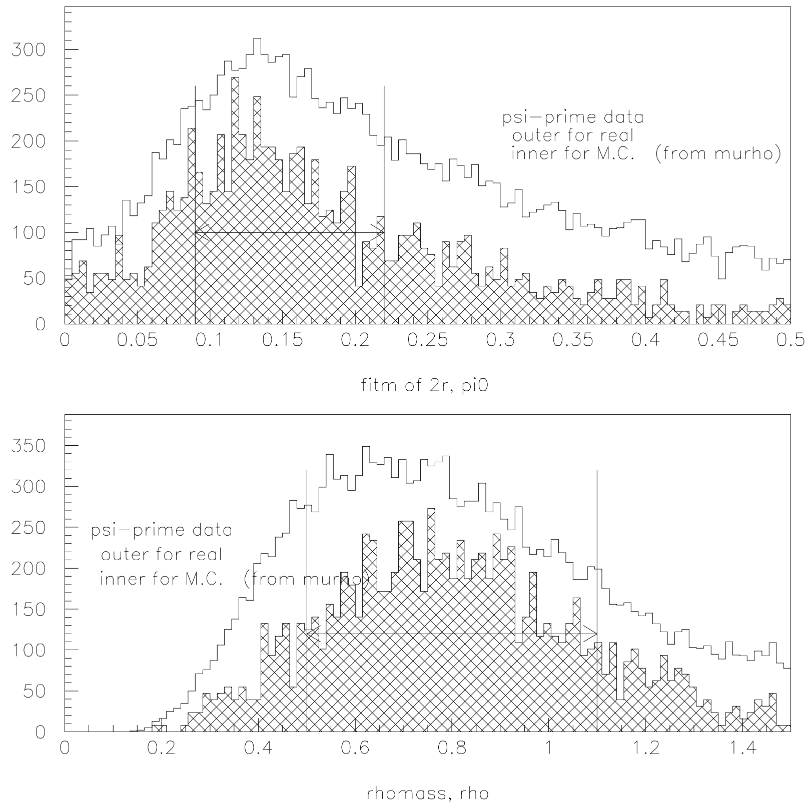

Figure 15: $\mu\rho$ channel, obtained after only a μ, a π and two γs identitys

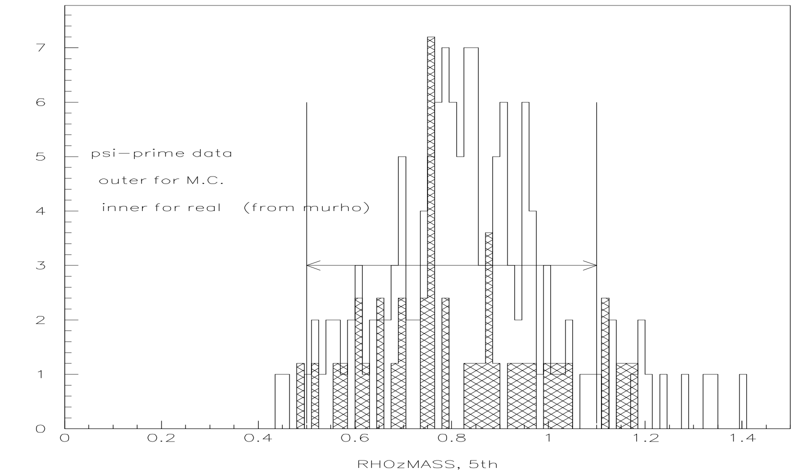

Figure 16: ρ_m, obtained after all cuts except for ρ_m cut(from $\mu\rho$ channel)

The different conditions for selecting the six channels are determined by studying the Monte Carlo data of $\psi' \to \tau\tau$, 93/94 ψ' data and J/ψ real data (the J/ψ data are used to estimate the $q\bar{q}$ background). The M.C. simulation data are compared to the 93/94 ψ' data as well as the J/ψ data as shown in the Figures from 1st to 16th.

$e\mu$ channel

- one track is an e, the other a μ, those momenta required $P_{min} \leq P_{e,\mu} \leq P_{max}$;
- no isolated photon;
- $acop \geq 10°$;
- $10° \leq acol \leq 170°$;
- $ptes \geq 0.1$.

$e\pi$ channel

- one track is an e, the other a π, those momenta required $P_{min} \leq P_e \leq P_{max}$, $P_\pi lo \leq P_\pi \leq P_\pi hi$;
- no isolated photon;
- $acop \geq 25°$;
- $10° \leq acol \leq 170°$;
- $ptes \geq 0.25$.

ee channel

- two tracks are es, those momenta required $P_{min} \leq P_e \leq P_{max}$;
- no isolated photon;
- $acop \geq 20°$;
- $10° \leq acol \leq 170°$;
- $ptes \geq 0.25$.

$\mu\pi$ channel

- one track is a μ, the other a π, those momenta required $P_{min} \leq P_\mu \leq P_{max}$, $P_\pi lo \leq P_\pi \leq P_\pi$hi;
- no isolated photon;
- $acop \geq 20°$;

- $10^\circ \leq acol \leq 170^\circ$;
- $ptes \geq 0.35$.

$e\rho$ channel

- one track is an e, the other a π, the momentum of e required $P_{min} \leq P_e \leq P_{max}$;
- the γs of fitting to π^0 demanded $Esc \geq 30MeV$, the angle between it and the charged track nearest to it $\theta_{open} \geq 3^\circ$;
- the mass of π^0, and the mass and momentum of ρ required:

$$90MeV/C^2 \leq M_{\pi^0} \leq 220MeV/C^2$$
$$500MeV/C^2 \leq M_\rho \leq 1100MeV/C^2$$
$$400MeV/C \leq P_\rho \leq 1100MeV/C$$

- the system of the e and fitted ρ demanded:

$$5^\circ \leq acol \leq 175^\circ$$
$$10^\circ \leq acop \leq 178^\circ$$
$$acol + acop \geq 50^\circ$$

- no other isolated photon, except for two photons making up π^0.

$\mu\rho$ channel

- one track is a μ, the other a π, the momentum of μ required $P_{min} \leq P \leq P_{max}$;
- the γs of fitting to π^0 demanded $Esc \geq 30MeV$, the angle between it and the charged track nearest to it $\theta_{open} \geq 3^\circ$;
- the mass of π^0, and the mass and momentum of ρ required:

$$90MeV/C^2 \leq M_{\pi^0} \leq 220MeV/C^2$$
$$500MeV/C^2 \leq M_\rho \leq 1100MeV/C^2$$
$$400MeV/C \leq P_\rho \leq 1100MeV/C$$

- the system of the μ and fitted ρ demanded:

$$5^\circ \leq acol \leq 175^\circ$$
$$10^\circ \leq acop \leq 178^\circ$$
$$acol + acop \geq 50^\circ$$

- no other isolated photon, except for two photons making up π^0.

Note: The previously used criteria for the ee and $\mu\pi$ modes have been modified to the above criteria so that the conditions of the particle identifications should be consistent with each other.

3.3 The background from $q\bar{q}$

The continuum background is estimated by use of the J/ψ data, which include three datasets, those runs from 1480 to 1616, from 1750 to 1940 and from 3579 to 3738, corresponding to 5 million $q\bar{q}$ events. Only 4, 6, 1, 0, 3, and 1 events meet the criteria for $e\mu, e\pi, ee, \mu\pi, e\rho$ and $\mu\rho$ respectively, corresponding to a $R_{bgd} < 10^{-3}$.

In addition, Monte Carlo study on the two-photon process has also been performed, no background event is found.

4 Result and discussion

The items measured and the value of $N_{\tau\tau}$ obtained are listed in table 2.

Table 2 the values of items used and $N_{\tau\tau}$

mode	n	n'	λ	σ'_{QED}	L'	ε_t	$N_{\tau\tau}$
$e\mu$	92	152	1.041	3.27	4680.9	0.99	8998.4 ± 1187.4
$e\pi$	61	103	0.892	3.27	4680.9	0.99	10261.2 ± 1657.9
ee	55	89	0.954	3.27	4680.9	0.99	10011.9 ± 1717.2
$\mu\pi$	40	75	0.967	3.27	4680.9	0.99	8995.5 ± 1761.2
$e\rho$	43	66	1.125	3.27	4680.9	0.99	8953.8 ± 1754.7
$\mu\rho$	36	52	1.066	3.27	4680.9	0.99	10040.7 ± 2177.0

in this table, $L'(nb^{-1})$ is determined by analyzing the wide-angle Bhabha events and $\sigma'_{QED}(nb)$ calculated theoretically.

The result of the weighted average for $N_{\tau\tau}$ is

$$N_{\tau\tau} = 9439.4 \pm 663.7 \pm 481.5 \tag{23}$$

where the systematic error include the contributions from the errors of L' ($\pm 5\%$) and ε_t ($\pm 1\%$).

Table 3 lists the differences between the previous measurement and the present check that result in the change of the value $N_{\tau\tau}$.

Table 3 changes of data and selection and their effects on $N_{\tau\tau}$

condition	present used	previous used	$\delta N_{\tau\tau}$
ψ' data	unfiltered	filtered	$\nearrow 3\%$
Ds data	93	92	$\searrow 7\%$
Esc, θ_{open} of γ	$\geq 60MeV, \geq 12°$	$\geq 40Mev, \geq 14°$	negligible

Furthermore, since the integrated luminosity of the Ds data has been corrected to increase by 3%, the value of $N_{\tau\tau}$ has a 3% increasement correspondingly.

In summary, all above-mentioned factors make the $N_{\tau\tau}$ reduce by about 0.9%.

If putting the values of $\sigma_{Q+I} = 2.237nb$ obtained by the theory analysis, $L = (2246 \pm 5 \pm 46)nb^{-1}$ measured by using the wide-angle Bhabha events and $N_{\psi'} =$

$(1271 \pm 4 \pm 111) \times 10^{+3}$ measured by using a method of detecting the inclusive J/ψ production from $\psi' \to \pi^+\pi^- J/\psi$ into the formula (2), we obtain

$$Br(\psi' \to \tau\tau) = (3.47 \pm 0.52 \pm 0.62) \times 10^{-3} \qquad (24)$$

which is consistent with the previous value of the $Br_{\tau\tau} = (3.54 \pm 0.61 \pm 0.63) \times 10^{-3}$.

The error sources of the $Br_{\tau\tau}$ are listed in table 4.

Table 4 the error sources of the $Br_{\tau\tau}$ (%)

error source	statistical error	systematic error
$\sigma_{N_{\tau\tau}}/(N_{\tau\tau} - L \bullet \sigma_{Q+I})$	15.03	10.91
$\sigma_{\sigma_L}/(N_{\tau\tau} - L \bullet \sigma_{Q+I})$	0.25	2.33
$\sigma_{N_{\psi'}}/(N_{\psi'})$	0.31	8.73
E_{cm} and its spread	-	11.0
$\sigma_{Br_{\tau\tau}}/Br_{\tau\tau}$	15.04	17.93

The value $Br(\psi' \to \tau\tau)/0.3885 = (8.93 \pm 1.34 \pm 1.60) \times 10^{-3}$ together with $Br_{ee} = (8.8 \pm 1.3) \times 10^{-3}$ and $Br_{\mu\mu} = (7.7 \pm 1.7) \times 10^{-3}$ are also in agreement with the $e - \mu - \tau$ universality hypothesis within the errors.

5 Acknowledgement

In this check, we obtain some useful helps and instructions from our colleagues at IHEP, we greatly acknowledge them. We also thank our colleagues in Hawaii University who provide us with the unfiltered reconstructed ψ' data.

The Preliminary Study of $\xi(2230)$ in $J/\psi \rightarrow \gamma\pi^0\pi^0$, $\gamma\eta\eta$ and $\gamma\eta\eta'$

Xiaoyan SHEN
Representing J/ψ Group
Institute of High Energy Physics, Academia Sinica,
Beijing 100039, P.R. China

Abstract

The decays $J/\psi \rightarrow \gamma\pi^0\pi^0$, $\gamma\eta\eta$ and $\gamma\eta\eta'$ have been analysed with the data collected by BES at Beijing Electron-Positron Collider (BEPC). The evidence for the existence of $\xi(2230)$ in these channels is shown and the preliminery fitting results are obtained.

1 Introduction

According to QCD, which is considered as an elementary theory describing the strong interaction, there exist 8 kinds of colored gauge boson – gluons and these gluons interact with each other. Thus, QCD predicts that two or more gluons can be bounded into a glueball. Therefore, the discovery of glueball will be of great significance in testing QCD directly and also in understanding the nature of the strong interaction.

1.1 Review of $\xi(2230)$

BES results confirmed the existence of $\xi(2230)$ in $J/\psi \rightarrow \gamma K^+K^-$ and $J/\psi \rightarrow \gamma K_s^0 K_s^0$, which was first observed by MARKIII collaboration [1] in $J/\psi \rightarrow \gamma K^+K^-$ and $J/\psi \rightarrow \gamma K_s^0 K_s^0$. BES also found two new non-strange decay modes of $\xi(2230) \rightarrow p\bar{p}$ and $\pi^+\pi^-$ [2]. The narrow width, the flavor-symmetric decay and the copious production of $\xi(2230)$ in J/ψ radiative decay reveal very important features of $\xi(2230)$.

1.2 Why study $J/\psi \rightarrow \gamma\eta\eta$, $J/\psi \rightarrow \gamma\eta\eta'$?

The knowledge about $\xi(2230)$ is still limited by the experimental facts. Thus, the study of other decay modes, such as $J/\psi \rightarrow \gamma\eta\eta$, $\gamma\eta\eta'$ etc., is very important in understanding the nature of $\xi(2230)$. Also, η and η' are considered to be strongly coupled to gluon. The signals appearing to be prominent in $\eta\eta$ and $\eta\eta'$ are traditionally regarded as glueball signatures. If $\xi(2230)$ is a glueball, it sounds that it should appear in $\eta\eta$ and $\eta\eta'$.

So far, no obvious $\xi(2230)$ signal has been found in $\eta\eta$ mass spectrum by GAMS, Crystal Ball, DM2, MARKIII and other collaborations. The first experiment which observed $\xi(2230)$ in $\eta\eta'$ is GAMS group [3]. They claimed that a peak near 2.22GeV, with a width less than 100MeV, was found in $\eta\eta'$ systems produced by 38GeV/c and 100GeV/c negative pions on protons. So, it's very important to have a look at $\eta\eta$ and $\eta\eta'$ mass spectra in J/ψ radiative decay to see if $\xi(2230)$ does exist in these two channels.

1.3 Why study $J/\psi \to \gamma\pi^0\pi^0$?

BES collaboration found two new non-strange decay modes of $\xi(2230)$ for the frist time. One of them is: $J/\psi \to \gamma\pi^+\pi^-$. If $\xi(2230)$ does exist in this channel, it should also appear in $\pi^0\pi^0$ mass spectrum and the branching ratio of $\xi(2230)$ to $\pi^0\pi^0$ should be half of that of to $\pi^+\pi^-$, whatever it is a glueball, $q\bar{q}$ or something else.

Study of $J/\psi \to \gamma\pi^0\pi^0$ is a test of $J/\psi \to \gamma\pi^+\pi^-$. Also, it is a good place to study the structures near 1500MeV and 1720MeV.

Therefore, the study of these channels is very important not only in $\xi(2230)$, but also in understanding other important structures, such as the structures around 1500MeV and 1720MeV.

2 Study of $J/\psi \to \gamma\pi^0\pi^0$

2.1 Events selection

The events without charged tracks and with the total tracks less than 12 but greater than 4 are needed. To obtain good photons, at least two layers of barrel shower counter should be hitted, the hit number of the first layer should be less than 6 and the energy of each photon should be larger than 50MeV. By using $\delta_c < 0.4$, the events which are not from the origin are excluded. Here,

$$\delta_c = (cosx - sccosx)^2 + (cosy - sccosy)^2 + (cosz - sccosz)^2, \tag{25}$$

cosx, cosy and cosz are the clusters' direction cosines, and sccosx, sccosy, sccosz are clusters' developing direction cosines in BSC. Then 4-C kinematic fit is performed to get 5 photons with the smallest χ^2. There are 15 combinations for 5 photons to construct 2 π^0s. The smallest δ is used to obtain the best combination of 2 π^0s, in which,

$$\delta = \sqrt{(m_{\gamma_1\gamma_2} - 0.135)^2 + (m_{\gamma_3\gamma_4} - 0.135)^2} \tag{26}$$

Further cuts, such as ${\chi_{4c}}^2 < 10.0$, $5 \leq N_{neu} \leq 6$ and $|m_{\gamma\gamma} - 0.135| < 0.05GeV$ are applied to get the clear $\gamma\pi^0\pi^0$ sample.

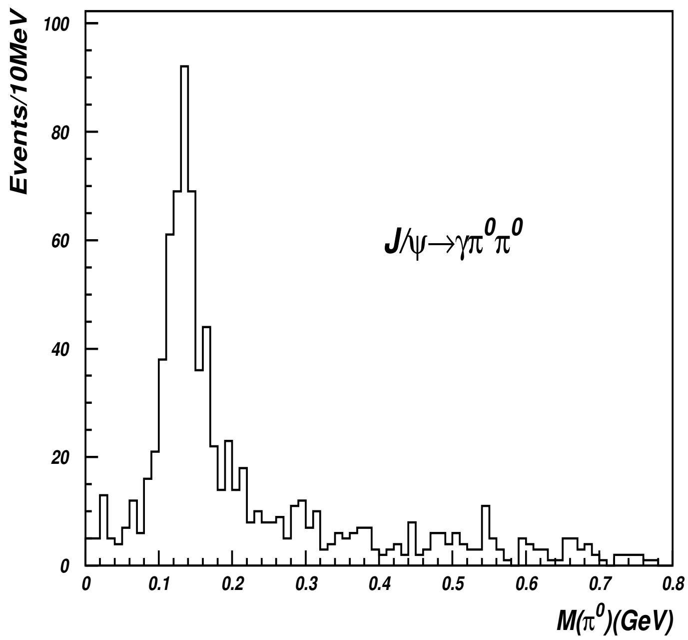

Figure 1: Invariant mass spectrum of $\gamma\gamma$

2.2 Results

Fig.1 shows us two π^0 signals. $\pi^0\pi^0$ invariant mass spectrum is shown in Fig. 2, which shows evidence for the existence of $\xi(2230)$ as well as other resonances, including $f_2(1270)$, $\theta(1710)$, $f_4(2050)$ and the so called shoulder of $f_2(1270)$ near 1.5 GeV. The fitting results and branching ratio are obtained as follows, after taking into account the mass resolution and the detection efficiency given from Monte-Carlo studies.

$$M_\xi = (2244 \pm 35)MeV \tag{27}$$

$$\Gamma_\xi = 20MeV(fixed) \tag{28}$$

$$Br(J/\psi \to \gamma\xi)Br(\xi \to \pi^0\pi^0) = (4.40 \pm 2.20 \pm 1.32) \times 10^{-5} \tag{29}$$

3 Study of $J/\psi \to \gamma\eta\eta$

3.1 Events selection

Using the similar techniques described above, we get the sample containing more than 4 good photons. After the 4-C kinematic fit, 6-C fit with $\chi_6c^2 < 15.0$ is used to retain $\gamma\eta\eta$ events.

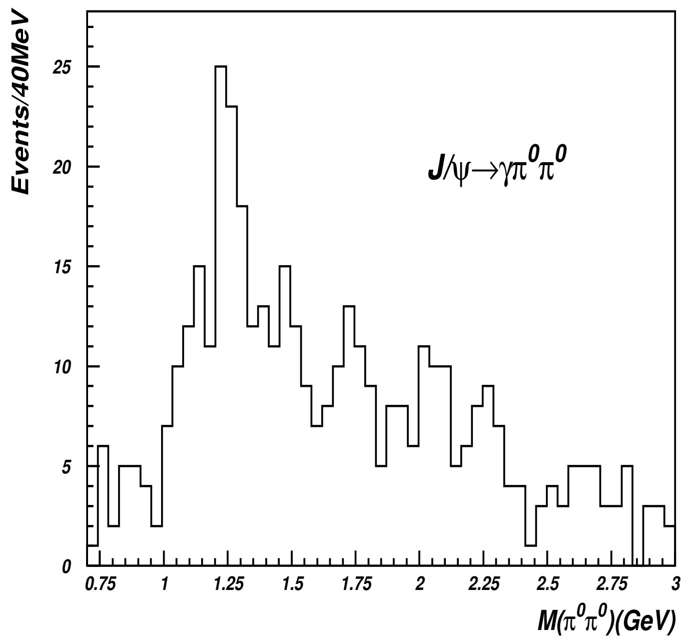

Figure 2: Invariant mass spectrum of $\pi^0\pi^0$

3.2 Results

Fig. 3 shows us the invariant mass spectrum of $\eta\eta$. A signal around 2.23 GeV can be seen. The fitting results are:

$$M_\xi = (2243 \pm 19) MeV \tag{30}$$

$$\Gamma_\xi = 20 MeV(fixed) \tag{31}$$

$$Br(J/\psi \to \gamma\xi)Br(\xi \to \eta\eta) = (2.66 \pm 1.20 \pm 0.79) \times 10^{-4} \tag{32}$$

4 Study of $J/\psi \to \gamma\eta\eta'$

4.1 Events selection

The events with 2 charged tracks and more than 3 neutral tracks are needed. For charged tracks, $R_{xy} < 0.02m$ and $Z < 0.2m$, the energy deposit of each charged track should be less than 600 MeV and $|cos\theta| < 0.8$. Here, θ is the angle between the charged track and Z direction. Then, TOF information is uesd to do the particle identification. Afterwards, the techniques as described in section 2.1 are used to choose good photons. We let the angle between each photon and its nearest charged track be larger than 15° to exclude the photons emitted from charged track. In order to get rid of the background from $\rho\pi$, the events with $|M_{\pi^+\pi^-} - 0.77| < 0.07GeV$ and $|P_{\rho^0} - 1.45| < 0.04GeV$ are excluded. After the above cuts, 4-C kinematic fit is performed and the events with the smallest ${\chi_{4c}}^2$ are remained.

For events which satisfy $|M_{\pi^+\pi^-} - 0.77| < 0.1GeV$, we consider the combination with the smallest

$$\delta = \frac{(M_{\gamma\gamma} - 0.547)^2}{{\sigma_\eta}^2} + \frac{(M_{\gamma\rho^0} - 0.958)^2}{{\sigma_{\eta'}}^2} \tag{33}$$

to be the best combination of $\eta\eta'$. Where, σ_η and $\sigma_{\eta'}$ are the mass resolutions of η and η', respectively. Fig. 4 shows the invariant mass spectrum of $\eta\eta'$. Except for the resonance of 1750 MeV, we can see clearly a structure around 2230 MeV. The following is the fitting results.

$$M_\xi = (2249 \pm 18) MeV \tag{34}$$

$$\Gamma_\xi = 20 MeV(fixed) \tag{35}$$

$$Br(J/\psi \to \gamma\xi)Br(\xi \to \eta\eta') = (1.02 \pm 0.54 \pm 0.31) \times 10^{-3} \tag{36}$$

5 Summary

We observed $\xi(2230)$ signal in J/ψ radiative decays to $\pi^0\pi^0$, $\eta\eta$ and $\eta\eta'$ and tested the existence of $\xi(2230)$ in non-strange decay mode through $\gamma\pi^0\pi^0$ channel. However, the errors are large due to not so good mass resolution and low statistics.

f(1500), f(1750) and f(2100), which were also observed by other groups, are found in these channels as well. It will be helpful for us to understand these states.

References

[1] R. M. Baltrusaitis *et al.*, Phys. Rev. Lett., 56 (1986)107;
K. F. Einsweiler, Ph.D thesis, SLAC Report No. SLAC-272, 1984 (unpublished)

[2] D. Alde *et al.*, Phys. Lett., B177 (1986) 120

[3] BES collaboration, Phys. Rev. Lett. 76 (1996) 3502

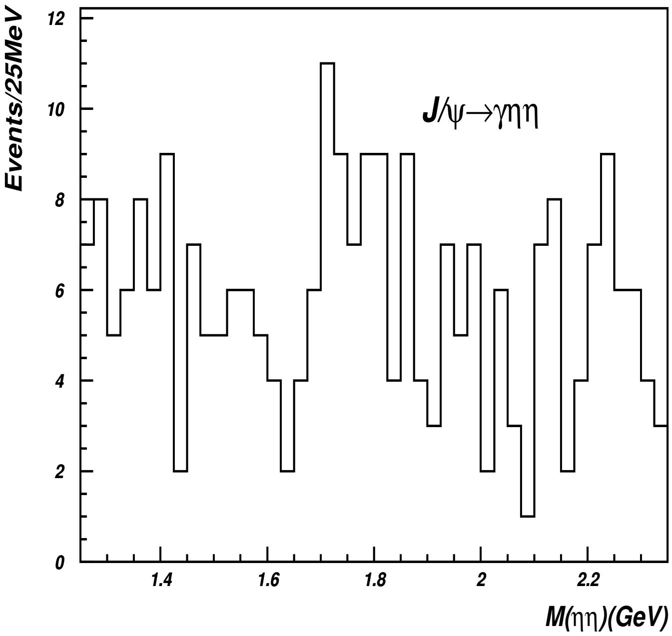

Figure 3: Invariant mass spectrum of $\eta\eta$

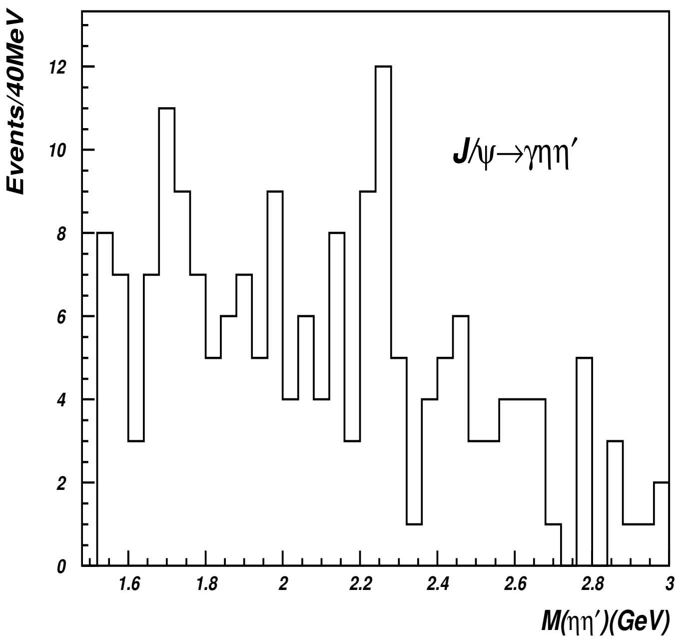

Figure 4: Invariant mass spectrum of $\eta\eta'$

The Structure Analysis of the $\mathbf{f_J(1710)}$ in the Radiative Decay $\mathbf{J/\psi \to \gamma K^+K^-}$

Lan-Chun LU (The BES J/ψ Group)

Institute of High Energy Physics, Beijing 100039, People's Republic of China

Abstract

The data on $J/\psi \to \gamma K^+K^-$ from the BES experiment at the Beijing electron-positron collider (BEPC) have been analysed. We find two resonances in 1.7 GeV region which were identified as $f_J(1710)$: a scalar with mass $1781 \pm 8^{+10}_{-31}$(MeV) and width $85 \pm 24^{+22}_{-19}$(MeV), and a tensor with mass $1696 \pm 5^{+9}_{-34}$(MeV) and width $103 \pm 18^{+30}_{-11}$(MeV). The resulting branching ratios $Br(J/\psi \to \gamma f_J)Br(f_J \to K^+K^-)$ are $(0.8 \pm 0.1^{+0.3}_{-0.1})10^{-4}$ for $J = 0$ and $(2.5 \pm 0.4^{+0.9}_{-0.4})10^{-4}$ for $J = 2$ respectively.

1 Introduction

There have been considerable recent interests in the $f_J(1710)$ and its role in the glueball spectroscopy. Phenomenologically, since the $f_J(1710)$ was first discovered by the Crystal Ball Collaboration in $J/\psi \to \gamma\eta\eta$ [1], it has been observed in other channels of J/ψ decay[2, 3], the pp central production[4], π^-p induced reactions [5, 6], in which the productions of glueballs are expected to be enhanced, while there is no evidence of the $f_J(1710)$ in $\gamma\gamma$ collisions[7] where the glueball production should be suppressed. Moreover, the $f_J(1710)$ has not been observed in the K^-p reaction[8], which suggests that it be unlikely an $s\bar{s}$ state. The recent investigation[9] shows that the nature of this state depends critically on whether its spin-parity is 0^{++} or 2^{++}; a scalar $f_J(1710)$ is likely a glueball state. The calculations on QCD lattice predict[10, 11] that the lightest glueball should be a scalar with mass $1.5 \sim 1.7$ GeV, which is consistent with the mass of $f_J(1710)$. The study[12] by Amsler and Close suggests that the $f_0(1500)$ should be a glueball mixed with the nearby flavourless member of the $^3P_0$ $q\bar{q}$ nonet. If this is indeed to be the case, another state orthogonal to the $f_0(1500)$ is believed in this region. Such a state orthogonal to the $f_0(1500)$ is expected to have a large branching ratio in its decay into $K\bar{K}$, as the data[13] from the Crystal Barrel show that the branching ratio of the $f_0(1500)$ decaying into $K\bar{K}$ is smaller than that expected for a glueball state. If the $f_J(1710)$ proves to be $J = 0$, it fits the profile of such a state and becomes an important glueball candidate. Thus, the reaction $J/\psi \to \gamma K\bar{K}$ would be a very important channel to investigate the $f_J(1710)$, because the production of a scalar glueball with relative large $K\bar{K}$ branching ratio is assumed to be enhanced in this reaction.

The spin of the $f_J(1710)$ has not been well determined experimentally. The report from the DM2 data indicated equal likelihoods of both 0^{++} and 2^{++}[2], and the result from Mark III showed that it is dominated by the spin zero state[14]. The $f_J(1710)$ produced in the central region of the reaction $pp \to p_f(K\bar{K})p_s$[4] favours strongly spin two at $m = 1713$ MeV, while a spin zero resonance with mass 1771 MeV is claimed in another reaction $\pi^-(23\text{GeV}/c^2)p \to K_s^0K_s^0n$ [5]. The recent analysis[15] of the $J/\psi \to \gamma\pi^+\pi^-\pi^+\pi^-$ data from the MARK III showed the presence of both 0^{++} and 2^{++} states in this region. In this report, we present an analysis of the recent $J/\psi \to \gamma K^+K^-$ data from BES experiment at BEPC. Our result clearly shows the existence of both scalar and tensor states in the $f_J(1710)$ region.

2 Event selection

The preliminary selection of the γK^+K^- events chooses those that have two opposite charged tracks, of which the momentum is smaller than the mass of J/ψ. Each charged track should have a good helix fit in order to ensure a correct corresponding error matrix in the kinematic fit. Moreover, more than one photon per event is allowed to consider the possible existence of the fake photons which come from the interactions of the charged tracks with the shower counter or from electronic noise in the shower counter. Following selection criteria are used to remove the Bhabha events

1. The opening angle of two tracks $\theta_{op} < 175°$.
2. The energy deposit of each track in BSC $E_{sc} < 1.0$ GeV.
3. The angle between each track and Z direction (positron beam direction) satisfies $|\cos\theta| < 0.7$.

If the two charged tracks are accollinear and the muon counter is hit, the event is rejected as a $\gamma\mu^+\mu^-$ event. It is required that the kinematic variable $|U| = |E_{miss} - |\mathbf{P}_{miss}|| < 0.1$, where E_{miss} and $\mathbf{P}_{miss}$ are the missing energy and missing momentum of all charged particles respectively, and they are calculated by assuming two charged particles as K^+K^- pair. This requirement can remove most background contributions from the events having multipion or other neutral particles. Another important cut $P_{t\gamma}^2 \equiv 4|\mathbf{P}_{miss}|^2\sin^2(\theta_{m\gamma}/2) < 0.0035$ GeV^2 is used to eliminated background photons, where $\theta_{m\gamma}$ is the angle between the missing momentum and the photon direction. The 4-C kinematic fits are performed by assuming the final state as a $\gamma\pi^+\pi^-$ or a γK^+K^- separately for each event, and the event is excluded if $\chi^2_{\gamma\pi^+\pi^-} < \chi^2_{\gamma K^+K^-}$. Thus, after all these cuts, the background from following reactions are greatly removed: (1) $J/\psi \to K^{*\pm}K^{\mp}$, (2)$J/\psi \to \rho^{\pm}\pi^{\mp}$, (3) $J/\psi \to \rho^0\pi^0$, (4) $J/\psi \to \gamma f_2(1270)$, (5) $J/\psi \to \gamma\eta(1440)$. The Monte Carlo simulations indicate that the efficiencies for these reactions are 3.3%, 0.7%, 0.02%, 0.2%, and 0.09% respectively. Furthermore, the most

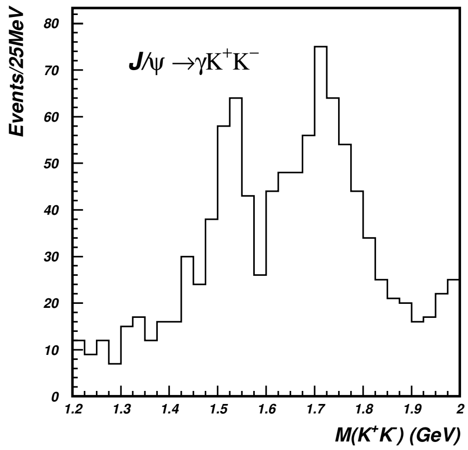

Figure 1: Mass distribution for $J/\psi \to \gamma K^+K^-$.

events with $K^{*\pm}K^{\mp}$ and $\rho^{\pm}\pi^{\mp}$ final states are distributed on high mass region (> 2 GeV). The K^+K^- invariant mass spectrum is shown in Fig. 1, wherein the resonance structure in 1.5 and 1.7 GeV region is clearly seen.

3 Spin-parity analysis of $\mathbf{f_J(1710)}$

For the process $J/\psi \longrightarrow VX(X \longrightarrow P\bar{P})$, the moment is defined as

$$T_r = \int W(\theta_V, \Omega) R_e[D^j_{0,-m}(0, \theta_V, 0) D^l_{m,0}{}^*(\Omega)] d\cos\theta_V d\Omega, \tag{37}$$

where $W(\theta_V, \Omega)$ is the angular distribution, r denotes (j, l, m), and P represents a pseudoscalar particle. The measured moment is

$$N'_\mu = \sum_{events} Re[D^j_{0,-m}(0, \theta_V, 0) \cdot D^l_{m,0}(\Omega)], \tag{38}$$

and the correlation matrix of N'_μ is

$$\begin{aligned} O_{\mu\nu} \quad = \quad & \sum_{events} R_e[D^{j'}_{0,-m'}(0, \theta_V, 0) D^{l'}_{m',0}(\Omega)] \\ & \cdot R_e[D^j_{0,-m}(0, \theta_V, 0) D^l_{m,0}(\Omega)], \end{aligned} \tag{39}$$

where μ and ν denote the indices (j', l', m') and (j, l, m) respectively.

The efficiency-corrected measured moment can be expressed as

$$N = C^{-1} N' \tag{40}$$

or

$$N_\mu = \sum_\nu C^{-1}_{\mu\nu} N'_\nu. \tag{41}$$

The quantity C in eqs. (40) and (41) is the efficiency correction matrix,

$$\begin{aligned} C_{\mu\nu} \; &= \; \frac{1}{N_g} \sum_{i=1}^{N_a} R_e[D^{j'}_{0,-m'}(0,\theta_V,0) D^{l'}_{m',0}(\Omega)] \\ &\cdot (2-\delta_{m0}) R_e[D^{j}_{0,-m}(0,\theta_V,0) D^{l}_{m,0}(\Omega)], \end{aligned} \tag{42}$$

The covariance matrix of N is

$$V = C^{-1} O (C^{-1})^T, \tag{43}$$

where N_a is the events number accepted by detector after the events selection, and N_g is the events number generated in Monte Carlo simulation.

Previous work by BES at BEPC [16] indicates that there exists a spin 0 and a spin 2 component in the mass region of $f_J(1710)$. The higher spin components are excluded as the results from PQCD[17] show that the contributions from the high spin (> 2) components are very small. The theoretical moments of radiative decay $J/\psi \longrightarrow \gamma X (X \to P\bar{P})$, $T_r \equiv T(j,l,m)$, with 0^{++} and 2^{++} components can be written as[18]

$$T(000) \sim 8[(A_{10}^2 + A_{11}^2 + A_{12}^2) + B_{10}^2], \tag{44}$$

$$T(200) \sim \frac{4}{5}[(A_{10}^2 - 2A_{11}^2 + A_{12}^2) + B_{10}^2], \tag{45}$$

$$T(020) \sim 8[\frac{1}{7}(2A_{10}^2 + A_{11}^2 - 2A_{12}^2) + \frac{1}{\sqrt{5}} A_{10} B_{10} \gamma], \tag{46}$$

$$T(220) \sim \frac{8}{5}[\frac{1}{7}(A_{10}^2 - A_{11}^2 - A_{12}^2) + \frac{1}{2\sqrt{5}} A_{10} B_{10} \gamma], \tag{47}$$

$$\begin{aligned} T(221) \;\; &\sim \;\; \tfrac{4}{5}[\tfrac{1}{7}(\sqrt{3} A_{10} A_{11} - -3\sqrt{2} A_{11} A_{12}) \\ &+ \frac{\sqrt{3}}{2\sqrt{5}} A_{11} B_{10} \gamma], \end{aligned} \tag{48}$$

$$T(222) \sim \frac{4\sqrt{6}}{5}[-\frac{2}{7} A_{10} A_{12} + \frac{1}{2\sqrt{5}} A_{12} B_{10} \gamma], \tag{49}$$

$$T(040) \sim \frac{8}{21}(6A_{10}^2 - 4A_{11}^2 + A_{12}^2), \tag{50}$$

$$T(240) \sim \frac{4}{105}(6A_{10}^2 + 8A_{11}^2 + A_{12}^2), \tag{51}$$

$$T(241) \sim \frac{4}{105}(3\sqrt{10} A_{10} A_{11} + \sqrt{15} A_{11} A_{12}), \tag{52}$$

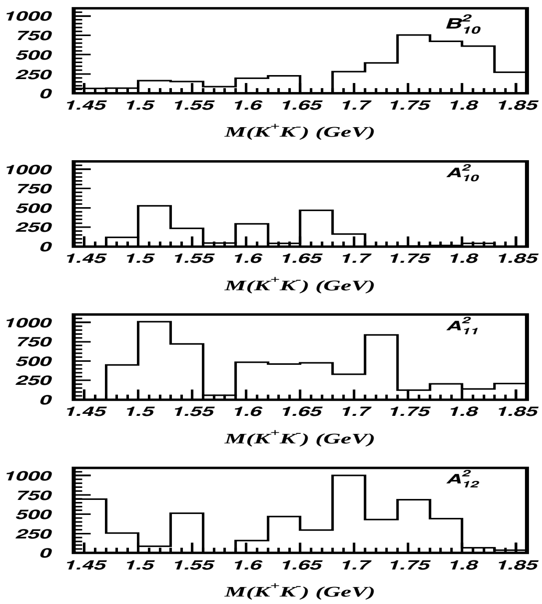

Figure 2: The helicity amplitudes versus invariant mass K^+K^-.

$$T(242) \sim \frac{4\sqrt{10}}{35} A_{10} A_{12}. \tag{53}$$

where B_{10} is the helicity amplitude for 0^{++} component, A_{10},A_{11} and A_{12} are those for 2^{++}, and $\gamma \equiv 2\cos\phi$ represents the interference between 0^{++} and 2^{++}.

4 Results

The objective function is defined as

$$\Lambda^2 = (N - T)V^{-1}(N - T) \tag{54}$$

and the standard Minuit Program in CERN LIBRARY is used to minimize Λ^2. The invaraint mass spectrum K^+K^-(from $1.44 - 1.86$ GeV/c^2) is divided into 14 bins with 30 MeV bin width in order to ensure both high statistics in each bin and small enough mass interval for performing a moment analysis. The helicity parameters are obtained for each bin respectively by minimizing the Λ^2, in which $\gamma \equiv 2\cos\phi$ ranges from -2 to 2. The helicity amplitudes B_{10}, A_{10}, $\cdots$ from above fits are shown in Fig. 2. There is a multi-solution problem for some bins, and we resolve this by finding all possible solutions for the bin and choosing the one that has the smallest Λ^2 and small errors of helicity amplitudes.

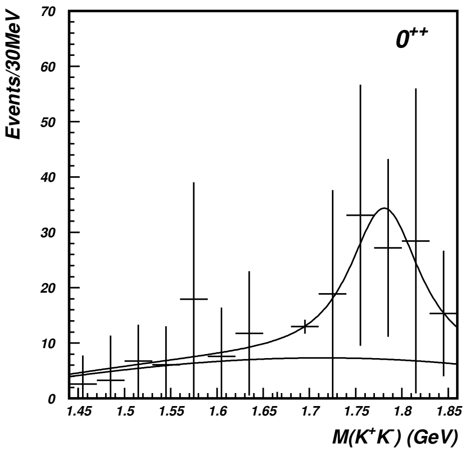

Figure 3: The separated 0^{++} from $f_J(1710)$.

Table 1: The masses, widths, and branching ratios of $X_{0^{++}}$ and $X_{2^{++}}$.

Spin	Mass(MeV)	Width(MeV)	$Br(J/\psi \to \gamma X)(X \to K^+K^-)(10^{-4})$
0^{++}	$1781 \pm 8^{+10}_{-31}$	$85 \pm 24^{+22}_{-19}$	$0.8 \pm 0.1^{+0.3}_{-0.1}$
2^{++}	$1696 \pm 5^{+9}_{-34}$	$103 \pm 18^{+30}_{-11}$	$2.5 \pm 0.4^{+0.9}_{-0.4}$
$f_2'(1525)$	$1516 \pm 5^{+9}_{-15}$	$60 \pm 23^{+13}_{-20}$	$1.6 \pm 0.2^{+0.6}_{-0.2}$

The contributions to the γK^+K^- mass spectrum from 0^{++} and 2^{++} components are shown in Fig. 3 and Fig. 4 respectively, which are renormalized to the observed mass spectrum.

The $f_2'(1525)$ is well reproduced in Fig. 4, and a second 2^{++} resonance $X_{2^{++}}$ appears in the lower part of the $f_J(1710)$ mass region. Fig. 3 shows the presence of a 0^{++} resonance $X_{0^{++}}$ in the higher part of $f_J(1710)$ mass region, and it accounts for thirty percent of $f_J(1710)$ with nearly ten percent uncertainty. The masses, widths and branching ratios of of 0^{++} and 2^{++} are given in Table I, in which the errors come from the Breit-Wigner fit and the uncertainties of the background shape and the bin widths respectively. The branching ratios are estimated by using the acceptance efficiency from Monte Carlo simulation and the fit of the spectra of these resonances.

The hadronic decay $J/\psi \to \omega K^+K^-$ is also useful to study the identification of the $f_J(1710)$ because the $f_2'(1525)$ in this channel is bellow the threshold. It is expected that this can be carried out with the upgraded BES and more J/ψ events in the near future.

In summary, a scalar and a tensor are separated from the broad resonance around 1.7 GeV. The scalar $X_{0^{++}}(1780)$ in the $f_J(1710)$ mass region is clearly established in our analysis. Further investigation on the other channels, such as $J/\psi \to \gamma 4\pi$

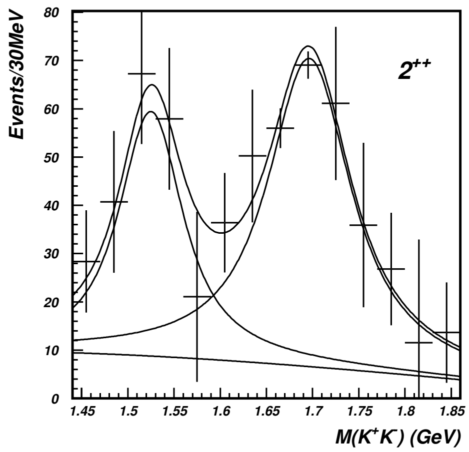

Figure 4: The separated 2^{++} from $f_J(1710)$.

and the $J/\psi \to \gamma\pi\pi$ will be helpful to understand the nature of the scalar and tensor.

Acknowledgment

This work was supported partly by the National Science Foundation of China under Contract No. 19290401. We would like to thank the staff of the BEPC accelerator and the IHEP Computing Center.

References

[1] C. Edwards et al., Phys. Rev. Lett. 48 (1982) 458.

[2] J.E. Augustin et al., Phys. Rev. Lett. 60 (1988) 2238.

[3] R.M. Baltrusaitis et al., Phys. Rev. D 35 (1987) 2077; T. Bolton, Ph.D thesis, MIT (1988).

[4] T.A. Armstrong et al., Phys. Lett. B 167 (1986) 133; Phys. Lett. B 227 (1989) 186.

[5] A. Etkin et al., Phys. Rev. D 25 (1982) 1786.

[6] B. Bolonkin et al., Nucl. Phys. B 309 (1988) 426.

[7] H. Aihara et al., Phys. Rev. Lett. 57 (1986) 404.

[8] D. Aston et al., Nucl. Phys. B 301 (1988) 525;

[9] F. Close, G. Farrar, and Zhenping Li, to be published.

[10] G. Bali et al., Phys. Lett. B 309 (1993) 378.

[11] D. Weingarten, Nucl. Phys. B (Proc. Suppl.) 34 (1994) 29; J. Sexton *et al.*, Phys. Rev. Lett. 75 (1995) 4563.

[12] C. Amsler and F. E. Close, Phys. Rev. D 53 (1996) 295.

[13] A. Abele, *et al*, Submitted to Phys. Lett. B; C. Amsler, *et al.*, Phys. Lett. B 335 (1995) 425.

[14] L.P. Chen, Ph.D thesis, SLAC-Repot-386 (1991).

[15] D. V. Bugg, *et al.* Phys. Lett. B 353 (1995) 378.

[16] Z.P. Zheng, The Report from the BES at BEPC. AIP Conference Proceedings 302, Lepton and photon Interactions, XVI international Sysmposim, Itheca, NY1993, p530; Z.D. Cheng, MS thesis, IHEP Beijing (1992).

[17] A. Billoire *et al.*, Phys. Lett. B 80 (1979) 381.

[18] H. Yu, Q.X. Shen, Y.C. Zhu, Z.P. Zheng and Z.D. Cheng, High Energy Phys. and Nucl. Phys. 17 (1993) 143.

Search For Hybrid states in J/ψ Decays

Jingtang HE Jimen WU Jinguo BIAN
Sheng FENG Zuhao LI Jimao MA
Institute of High Energy Physics, Chinese Academy of Sciences
100039, Beijing, PRC

Abstract

A search for hybrid states in J/ψ decays were carried out,several candidates of hybrid state were found. In J/$\psi \rightarrow \rho + \pi$ $f_2(1520)$ and J/$\psi \rightarrow \rho + \pi f_2(1270)$decays, the peaks of M($\pi f_2$) at about 1.9 GeV were found with different charge combinations.In J/$\psi \rightarrow \phi + K^+K^-\eta$ decay, a peak of M($K^+K^-\eta$) at about 1.9 GeV was also found. These peaks could be explained as evidence of existing hybrid ρ and hybrid ϕ state.

I. Introduction

The well-known candidates of glueball are $\iota(1440)$,G(1590), $\theta(1720)$,$\xi(2230)$,$g_T(2050)$, $g_T(2200)$,$g_T(2350)$.None of them is fixed as glueball. Some candidate found in fixed target experiment without corresponding candidate in J/ψ decays, such as G(1590), g_T states, which never be found in J/ψ decays. Another difficulty of searching for glueball is that glueball is an isospin singlet, it means that the numbers of glueball are limited. Contrariwise,hybrid states can be produced by radiative decays or by hadronic decays in J/ψ decays,it means that we could use more channels in J/ψ decays to search for hybrid states. The quantum number of J/ψ is well-known. If the hybrid state is produced by two body decay in J/ψ decays, if one of the two particles is well-known, the quantum number of another particle should be set to a certain value, one could use this properties to see it is normal $q\bar{q}$ meson or exotic meson. For hybrid states, it could be isospin singlet or isospin multiplet. If one found a hybrid family with I=1, I_3=+1,0,-1, the mass of these states are nearly the same, like that of π^+, π^-, π^0 family. This fact itself is a good evidence of existence of hybrid states.

There are some hints of existence of hybrid states from experiment abroad.[1][2][3] The light $q\bar{q}g$ hybrid meson multiplet arises when each $q\bar{q}$ is in the lowest (1S) mode and the gluon is in the lowest TE(J^p) = 1^+ mode. This leads to the following quantum number:[4] $J^{pc} = 2^{-+}, 1^{-+}, 0^{-+}, 1^{--}$. Fig.1.describes the productions of hybrid states in J/ψ decays. As can be seen that there are four kind of hybrid states: hybrid ρ, hybrid ϕ, hybrid ω and hybrid K states. The way to find hybrid states in J/ψ decays is following:
For hybrid ρ, J/$\psi \rightarrow \rho$ + H_ρ,
For hybrid ϕ, J/$\psi \rightarrow \phi$ + H_ϕ,
For hybrid ω, J/$\psi \rightarrow \eta$ + H_ω,
For hybrid K, J/$\psi \rightarrow$K+H_K.
The mass of hybrid states predicted by different model are different. F.Close et al[4]using Bag Model predicted that the mass of hybrid states with different quantum number are different as shown in Fig.2. N.Isgur et al [5] using Flux Tube Model predicted that the mass of hybrid states with different quantum number are serious degenerated, its mass will be concentrated between 1.8 GeV to 2.2 GeV with 0.2 GeV errors, as shown in Fig.3.

II. Some hints from our group

A. J/$\psi \rightarrow \rho$ + X$\rightarrow \rho$ + πf_2(1520)

1.Events selections

(1) The criteria of selections for charged tracks:
The numbers of charged tracks N_{charge}=4 was required. Requiring M_{fit}=2 or -19 to get good quarlity of charged tracks. The total charge of these four charged tracks should equal to zero. To guarantee the tracks come from interaction point, requiring:

$$\sqrt{X_0^2 + Y_0^2} < 2cm$$

$$\mid Z_0 \mid < 20cm$$

We take the tracks in the barrel part only. Using TOF or dE/dX information to identify pions, requiring W(π)>W(K,P).
(2)The criteria of selections for photons:
The numbers of photons are large then 2 and less then 6. To reject fake photons, $E_\gamma > 50MeV$ was required. From selected photons and 4π informations, a 4C-fit was made to select 2 good photons, if χ^2<50, then take the selected 2 photons as 2 real photons.
(3)For π^0 selections, to reject fake photons, M($\pi^+\pi^-$ $\pi^+\pi^-$)<(3.1GeV-0.15GeV)<2.9GeV was required. Requiring |$M_{\gamma\gamma}$-0.135|<60MeV.
(4)Using 5C-fit, requiring χ^2<30 to select π^+ $\pi^-\pi^+\pi^-\pi^0$ events.
(5) To select ρ^0, defining:
$\Delta\rho^0$=|M($\pi_i^+\pi_j^-$)-0.77| ^{2} i,j=1,2
ΔK^0=|M($\pi_i^+\pi_j^-$)-0.498| ^{2} i,j=1,2

$\Delta f_0 = |M(\pi_i^+\pi_j^-)\text{-}0.98|^2$ i,j=1,2
Requiring $\Delta\rho<\Delta K$ and $\Delta\rho<\Delta f_0$
(6)For $f_2(1520)$ selection, requiring $|M(\pi^+\pi^-)$ -1.52$|$<100MeV
(7)To reject background, defining:

$$\Delta = \frac{1}{1+(\frac{M_{\gamma\gamma}-0.135}{\sigma_{\pi^0}})^2} \times \frac{1}{1+(\frac{M_\rho-0.77}{\sigma_\rho})^2} \times \frac{1}{1+(\frac{M_{f_2}-1.52}{\sigma_{f_2}})^2}$$

Δ>0.3 was required.
The same principles were used to events selections for $J/\psi\to\rho + \pi f_2(1270)$ and $J/\psi\to\phi + K^+K^-\eta$ decays.

2. Preliminary results

The preliminary results of $J/\psi\to\rho+\pi f_2(1520)$ are shown in Fig.4. Fig.4.a. is the invariant mass distribution of $M(\pi^+f_2(1520))$ in $J/\psi\to\rho^- + \pi^+f_2(1520)$ decays, Fig.4.b. is the invariant mass distribution of $M(\pi^-f_2(1520))$ in $J/\psi\to\rho^+ + \pi^-f_2(1520)$ decays, Fig.4.c. is the invariant mass distribution of $M(\pi^0f_2(1520))$ in $J/\psi\to\rho^0 + \pi^0f_2(1520)$ decays, Fig.4.d. is the invariant mass distribution of $M(\eta f_2(1520))$ in $J/\psi\to\rho^0 + \eta f_2(1520)$ decays. It can be seen that there are peaks of $M(\pi f_2)$ at about 1.9GeV. Fig.5.a. is the result of adding up of Fig.4.a. and Fig.4.b. Using one B-W peak to fit the curve, the result is $M(X^\pm)=(1.926\pm0.004)$GeV, 3σ significance. Fig.5.b. is the peak fitting for $M(\pi^0f_2)$, the result is $M(X^0)=(1.888\pm0.006)$GeV, 3.5σ significance. We can get: $M(X^\pm) - M(X^0) \simeq 38MeV$.

B. $J/\psi\to\rho$ + $X\to\rho$ + πf_2(1270)

The preliminary results of $J/\psi\to\rho + \pi f_2(1270)$ are shown in Fig.6. Fig.6.a. is the invariant mass distribution of $M(\pi^+f_2(1270))$ in $J/\psi\to\rho^- + \pi^+f_2(1270)$ decays, Fig.6.b. is the invariant mass distribution of $M(\pi^-f_2(1270))$ in $J/\psi\to\rho^+ + \pi^-f_2(1270)$ decays, Fig.6.c. is the invariant mass distribution of $M(\pi^0f_2(1270))$ in $J/\psi\to\rho^0 + \pi^0f_2(1270)$ decays, Fig.6.d. is the invariant mass distribution of $M(\eta f_2(1270))$ in $J/\psi\to\rho^0 + \eta f_2(1270)$ decays. It can be seen that there are two well-known peaks of $M(\pi f_2)$ named $\pi_2(1670)$, $\pi_2(2100)$ and one peak named $\pi(1770)\to\ \pi f_0(1300)$. These three peaks can serve as calibration peaks. In addition, there is one more new peak with mass of about 1.9GeV.

C. $J/\psi\to\phi$ + $Y\to\phi$ + $K^+K^-\eta$

The preliminary result of $J/\psi\to\phi + K^+K^-\eta$ is shown in Fig.7. There is a peak of $M(K^+K^-\eta)$ at about 1.9GeV.

III. Discussion

From our data, there seems a isospin multiplet family of X particles with I=1, I_3=+1,0,-1 and the state of Y with I=0, I_3=0. From our preliminary results,if we suppose above X particle as hybrid $\rho(H\rho)$ and the Y particle as hybrid $\phi(H\phi)$, it seems that the mass of H_ρ and H_ϕ are concentrated at about 1.9GeV. This phenomenon was predicted by Flux Tube Model. In the normal $q\bar{q}$ meson picture, there is no place for these new particles. We think that there are rich physics in "Search for hybrid states in J/ψ decays."

References

[1] M.Amelin et al Proc. of XXVII High Energy Phy.Conf.P.1409

[2] L3 group Phys.Lett.B363(1995)118

[3] M.Feindt DESY 90-128

[4] F.E.Close Rep.Proc.Phy.51(1988)833

[5] N.Isgur and J.Paton Phys.Rev.D31(1985)2910

Results on J/$\psi \to \gamma + \eta\pi^+\pi^-$ and J/$\psi \to \gamma + \eta\eta'$ Decays

Hong YE Jingtang HE Jimao MA
Institute of High Energy Physics, Chinese Academy of Sciences
100039, Beijing, PRC

Abstract

The results on J/$\psi \to \gamma + \eta\pi^+\pi^-$ and J/$\psi \to \gamma + \eta\eta'$ decays are presented. Three peaks of M($\eta\pi^+\pi^-$) with mass at about 1280, 1400 and 1500 MeV in J/$\psi \to \gamma + \eta\pi^+\pi^-$ were found. A peak of M($\eta\eta'$) with mass at about 2.2GeV in J/$\psi \to \gamma + \eta\eta'$ was also found. The peak of M($\eta\eta'$) with mass at about 2.2GeV could be explained as evidence of $\xi(2230) \to \eta\eta'$.

I. Results on J/$\psi \to \gamma + \eta\pi^+ \pi^-$ decays

1. Introduction

The discovery of glueball candidate of $\iota(1440)$ in J/$\psi\to \gamma$ + K$\bar{K}\pi$ decay stimulates the search for $\iota(1440)$ in another J/ψ channels. Since $\iota(1440)$ can decay to K$\bar{K}\pi$ through intermediate state a$_0$(980)π, so that $\iota(1440)$ decays to the final state $\eta\pi^+\pi^-$ is expected. Since[1]

$$\frac{Br(a_0 \to K\bar{K})}{Br(a_0 \to \eta\pi)} \simeq \frac{1}{10}$$

if $\iota(1440)$ could decay through intermediate state a$_0$(980)π, one could expect:

$$Br(\iota(1440) \to \eta\pi^+\pi^-) > 10 Br(\iota(1440) \to K\bar{K}\pi)$$

2.Events selections

(1) The criteria of selections for charged tracks:
The numbers of charged tracks N_{charge}=2 was required. Requiring M_{fit}=2 or -19 to get good quarlity of charged tracks. The total charge of these two charged tracks should equal to zero. To guarantee the tracks come from interaction point, requiring:

$$\sqrt{X_0^2 + Y_0^2} < 2cm$$

$$\mid Z_0 \mid < 20cm$$

We take the tracks in the barrel part only. Using TOF information to identify pions, requiring $W(\pi) > W(K,P)$.
(2)The criteria of selections for photons:
The numbers of photons are larger than 3 and less then 8. To reject fake photons, $E_\gamma > 80MeV$ was required. The angle between the direction of shower development and the line of interaction point and first hit point of photon in the shower counter $<30^0$. The angle between charged tracks and photon larger than 12^0 is required. From selected photons and 2π informations, a 4C-fit was made to select 3 good photons, if $\chi^2 < 50$, then take the selected 3 photons as 3 real photons.
(3)defining $\alpha_{\gamma\eta}$ for η selections
The definition of $\alpha_{\gamma\eta}$ is shown in Fig.1.1. One could calculate the direction of γ_1 in the framework of $\pi^+\pi^-$ from $J/\psi \to \eta\pi^+\pi^-$ and from data, one could measure the direction of γ_1

$$\alpha_{\gamma\eta} = cos(\vec{P}(\gamma_1, expected)) \bullet (\vec{P}(\gamma_1, measured))$$

To select real $J/\psi \to \eta\pi^+\pi^-$ event, making different combination from selected 3 real photons, selecting event with $\alpha_{\gamma\eta} \simeq 1$ as the $J/\psi \to \eta\pi^+\pi^-$ candidate event, then doing η mass constrain and momentum constrain 5C-fit, requiring $\chi^2 < 11$.
(4) Background rejections:
(a)$J/\psi \to \gamma + \pi^0\pi^+\pi^-$
Defining $\alpha_{\gamma\pi^0}$ as above $\alpha_{\gamma\eta}$, rejecting the event with $\alpha_{\gamma\pi^0} \simeq 1$.
(b)$J/\psi \to \gamma + \pi^+\pi^- +$ neutrons
Defining $P_{tr}^2 = 4 \mid \vec{P}_{miss} \mid^2 \bullet sin^2\Theta/2$, requiring $P_{tr}^2 < 0.1$.
(c)$J/\psi \to \rho^0 + \pi^0$
From the two body decay of $J/\psi \to \rho^0 + \pi^0$, $\vec{P}_{\rho^0}$=1.449GeV,rejecting events with

$$\mid \vec{P}_{\pi^+\pi^-} - 1.449 \mid \leq 0.04GeV$$

$$\mid M_{\pi^+\pi^-} - 0.768 \mid \leq 0.075GeV$$

(d)Another background:
$J/\psi \to \omega\eta, \omega\pi^0, \pi^+\pi^-\pi^0$, rejecting events with $\mid M_{\gamma\gamma} - M_{\pi^0} \mid < 40$MeV.
(5)Calibration
Taking $J/\psi \to \gamma + \eta' \to \gamma + \eta\pi^+\pi^-$ as calibration peak. The result is shown in Fig.1.2, from our data fit:

$$M(\eta') = 956.8MeV$$

$$\Gamma(\eta') = 5MeV$$

From PDG data:

$$M(\eta') = (957.7 \pm 0.14)MeV$$

$$\Gamma(\eta') = (0.201 \pm 0.016)MeV$$

Our data is in good agreement with PDG data.
(6) Intermediate state $a_0(980) \rightarrow \eta\pi$ cut, requiring $\mid M(\eta\pi) - 980 \mid < 80MeV$.

3.Preliminary results

There are three peaks of M($\eta\pi^+\pi^-$) in J/$\psi \rightarrow \gamma + a_0\pi \rightarrow \gamma + \eta\pi^+\pi^-$, the results are shown in Fig.1.3.

$$X(1280) 3.4\sigma significance$$
$$X(1400) 3.5\sigma significance$$
$$X(1510) 3.0\sigma significance$$
$$M(1280) = (1269 \pm 11)MeV$$
$$\Gamma(1280) = (50 \pm 32)MeV$$
$$Br(J/\psi \rightarrow \gamma + X(1280)) \bullet Br(X(1280) \rightarrow a_0\pi) = (2.5 \pm 0.9 \pm 1.0) \times 10^{-4}$$
$$M(1400) = (1382 \pm 7)MeV$$
$$\Gamma(1400) = (27 \pm 21)MeV$$
$$Br(J/\psi \rightarrow \gamma + X(1400)) \bullet Br(X(1400) \rightarrow a_0\pi) = (2.7 \pm 0.9 \pm 0.8) \times 10^{-4}$$
$$M(1510) = (1515 \pm 5)MeV$$

There is no sign of J/$\psi \rightarrow \gamma + \iota(1440) \rightarrow \gamma + \eta\pi^+\pi^-$. The up limit for J/$\psi \rightarrow \gamma + \iota(1440) \rightarrow \gamma + \eta\pi^+\pi^-$ is:

$$Br(J/\psi \rightarrow \gamma\iota) \bullet Br(\iota \rightarrow \eta\pi^+\pi^-) < 1.9 \times 10^{-4}$$

90 percent C.L.

II.Result on J/$\psi \rightarrow \gamma + \eta\eta'$ decay

1.Introduction

In 1986,GAMS group in $\pi^- P \rightarrow \eta\eta' n$ reaction,found that M($\eta\eta'$)=(2.220 $\pm$ 0.010)GeV[2]. Mark-III group in J/$\psi \rightarrow \gamma + K^+K^-$ and J/$\psi \rightarrow \gamma + K_s^0 K_s^0$ found that[3]

$$M(K^+K^-) = (2230 \pm 6 \pm 14)MeV$$
$$M(K_s^0 K_s^0) = (2232 \pm 7 \pm 7)MeV$$

and named this particle as $\xi(2.2)$. But,DM2 group has not found ξ particle in 8.6×10^6 J/ψ event data samples.[4] In BES group,Dr Jin San comfirmed the discoveries of ξ particle from Mark-III in K^+K^- and $K_s^0 K_s^0$ channels,and Dr Jin San found another two new channels of ξ particle:

$$J/\psi \rightarrow \gamma + \xi(2230) \rightarrow \gamma + \pi^+\pi^-$$
$$J/\psi \rightarrow \gamma + \xi(2230) \rightarrow \gamma + P\bar{P}$$

It is interesting to search for ξ particle in another J/ψ decay channels.Our group made an analysis of J/$\psi \rightarrow \gamma + \xi(2.2) \rightarrow \gamma + \eta\eta'$ based on about 8×10^6 J/ψ events from BES.

2.Event Selections and Background Rejections

The princples of event selection are the same as that in J/$\psi \to \gamma + \eta\pi^+\pi^-$. Now in J/$\psi \to \gamma + \eta\eta$' with $\eta \to \gamma\gamma$ and $\eta' \to \gamma\rho$, 4γ and 2 prong tracks were selected. The main background come from J/$\psi \to \rho^0\pi^0$,KK+neutrals,p$\bar{p}$ + neutrals,using TOF information to reject KK,p$\bar{p}$ events,for $\rho^0\pi^0$ background,requiring | $\vec{P}_{\rho^0}$ -1.45|≥0.04 GeV to reject $\rho^0\pi^0$ events. Defining:

$$\Delta = \frac{1}{1+(\frac{M_{\gamma\gamma}-0.548}{\sigma_\eta})^2} \times \frac{1}{1+(\frac{M_{\eta'}-0.958}{\sigma_{\eta'}})^2} \times \frac{1}{1+(\frac{M_{\rho^0}-0.768}{\sigma_{\rho^0}})^2}$$

where σ_η,$\sigma_{\eta'}$,σ_{ρ^0} obtained from MC simulations. Requiring:

$$\Delta \geq 0.4$$

$$| M_{\rho^0} - 0.768 | < 0.075 GeV$$

$$P_{tr}^2 < 0.1$$

$$\chi^2 \leq 15.$$

3.Preliminary Results

The full structure of M($\eta\eta$') is shown in Fig2.1. There are two peaks of M($\eta\eta$'): one in 1.7-1.8GeV region,another in 2.2-2.3 GeV region. For the second peak,the result is shown in Fig2.2,from BW Fit,we got:

$$M(\eta\eta') = (2248 \pm 13)MeV$$

$$\Gamma = (35 \pm 48)MeV$$

$$Br(J/\psi \to \eta\eta') \bullet Br(\eta \to \gamma\gamma) = (1.4 \pm 0.6 \pm 0.4) \times 10^{-3}$$

4σ statistical significance at 90 percent C.L.

4.Discussion

This peak of M($\eta\eta$')=(2248±13)MeV could be explained as evidence of existence of J/$\psi \to \gamma + \xi(2.2)$, $\xi(2.2) \to \eta\eta'$.

References

[1] Review of particle properties Phys.Lett.170B(1986)5

[2] D.Alde et al Phys.Lett.177(1986)120

[3] R.M.Baltrusaitis et al Phys.Rev.Lett.56(1986)107

[4] J.Augustin et al Phys.Rev.Lett.60(1988)2238

Kaon Production in e^+e^- Annihilation

Yang Chunbin and Cai Xu

Institute of Particle Physics, Hua-Zhong Normal University, Wuhan 430070

Abstract

Based on isospin conservation and strangeness suppression, $\langle \frac{K^+}{\pi^+} \rangle$ and $\langle \frac{K^-}{\pi^-} \rangle$ together with $\langle K^+/\pi^+ \rangle / \langle K^-/\pi^- \rangle$ in processes $e^+e^- \to$ hadrons are calculated. It is shown that those ratios as functions of hadron multiplicity of final state depend on the isospin structures of the quark-antiquark pair from which the fragmentation takes place and they can be used for determining the flavor contents of the quark-antiquark pair.

PACS number: 13.65.+i, 13.87.Fb, 13.75.Lb

Kaons, since being discovered, have long been proposed as one of the most promising messengers of the primary stages of hadron-hadron, e^+e^- and heavy-ion collisions. Since s and $\bar{s}$ quarks exists only in the sea of normal particles such as nucleons and nucleus, kaon production is sensitive to the mechanisms postulated for the processes and the internal structure of particles involved. However, due to the complexity of the not well-known reaction dynamics and uncertainties in elementary kaon production processes, the physics extracted from kaon data is still very limited in spite of extensive efforts in the past years. To explain the firmly established increase of the ratio $R^{\pm}$ of strange over non-strange particles from nucleon-nucleon to central nucleus-nucleus collisions in various experiments, people have proposed many models. Some believe that the enhanced production of strange particles is a possible signature of deconfinement of quarks in ultra-relativistic heavy-ion collisions [1]. Due to the fact that the process of hadronization can affect the final number of strange particles [2], the simple picture of an equilibrated quark-gluon plasma is replaced by more complicated and more mundane ones. Almost all models can explain some respect of experimental data but fail to face the whole data. For example, the independent string models, such as the Dual Parton Model and Quark Gluon String Model [3], allow to understand the observed enhancement of K^-, but not K^+ and K^0_S. Meanwhile, to find out if such an enhancement can be worked out in hadronic scenario, several purely hadronic models have been developed [4]. In those models some delicate but artificial mechanisms have been assumed, but their answers are not the same, some even opposite to each other.

In one of our earlier works [5], we surmised in a completely different way that the enhanced strangeness production may be a result of fundamental conservation laws such as isospin conservation. To see what our idea will work out for hadron-hadron